PART I - THE RADIATION OF ELASTIC WAVES FROM A SPHERICAL CAVITY IN A HALF SPACE

PART II - PRECISION DETERMINATION OF FOCAL DEPTHS AND EPICENTERS OF EARTHQUAKES

Thesis by

Armando Cisternas

In Partial Fulfillment of the Requirements

For the Degree of

Doctor of Philosophy

California Institute of Technology

Pasadena, California

1964

(Submitted May 28, 1964)

ACKNOWLEDGMENTS

The author most gratefully acknowledges the guidance and constant support of Dr. Frank Press throughout this study. The author is especially indebted to Dr. Ari Ben-Menahem with whom he collaborated in a part of the first problem, and had many stimulating discussions. Dr. Charles F. Richter, Dr. Clarence Allen and Mr. John Nordquist gave valuable advice for Part II, and the latter two read the manuscript critically. Dr. John H. Healy of the U.S. Geological Survey (Crustal Studies Branch) furnished refraction data in advance of publication.

Mr. Laszlo Lenches deserves special credit for the preparation of the figures, and Mrs. Virginia Gilliam and Mrs. Barbara Sloan for typing the manuscript.

The research was partially supported by contract AF-49(638)-1337. During these studies the author was under the sponsorship of the Agency for International Development and received partial support from the University of Chile.

ABSTRACT

Part I: The dynamic response of an elastic half space to an explosion in a buried spherical cavity is investigated by two methods. The first is implicit, and the final expressions for the displacements at the free surface are given as a series of spherical wave functions whose coefficients are solutions of an infinite set of linear equations. The second method is based on Schwarz's technique to solve boundary value problems, and leads to an iterative solution, starting with the known expression for the point source in a half space as first term. The iterative series is transformed into a system of two integral equations, and into an equivalent set of linear equations. In this way, a dual interpretation of the physical phenomena is achieved. The systems are treated numerically and the Rayleigh wave part of the displacements is given in the frequency domain. Several comparisons with simpler cases are analyzed to show the effect of the cavity radius-depth ratio on the spectra of the displacements.

PART II: A high speed, large capacity, hypocenter location program has been written for an IBM 7094 computer. Important modifications to the standard method of least squares have been incorporated in it. Among them are a new way to obtain the depth of shocks from the normal equations, and the computation of variable travel times for the local

shocks in order to account automatically for crustal variations. The multiregional travel times, largely based upon the investigations of the United States Geological Survey, are confronted with actual traverses to test their validity.

It is shown that several crustal phases provide control enough to obtain good solutions in depth for nuclear explosions, though not all the recording stations are in the region where crustal corrections are considered. The use of the European travel times, to locate the French nuclear explosion of May 1962 in the Sahara, proved to be more adequate than previous work.

A simpler program, with manual crustal corrections, is used to process the Kern County series of aftershocks, and a clearer picture of tectonic mechanism of the White Wolf fault is obtained.

Shocks in the California region are processed automatically and statistical frequency-depth and energy-depth curves are discussed in relation to the tectonics of the area.

TABLE OF CONTENTS

PART I

THE RADIATION OF ELASTIC WAVES FROM A SPHERICAL CAVITY IN A HALF SPACE

PART II

PRECISION DETERMINATION OF FOCAL DEPTHS AND EPICENTERS OF EARTHQUAKES

PART I

THE RADIATION OF ELASTIC WAVES FROM A SPHERICAL CAVITY IN A HALF SPACE

INTRODUCTION

Problems of seismic wave propagation from a point-source in a half-space or from a pressurized cavity in an infinite elastic medium were studied long ago and their solutions are well known, (Ewing et al., 1957). However, it is extremely more complex to achieve results in the field of wave propagation in media with mixed boundaries. A problem of this kind has recently arisen in connection with the use of large cavities to reduce seismic signals from underground nuclear explosions, (Latter et al., 1961). One is faced here with the problem of obtaining the transient displacements over the free surface, caused by an explosion in a pre-existing cavity. An explosion in a smaller cavity can also be represented by the same theory, assuming the size of the source to be given by the boundary of the non-elastic zone. Although cylindrical symmetry exists in the mathematical model, conventional methods cannot be applied because the Helmholtz wave equation does not separate in the bispherical coordinate system, which is natural to the boundaries. Some progress has recently been made with regard to non-separable coordinate systems (Weston, 1957), but we could not find ways to apply these techniques to our case.

To bypass the inherent difficulty of the problem we use two systems with a common origin: The cylindrical and

the spherical systems fit the plane surface and the walls of the cavity respectively. Moreover, the vector wave equation separates in both of them. It is only necessary to transform the wave-functions from one coordinate system to the other so as to be able to specify the complete field on both boundaries. Along these lines we describe two different methods:

The first one, introduced by Grinberg (1948), was used by D'Yakonov (1959) to treat the equivalent electromagnetic problem in which he studied the diffraction of electromagnetic waves by a spherical inclusion within a conducting sphere. Here the field is completely specified at once. The half-space is obtained as that case in which the radius of the conducting sphere is increased to infinity. Our analysis becomes simpler due to the direct transformation of spherical waves to cylindrical waves; thus the limiting process is avoided. Nevertheless, numerical computations were not possible.

The second approach is based on a technique introduced by Schwarz (Kantorovich and Krylov, 1958) to solve boundary value problems for regions that are the union or the intersection of simpler ones. It consists in the modification of an initial trial solution in order to satisfy alternatively the different boundary conditions, and is a generalization of the known iterative procedures to solve integral equations. This method has been used

with success by Kane (1962) and by Kane and Spence (1963), to solve some elastodynamic problems with mixed boundaries. We will show how to apply this general criterion to obtain a solution to the problem of radiation of waves from a spherical cavity in an elastic half-space.

With this method the computations are possible because a fast convergence is expected in the case in which the introduction of an additional boundary (the sphere) perturbs the wave functions only slightly. Kane and Spence (1963, in press) obtained a good fit to experimental data after only one approximation. In our problem, if the spherical cavity is small in comparison with the wave length, it would be enough to consider only the first order terms. Otherwise, the complexity of the expressions involved makes it impossible to handle the exact solution numerically.

Cavities that are not spheres can be studied in the same way.

THE FIELD POTENTIALS

Consider an homogeneous, isotropic elastic half-space with a spherical cavity of radius "a", at depth "h" below the free surface (Figure 1-1). It is convenient to assume Poisson's hypothesis $\sigma = \frac{1}{4}$. We choose the center of the cavity as the origin of a spherical and a cylindrical coordinate system. The z - axis points downwards.

A point P, inside the half space has coordinates (r,φ,z) in the cylindrical system and (R,φ,θ) in the spherical system. These frames of reference are tied by the relations $r = R\sin\theta$, $z = R\cos\theta$. The medium is excited by the application of a spherically symmetric pressure impulse upon the surface of the cavity: $P(t) = P_0 H(t)$, where $H(t)$ is the step function. A more general time function can be considered. Because of the source symmetry the field will be independent of the angle φ . The expressions we will consider are in the frequency domain. The time domain quantities can be obtained from them by a Fourier synthesis. From now on, the factor $e^{-i\omega t}$ will be suppressed.

It is well known that the displacement vector $\vec{u}$ is completely determined by a scalar potential Φ , and a vector potential $\vec{B}$:

$$\vec{u} = \nabla\Phi - \nabla\times\nabla\times\vec{B} \qquad (1\text{-}1)$$

The choice of the vector $\vec{B}$ usually depends on the geometry of the problem. Here we must take $\vec{B} = \Delta\hat{k}$ ($\hat{k}$ is a unit vector in the positive z - direction) to secure the separability of the boundary conditions over both the half-space and the spherical cavity. The functions Φ and Δ satisfy the scalar Helmholtz equations $\nabla^2\Phi + k_\alpha^2\Phi = 0$, $\nabla^2\Delta + k_\beta^2\Delta = 0$, for compressional and shear waves respectively. The quantities

$k_\alpha = \frac{\omega}{c_\alpha}$ and $k_\beta = \frac{\omega}{c_\beta}$ are the corresponding wave numbers.

Now we can proceed to give a representation of the field in spherical coordinates. We make use of the spherical eigenfunctions:

$$\Phi = \sum_{n=0}^{\infty} [A_n h_n^{(1)}(k_\alpha R) + B_n h_n^{(2)}(k_\alpha R)] P_n(\cos\theta) \qquad (1\text{-}2)$$

$$\Delta = \sum_{n=0}^{\infty} [C_n h_n^{(1)}(k_\beta R) + D_n h_n^{(2)}(k_\beta R)] P_n(\cos\theta) \qquad (1\text{-}3)$$

Here, $h_n^{(1)}(k_\alpha R) P_n(\cos\theta)$, the product of the spherical Hankel function of the first kind by the Legendre polynomial, represents an outgoing elementary wave of order n. On the other hand, the term with the spherical Hankel function of the second kind represents an elementary incoming wave of order n. Together they form a complete system of eigenfunctions for the wave equation with the boundary conditions of the theory of elasticity, and a source function that can be expressed as a uniformly convergent series of Legendre polynomials over the surface of the sphere. The coefficients A_n, B_n, C_n and D_n measure the strength of the different elementary waves.

We will now show that the vector $\nabla x \vec{B}$ can be separated in both system of coordinates. In the

cylindrical system we obtain $\nabla \times \vec{B} = -\frac{\partial \Delta}{\partial r}\hat{e}_\varphi$, and the separability is obvious, because if Δ is the product of a function of Z and a function of r , $\frac{\partial \Delta}{\partial r}$ is also . In spherical coordinates we write the operator $\frac{\partial}{\partial r}$ in the form $\sin\theta \frac{\partial}{\partial R} + \frac{\cos\theta}{R}\frac{\partial}{\partial \theta}$, and make use of some results in the theory of spherical Bessel functions and the Legendre polynomials to obtain (Appendix I-1):

$$-\frac{\partial \Delta}{\partial r} = \sum_{n=1}^{\infty} \left[\Gamma_n h_n^{(1)}(k_\beta R) + \Delta_n h_n^{(2)}(k_\beta R) \right] \frac{\partial P_n(\cos\theta)}{\partial \theta} \qquad (I-4)$$

with $\Gamma_n = -k_\beta \left(\frac{C_{n+1}}{2n+3} + \frac{C_{n-1}}{2n-1} \right)$; $\Delta_n = -k_\beta \left(\frac{D_{n+1}}{2n+3} - \frac{D_{n-1}}{2n-1} \right)$

Thus $\frac{\partial \Delta}{\partial r}$ can be expressed as a sum of products of functions of R and θ , and therefore it is separable. The separability condition implies a mode conversion at the surface of the cavity, where each mode is tied up with its two adjacent modes, as stated by equation (I-4).

This phenomenon of mode conversion will be present at each stage of this theory. It is due to the fact that the geometry of one wave representation doesn't fit all of the boundaries. The wave equations have a separation variable n in spherical coordinates, and a separation variable k in cylindrical coordinates; they provide a dual representation of the events, and the normal modes of vibration of the system. They are going to be split when an elementary wave incides upon a boundary that is not natural to its geometry.

The relations for the coefficients in equation (I-4), can be treated as difference equations, and solved for Cn under the assumption $C_n \to 0$ as $n \to \infty$. It results:

$$C_n = -\frac{2n+1}{K_\beta} \sum_{p=0}^{\infty} (-1)^p \Gamma_{n+2p+1}$$

which will be useful further on in the derivation of the integral equations (I-73), (I-74).

TRANSFORMATION TO CYLINDRICAL COORDINATES

Up to now we have constructed the field potential Φ and Λ in terms of spherical wave functions. Keeping in mind the invariance of the physical field under a transformation of the coordinate system, we shall next search for a suitable way to express our field potentials in cylindrical coordinates so as to be able to satisfy the boundary conditions on the free surface. To this purpose we need the operational representation of the spherical wave functions as given by Van der Pol (1936) and Erdelyi (1937).

$$h_n^{(1)}(k_\alpha R) P_n(\cos\theta) = i^{-n} P_n\left(\frac{\partial}{\partial i k_\alpha z}\right) h_0^{(1)}(k_\alpha R) \qquad (I-5)$$

The argument of the Legendre Polynomial on the right side of equation (I-5) is the operational derivative with respect to the argument $ik_\alpha z$.

The beauty of the relationship (I-5) lies in the fact that the spherical wave function of order zero $h_0^{(1)}(k_\alpha R)$ can be expressed by the Sommerfeld integral

representation in terms of cylindrical wave functions:

$$h_o^{(1)}(k_\alpha R) = \frac{1}{i k_\alpha} \int_o^\infty e^{-\nu|z|} J_o(kr) \frac{k\,dk}{\nu} \quad ; \quad \nu = \sqrt{k^2 - k_\alpha^2} \qquad (1\text{-}6)$$

The application of formula (1-5) to the relation (1-6) implies the use of the operator $P_n\left(\frac{\partial}{\partial i k_\alpha z}\right)$ under the integral sign. The operator acts upon the exponential term only, modifying the integrand by a factor $P_n\left(\frac{i\nu}{k_\alpha}\right)$. Therefore the result is an absolutely convergent integral, and we have

$$h_n^{(1)}(k_\alpha R) P_n(\cos\theta) = \frac{i^{-n-1}}{k_\alpha} \int_o^\infty P_n\left(\frac{i\nu}{k_\alpha}\right) e^{-\nu|z|} J_o(kr) \frac{k\,dk}{\nu} \qquad (1\text{-}7)$$

A similar expression can be constructed for the Hankel functions of the second kind by taking the complex conjugate of (1-7). In this way we obtain the higher order wave functions in cylindrical coordinates as we sought.

The field potentials can be rewritten in the form:

$$\Phi = \int_o^\infty \left[\alpha(\nu) \frac{e^{-\nu|z|}}{\nu} - \beta(\bar{\nu}) \frac{e^{-\bar{\nu}|z|}}{\bar{\nu}}\right] J_o(kr)\, k\,dk \qquad (1\text{-}8)$$

$$\Lambda = \int_o^\infty \left[\gamma(\nu') \frac{e^{-\nu'|z|}}{\nu'} - \delta(\bar{\nu}') \frac{e^{-\bar{\nu}'|z|}}{\bar{\nu}'}\right] J_o(kr)\, k\,dk \qquad (1\text{-}9)$$

where $\nu' = \sqrt{k^2 - k_\beta^2}$, $\bar{\nu}$ and $\bar{\nu}'$ are complex conjugate of ν and ν' and

$$\alpha(\nu) = \frac{1}{i k_\alpha} \sum_{n=0}^\infty i^{-n} A_n P_n\left(\frac{i\nu}{k_\alpha}\right) \qquad (1\text{-}10)$$

with similar expressions for $\beta(\bar{\nu})$, $\gamma(\nu')$ and $\delta(\bar{\nu}')$.

To obtain the surface displacements we write equation (1-1) explicitly for the radial and vertical components:

$$u_r = \frac{\partial \Phi}{\partial r} - \frac{\partial^2 \Delta}{\partial r \partial z} \quad ; \quad u_z = \frac{\partial \Phi}{\partial z} + \frac{1}{r}\frac{\partial}{\partial r}\left(r\frac{\partial \Delta}{\partial r}\right) \tag{1-11}$$

Performing the necessary operations we have:

$$u_r = -\int_0^\infty \left[\alpha(\nu)\frac{e^{-\nu z}}{\nu} - \beta(\bar{\nu})\frac{e^{-\bar{\nu} z}}{\bar{\nu}} + \gamma(\nu')e^{-\nu' z} - \delta(\bar{\nu}')e^{-\bar{\nu}' z}\right] J_1(kr)k^2 dk \tag{1-12}$$

$$u_z = -\int_0^\infty \left[\alpha(\nu)e^{-\nu z} - \beta(\bar{\nu})e^{-\bar{\nu} z} + \gamma(\nu')k^2\frac{e^{-\nu' z}}{\nu'} - \delta(\bar{\nu}')k^2\frac{e^{-\bar{\nu}' z}}{\bar{\nu}'}\right] J_0(kr)k\,dk \tag{1-13}$$

We next derive the normal and tangential stresses at the free surface; starting from the relations

$$\frac{1}{\mu}\sigma_{zr} = \frac{\partial u_r}{\partial z} + \frac{\partial u_z}{\partial r} \quad ; \quad \frac{1}{\mu}\sigma_{zz} = \nabla\cdot\vec{u} + 2\frac{\partial u_z}{\partial z} \tag{1-14}$$

we obtain after replacing $z = h$

$$\sigma_{zz} = \mu\int_0^\infty \left[\alpha(\nu)\frac{2k^2-\kappa_\beta^2}{\nu}e^{-\nu h} - \beta(\nu')\frac{2k^2-\kappa_\beta^2}{\bar{\nu}}e^{-\bar{\nu} h} + 2k^2\gamma(\nu')e^{-\nu' h} - 2k^2\delta(\bar{\nu}')e^{-\bar{\nu}' h}\right] J_0(kr)k\,dk \tag{1-15}$$

$$\sigma_{zr} = \mu\int_0^\infty \left[2\alpha(\nu)e^{-\nu h} - 2\beta(\bar{\nu})e^{-\bar{\nu} h} + \gamma(\nu')\frac{2k^2-\kappa_\beta^2}{\nu'}e^{-\nu' h} - \delta(\bar{\nu}')\frac{2k^2-\kappa_\beta^2}{\bar{\nu}'}e^{-\bar{\nu}' h}\right] J_1(kr)k^2 dk \tag{1-16}$$

The application of the boundary conditions over the spherical cavity is straightforward. The normal and tangential stress are derived from the formulas:

$$\frac{1}{\mu}\sigma_{RR} = \left(3\frac{\partial}{\partial R} + \frac{2}{R}\right)u_R + \frac{1}{R\sin\theta}\frac{\partial}{\partial\theta}(\sin\theta\, u_\theta) \tag{1-17}$$

$$\frac{1}{\mu}\sigma_{R\theta} = \frac{1}{R}\frac{\partial u_R}{\partial\theta} + \left(\frac{\partial}{\partial R} - \frac{1}{R}\right)u_\theta \tag{1-18}$$

Substitution of the expressions for the displacements yields:

$$\sigma_{RR} = \mu \sum_{n=0}^{\infty} \left\{ L_1 \left[A_n h_n^{(1)}(K_\alpha R) + B_n h_n^{(2)}(K_\alpha R) \right] + n(n+1) L_2 \left[\Gamma_n h_n^{(1)}(K_\beta R) + \Delta_n h_n^{(2)}(K_\beta R) \right] \right\} P_n(\cos\theta) \quad (1-19)$$

$$\sigma_{R\theta} = \mu \sum_{n=0}^{\infty} \left\{ L_2 \left[A_n h_n^{(1)}(K_\alpha R) + B_n h_n^{(2)}(K_\alpha R) \right] + L_3 \left[\Gamma_n h_n^{(1)}(K_\beta R) + \Delta_n h_n^{(2)}(K_\beta R) \right] \right\} \frac{\partial P_n(\cos\theta)}{\partial \theta} \quad (1-20)$$

L_1, L_2, and L_3 are linear differential operators:

$$L_1(n) = \frac{2n(n+1)}{R^2} - K_\beta^2 - \frac{4}{R}\frac{d}{dR}$$

$$L_2 = \frac{2}{R}\left(\frac{d}{dR} - \frac{1}{R}\right) \quad (1-21)$$

$$L_3(n) = \frac{2n(n+1)-2}{R^2} - K_\beta^2 - \frac{2}{R}\frac{d}{dR} = L_1 + L_2$$

These operators have been simplified by the elimination of the second derivatives through the use of Bessel's differential equation.

BOUNDARY CONDITIONS

The use of the boundary conditions gives the necessary equations to determine the amplitudes of the spherical wave fields. The boundary conditions on the plane surface give $\sigma_{zz} = \sigma_{zr} = 0$. From (1-15) and (1-16) we see that stresses on the plane surface depend only upon r , via the Bessel functions. If we expand Bessel functions in Taylor series around the origin, the stresses will be given in power series of r . After replacing

$$J_0(kr)=\sum_{h=0}^{\infty}(-1)^h\frac{\left(\frac{kr}{2}\right)^{2h}}{(h!)^2}\quad,\qquad J_1(kr)=\frac{kr}{2}\sum_{h=0}^{\infty}(-1)^h\frac{\left(\frac{kr}{2}\right)^{2h}}{h!\,(h+1)!}$$

in the equation for the stresses (I-15) and I-16) and reversing the order of summation and integration and finally equating each coefficient of the powers of r to zero, we have:

$$\int_0^{\infty}k^{2m}\kappa\,dk\left[2\alpha(\nu)e^{-\nu h}-2\beta(\bar\nu)e^{-\bar\nu h}+\frac{2k^2-\kappa_\beta^2}{\nu'}e^{-\nu' h}\gamma(\nu')-\frac{2k^2-\kappa_\beta^2}{\bar\nu'}e^{-\bar\nu' h}\delta(\bar\nu')\right]=0 \qquad (I-22)$$

$$m=1,2,3....$$

$$\int_0^{\infty}k^{2m}\kappa\,dk\left[\frac{2k^2-\kappa_\beta^2}{\nu}e^{-\nu h}\alpha(\nu)-\frac{2k^2-\kappa_\beta^2}{\bar\nu}e^{-\bar\nu h}\beta(\bar\nu)+2k^2e^{-\nu' h}\gamma(\nu')-2k^2e^{-\bar\nu' h}\delta(\bar\nu')\right]=0 \qquad (I-23)$$

$$m=0,1,2,3....$$

The factor k^2 can be generated by taking the second derivative of the exponentials within the integral sign. This fact leads to the introduction of the operators $L_\alpha=\frac{d^2}{dh^2}+k_\alpha^2$; $L_\beta=\frac{d^2}{dh^2}+k_\beta^2$. The application of these operators together with the already known results: $\int_0^{\infty}P_n\left(\frac{i\nu}{k_\alpha}\right)e^{-\nu h}\frac{\kappa\,dk}{\nu}=k_\alpha i^{n+1}h_n^{(1)}(k_\alpha h)$, and the like, to (I-22) and I-23) yields

$$-2L_\alpha^m\frac{d}{dh}\Phi_E+L_\beta^m(2L_\beta-k_\beta^2)\Delta_E=0 \quad ; \; m=1,2,3.... \qquad (I-24)$$

$$L_\alpha^m (2L_\alpha - K_\beta^2)\,\Phi_E - 2L_\beta^{m+1}\frac{d}{dh}\,\Lambda_E = 0 \quad ; \; m = 0,1,2,3,\ldots \qquad (1\text{-}25)$$

where L^m means that the operator L is repeated m times. Φ_E and Λ_E are the field potentials, evaluated at the epicenter E.

$$\Phi_E = \sum_{n=0}^{\infty} [A_n h_n^{(1)}(K_\alpha h) + B_n h_n^{(2)}(K_\alpha h)]$$
$$\Lambda_E = \sum_{n=0}^{\infty} [C_n h_n^{(1)}(K_\beta h) + D_n h_n^{(2)}(K_\beta h)] \qquad (1\text{-}26)$$

The transformed input pressure on the walls of the cavity is $\frac{P_o}{2\pi i\omega}$, and the conditions that determine the problem completely are $\sigma_{RR} = \frac{P_o}{2\pi i\omega}$; $\sigma_{R\theta} = 0$ at R = a. We then use equations (1-19) and (1-20), observing that the terms that involve a θ - dependence should vanish.

$$L_1 [A_o h_o^{(1)}(K_\alpha a) + B_o h_o^{(2)}(K_\alpha a)] = \frac{P_o}{2\pi\mu i\omega} \qquad (1\text{-}27)$$

$$L_1 [A_n h_n^{(1)}(K_\alpha a) + B_n h_n^{(2)}(K_\alpha a)] + n(n+1) L_2 [\Gamma_n h_n^{(1)}(K_\beta a) + \Delta_n h_n^{(2)}(K_\beta a)] = 0 \qquad (1\text{-}28)$$
$$n = 1, 2, 3, \ldots$$

$$L_2 [A_n h_n^{(1)}(K_\alpha a) + B_n h_n^{(2)}(K_\alpha a)] + L_3 [\Gamma_n h_n^{(1)}(K_\beta a) + \Delta_n h_n^{(2)}(K_\beta a) = 0 \qquad (1\text{-}29)$$
$$n = 1, 2, 3, \ldots$$

We rewrite the conditions (I-24), (I-25) in a more explicit way

$$-2\left(\frac{d^2}{dh^2}+K_\alpha^2\right)^m \frac{d}{dh}\sum_{j=0}^{\infty}\left[A_j h_j^{(1)}(K_\alpha h)+B_j h_j^{(2)}(K_\alpha h)\right] + \qquad (I-30)$$

$$+\left(\frac{d^2}{dh^2}+K_\beta^2\right)^m\left(2\frac{d^2}{dh^2}+K_\beta^2\right)\sum_{j=0}^{\infty}\left[C_j h_j^{(1)}(K_\beta h)+D_j h_j^{(2)}(K_\beta h)\right]=0$$

$$m=1,2,3,\ldots\ldots$$

$$\left(\frac{d^2}{dh^2}+K_\alpha^2\right)^m\left(2\frac{d^2}{dh^2}-K_\alpha^2\right)\sum_{j=0}^{\infty}\left[A_j h_j^{(1)}(K_\alpha h)+B_j h_j^{(2)}(K_\alpha h)\right]- \qquad (I-31)$$

$$-2\left(\frac{d^2}{dh^2}+K_\beta^2\right)^{m+1}\frac{d}{dh}\sum_{j=0}^{\infty}\left[C_j h_j^{(1)}(K_\beta h)+D_j h_j^{(2)}(K_\beta h)\right]=0$$

$$m=0,1,2,3,\ldots\ldots$$

Equations (I-27) to (I-31) form a set of linear equations with unknowns An, Bn, Cn, Dn. If we can solve exactly this infinite system, we can obtain the whole field at once. We will discuss the numerical properties of it at the end of the paragraph, but before we will give the surface displacements in a more suitable way. To this effect it is convenient to go back to equations (I-15) and (I-16), and note that an alternative way to write the boundary conditions at the plane surface, can be obtained by equating to zero the factors in front of the Bessel functions, since the stresses should vanish independently of r. We thus write:

$$\frac{2K^2-K_\beta^2}{\nu}e^{-\nu h}\alpha(\nu)-\frac{2K^2-K_\beta^2}{\bar{\nu}}e^{-\bar{\nu}h}\beta(\bar{\nu})+2K^2e^{-\nu' h}\gamma(\nu')-2K^2e^{-\bar{\nu}' h}\delta(\bar{\nu}')=0 \qquad (I-32)$$

$$2e^{-\nu h}\alpha(\nu) - 2e^{-\bar{\nu} h}\beta(\bar{\nu}) + \frac{2k^2 - k_\beta^2}{\nu'}e^{-\nu' h}\gamma(\nu') - \frac{2k^2 - k_\beta^2}{\bar{\nu}'}e^{-\bar{\nu}' h}\delta(\bar{\nu}') = 0 \quad (1\text{-}33)$$

This system can be solved for $\alpha(\nu)$ and $\gamma(\nu')$ in terms of $\beta(\bar{\nu})$ and $\delta(\bar{\nu}')$. Substituting $\alpha(\nu)$ and $\gamma(\nu')$ back into equations (1-12) and 1-13), and collecting terms we obtain an expression for the displacements at the surface in a more familiar form:

$$u_r = \int_0^\infty \frac{J_1(kr)\,k^2\,dk}{F(k)}\left[2k_\beta^2\nu'\left(1 - \frac{\nu}{\bar{\nu}}\right)e^{-\bar{\nu} h}\beta(\bar{\nu}) - k_\beta^2(2k^2 - k_\beta^2)\left(1 - \frac{\nu'}{\bar{\nu}'}\right)e^{-\bar{\nu}' h}\delta(\bar{\nu}')\right] \quad (1\text{-}34)$$

$$u_z = \int_0^\infty \frac{J_0(kr)\,k\,dk}{F(k)}\left[-k_\beta^2(2k^2 - k_\beta^2)\left(1 - \frac{\nu}{\bar{\nu}}\right)e^{-\bar{\nu} h}\beta(\bar{\nu}) + 2k_\beta^2 k^2\nu\left(1 - \frac{\nu'}{\bar{\nu}'}\right)\delta(\bar{\nu}')\right]$$

This is a solution of the problem if the functions $\beta(\bar{\nu})$ and $\delta(\bar{\nu}')$ are known. They are determined as functions of the coefficients Bn and Dn, which are to be determined by the use of the boundary conditions. However, for our purpose, there are critical difficulties that force us to change the procedure. Any attempt to

solve the system by approximants, runs into very delicate problems due to very large round-off errors. The Hankel functions give very large values for small arguments, which is the case here, if we examine a long wavelength approximation. Furthermore, analytic cancellation of the leading terms helps in the loss of the significant figures. Despite the theoretical interest of the method, we believe it is unsuitable to extract a numerical solution from it, with the methods accessible to us at this time.

THE METHOD OF H. A. SCHWARZ

In this second approach to the problem, we keep the same geometry and general equations of the previous paragraphs. We change only the form of the wave functions and the technique to arrive at the solution.

A few words about the steps to be followed will help to clarify the procedure: We begin with a cavity of radius "a" in an infinite space. The solution to the elastic problem when a pressure P is applied to the walls of the cavity, and kept in time, was given by Jeffreys (1932), Sharpe (1942), Blake (1952) and others. Next, the introduction of a plane boundary at a distance "h" from the center of the cavity, results in nothing more than Lamb's problem. The only difference is a source function equal to the ratio of the spectra of the

displacements from a cavity and from a point source in the infinite space. This term, which depends upon the radius of the cavity, multiplies Lamb's integrals which in turn depend only upon the depth. At this stage the depth and the radius of the cavity act independently of each other. This problem was analyzed by Byatt and De Vault (1961).

The following steps are no longer simple. The modification of the solution to satisfy the boundary conditions at the surface of the cavity is rather involved, but it gives the spatial dependence on the source. Further steps can still be carried out formally to satisfy again the condition of vanishing normal and tangential stresses at the free surface, and at the surface of the sphere.

The scalar potentials are expanded in series in order to account for the different steps to be followed.

$$\Phi = \Phi_0 + \Phi_1 + \Phi_2 + \cdots\cdots \qquad (1\text{-}35)$$

$$\Delta = \Delta_1 + \Delta_2 + \cdots\cdots \qquad (1\text{-}36)$$

The odd order terms are introduced to satisfy the boundary conditions at the free surface, and the even ones to satisfy the conditions at the surface of the cavity.

We begin with a source potential which already satisfies the cavity conditions:

$$\Phi_0 = \mathcal{A}(\omega)\frac{1}{R}e^{ik_\alpha R} = \mathcal{A}(\omega)\int_0^\infty J_0(kr)e^{-\nu|z|}\frac{kdk}{\nu} \qquad (1\text{-}37)$$

where

$$\mathcal{A}(\omega) = -\frac{P(\omega)a^3}{\mu}\frac{e^{ik_\alpha a}}{4-4ik_\alpha a-3k_\alpha^2 a^2} \qquad (1\text{-}38)$$

Here $P(\omega)$ is the spectrum of the source function; $P(\omega) = \frac{P_0}{2\pi i\omega}$ in case of a step function.

In order to satisfy the conditions at the surface of the earth, we introduce scalar potentials in cylindrical coordinates in the way shown by Ewing et al. (1957)

$$\Phi_1 = \mathcal{A}(\omega)\int_0^\infty B(k)\,J_0(kr)e^{-\nu z}\frac{kdk}{\nu} \qquad (1\text{-}39)$$

$$\Delta_1 = \mathcal{A}(\omega)\int_0^\infty C(k)\,J_0(kr)e^{-\nu' z}\frac{kdk}{\nu'} \qquad (1\text{-}40)$$

The contour of integration is shown in Figure 1-2, it passes above the branch points k_α, k_β, the Rayleigh pole and gives Cauchy's principal value of the integral. $B(k)$ and $C(k)$ are chosen to satisfy the boundary conditions at the free surface $z = h$. They are:

$$B(k) = \frac{(2k^2-k_\beta^2)^2+4k^2\nu\nu'}{-F(k)}\, e^{-2\nu h} \qquad (1-41)$$

$$C(k) = \frac{4\nu'(2k^2-k_\beta^2)}{F(k)}\, e^{-(\nu+\nu')h} \qquad (1-42)$$

where $F(k) = (2k^2-k_\beta^2)^2 - 4k^2\nu\nu'$ is the Rayleigh denominator.

To continue with the process we add new potentials Φ_2 and Δ_2, such that $\Phi_1+\Phi_2$, and $\Delta_1+\Delta_2$ satisfy the boundary conditions at the cavity. We should remember here that Φ_o was already constructed to satisfy them. It is natural to select these new potentials in spherical coordinates in terms of outgoing waves:

$$\Phi_2 = \mathcal{A}(\omega) \sum_{n=o}^{\infty} A_n h_n^{(1)}(k_\alpha R)\, P_n(\cos\theta) \qquad (1-43)$$

$$\Delta_2 = \mathcal{A}(\omega) \sum_{n=o}^{\infty} C_n h_n^{(1)}(k_\beta R)\, P_n(\cos\theta) \qquad (1-44)$$

To transform Φ_1 and Δ_1 into spherical coordinates, we make use of the relationship, (Stratton, 1941):

$$J_o(kr)\, e^{-\nu z} = \sum_{n=o}^{\infty} i^n(2n+1)\, P_n\left(\frac{i\nu}{k_\alpha}\right) j_n(k_\alpha R) P_n(\cos\theta) \qquad (1-45)$$

and a similar one, changing ν by ν', and k_α by k_β. This series development is uniformly convergent in any bounded region of the ν-plane. (Appendix 1-2)

Changing the order of summation and integration we obtain the expressions in spherical coordinates: (For justification of this step, see Appendix I-2)

$$\Phi_1 = \mathcal{A}(\omega) \sum_{n=0}^{\infty} a_n j_n(k_\alpha R) P_n(\cos\theta) \tag{I-46}$$

and

$$\Delta_1 = \mathcal{A}(\omega) \sum_{n=0}^{\infty} c_n j_n(k_\beta R) P_n(\cos\theta) \tag{I-47}$$

where $$a_n = (2n+1) i^n \int_0^\infty \frac{k\,dk}{\nu} B(k) P_n\left(\frac{i\nu}{k_\alpha}\right) \tag{I-48}$$

and $$c_n = (2n+1) i^n \int_0^\infty \frac{k\,dk}{\nu'} C(k) P_n\left(\frac{i\nu'}{k_\beta}\right) \tag{I-49}$$

Once we know a_n and c_n, we may proceed as in Section 4, to write the conditions at the surface of the cavity:

$$A_n L_1 h_n^{(1)}(k_\alpha a) + n(n+1)\Gamma_n L_2 h_n^{(1)}(k_\beta a) = -a_n L_1 j_n(k_\alpha a) - n(n+1)\delta_n^* L_2 j_n(k_\beta a) \tag{I-50}$$

$n = 0, 1, 2, 3, \ldots\ldots$

$$A_n L_2 h_n^{(1)}(k_\alpha a) + \Gamma_n L_3 h_n^{(1)}(k_\beta a) = -a_n L_2 j_n(k_\alpha a) - \delta_n L_3 j_n(k_\beta a) \tag{I-51}$$

$n = 1, 2, 3, \ldots\ldots$

L_1, L_2, and L_3 are defined as in paragraph IV.

$$\Gamma_n = -K_\beta \left(\frac{C_{n+1}}{2n+3} - \frac{C_{n-1}}{2n-1} \right) \quad ; \quad \gamma_n = -K_\beta \left(\frac{e_{n+1}}{2n+3} - \frac{e_{n-1}}{2n-1} \right) \qquad (I\text{-}52)$$

$n = 1, 2, 3, \ldots\ldots$

The system (I-50), (I-51), permits us to compute A_n and Γ_n once we know the integrals for a_n and e_n .

The computation of these integrals is the more interesting feature of this theory, because of the role they play in the interpretation of the interaction of the fields between the free surface and the walls of the cavity. The analysis and their numerical evaluation is given in Appendix I-3.

The solution of the system (I-50), (I-51), involves the evaluation of five 2 x 2 determinants. Appendix I-4 shows a way to avoid loss of significant figures in their calculation. It is also shown there that the coefficients A_n and Γ_n are of the order $O[(K_\alpha a)^{2n-1}]$ for small values of $K_\alpha a$ and $n \geq 2$. A_0 , A_1 , and Γ_1 are of the order $O[(K_\alpha a)^3]$.

Once Γ_n is known, it is possible to find C_n by means of (I-52) rewritten in the more convenient way

$$C_{n-1} = -\frac{2n-1}{K_\beta} \Gamma_n - \frac{2n-1}{2n+3} C_{n+1} \qquad (I\text{-}53)$$

If Γ_m has been computed for $1 \leq n \leq m$, then we take $C_m = C_{m+1} = 0$ as initial values, and proceed backwards down to C_o. The coefficient C_{n-1} is of the order of Γ_n, that is to say $C_{n-1} = O[(k_\alpha a)^{2n-1}]$, but C_o and C_1 are of the order $O[(k_\alpha a)^3]$.

Once A_n and C_n are known, it is easy to compute Φ_2 and Δ_2 from equations (I-43) and (I-44).

A last step directed to obtain a solution with zero stresses at the free surface, requiresadditional potentials Φ_3 and Δ_3. By the use of the Van der Pol – Erdelyi transformation, Φ_2 and Δ_2 can be expressed in the cylindrical system.

$$\Phi_2 = \mathcal{A}(\omega) \int_o^\infty \alpha(\nu)\, J_o(kr) e^{-\nu z} \frac{k\,dk}{\nu} \qquad (I\text{-}54)$$

$$\Delta_2 = \mathcal{A}(\omega) \int_o^\infty \gamma(\nu')\, J_o(kr) e^{-\nu' z} \frac{k\,dk}{\nu'} \qquad (I\text{-}55)$$

where $\alpha(\nu) = \frac{1}{ik_\alpha} \sum_{n=o}^{\infty} i^{-n} A_n P_n\left(\frac{i\nu}{k_\alpha}\right)$, etc. ; then:

$$\Phi_3 = \mathcal{A}(\omega) \int_o^\infty B_3(k)\, J_o(kr) e^{-\nu z} \frac{k\,dk}{\nu} \qquad (I\text{-}56)$$

$$\Delta_3 = \mathcal{A}(\omega) \int_o^\infty C_3(k)\, J_o(kr) e^{-\nu' z} \frac{k\,dk}{\nu'} \qquad (I\text{-}57)$$

where $B_3(k)$ and $C_3(k)$ are functions to be determined. Since $\Phi_o + \Phi_1$ and Δ_1 already satisfy the boundary conditions at the surface, we have to impose them only on $\Phi_2 + \Phi_3$ and $\Delta_2 + \Delta_3$. After some algebra we finally

arrive at:

$$B_3(\kappa) = \frac{e^{-\nu h}}{F(\kappa)} \left[-\tilde{F}(\kappa)\alpha(\nu)e^{-\nu h} + 4\kappa^2\nu(2\kappa^2 - k_\beta^2)\gamma(\nu')e^{-\nu' h} \right] \qquad (1\text{-}58)$$

$$C_3(\kappa) = \frac{e^{-\nu' h}}{F(\kappa)} \left[4\nu'(2\kappa^2 - k_\beta^2)\alpha(\nu)e^{-\nu h} - \tilde{F}(\kappa)\gamma(\nu')e^{-\nu' h} \right] \qquad (1\text{-}59)$$

Here $\tilde{F}(\kappa) = (2\kappa^2 - k_\beta^2)^2 + 4\kappa^2\nu\nu'$.

We are now in condition to write down the displacement at the free surface due to the potentials $\Phi_2 + \Phi_3$ and $\Delta_2 + \Delta_3$. They are obtained through equations (1-11):

$$u_r^2 + u_r^3 = \mathcal{A}(\omega) \int_0^\infty \frac{\kappa^2 d\kappa}{F(\kappa)} \left[4\kappa^2\nu'\alpha(\nu)e^{-\nu h} - 2k_\beta^2(2\kappa^2 - k_\beta^2)\gamma(\nu')e^{-\nu' h} \right] J_1(\kappa r) \qquad (1\text{-}60)$$

$$u_z^2 + u_z^3 = \mathcal{A}(\omega) \int_0^\infty \frac{\kappa d\kappa}{F(\kappa)} \left[-2k_\beta^2(2\kappa^2 - k_\beta^2)\alpha(\nu)e^{-\nu h} + 4k_\beta^2\kappa^2\nu\gamma(\nu')e^{-\nu' h} \right] J_0(\kappa r) \qquad (1\text{-}61)$$

The main contribution to the field comes from the potentials $\Phi_0 + \Phi_1$, and Δ_1 . The displacements due to these functions are:

$$u_r^0 + u_r^1 = 4k_\beta^2 \mathcal{A}(\omega) \int_0^\infty \frac{\kappa^2 d\kappa}{F(\kappa)} \nu' e^{-\nu h} J_1(\kappa r) \qquad (1\text{-}62)$$

$$u_z^0 + u_z^1 = -2k_\beta^2 \mathcal{A}(\omega) \int_0^\infty \frac{\kappa d\kappa}{F(\kappa)} (2\kappa^2 - k_\beta^2) e^{-\nu h} J_0(\kappa r) \qquad (1\text{-}63)$$

The combination of these two sets of displacements gives a spectrum of the field which is accurate for small values of $k_\alpha a$:

$$u_r = \mathcal{A}(\omega) \int_0^\infty \frac{\kappa^2 d\kappa}{F(\kappa)} \left\{ 4k_\beta^2\nu'[1 + \alpha(\nu)]e^{-\nu h} - 2k_\beta^2(2\kappa^2 - k_\beta^2)\gamma(\nu')e^{-\nu' h} \right\} J_1(\kappa r) \qquad (1\text{-}64)$$

$$u_z = \mathcal{A}(\omega) \int_0^\infty \frac{k\,dk}{F(k)} \left\{ -2k_\beta^2(2k^2-k_\beta^2)[1+\alpha(\nu)]e^{-\nu h} + 4k_\beta^2 k^2 \nu\, \gamma(\nu')e^{-\nu' h} \right\} J_0(kr) \quad (1\text{-}65)$$

THE EXACT FORMAL SOLUTION

The repeated application of this iterative procedure leads to the exact solution of the problem as an infinite series of terms in the form given in (1-35) and 1-36). The formalism developed in the previous paragraph is enough to show us what the complete series should be. It is sufficient to look at equations (1-58), (1-59), (1-50), (1-51), and (1-48), (1-49) to write the final form of the displacements in a formula that generalizes (1-64), (1-65):

$$u_r = \mathcal{A}(\omega) \int_0^\infty \frac{k^2\,dk}{F(k)} \left\{ 4k_\beta^2 \nu' [1+\sum_{i=1}^{\infty} \alpha^{(i)}(\nu)]e^{-\nu h} - 2k_\beta^2(2k^2-k_\beta^2) \sum_{i=1}^{\infty} \gamma^{(i)}(\nu')e^{-\nu' h} \right\} J_1(kr) \quad (1\text{-}66)$$

$$u_z = \mathcal{A}(\omega) \int_0^\infty \frac{k\,dk}{F(k)} \left\{ -2k_\beta^2(2k^2-k_\beta^2)[1+\sum_{i=1}^{\infty} \alpha^{(i)}(\nu)]e^{-\nu h} + 4k_\beta^2 k^2 \nu \sum_{i=1}^{\infty} \gamma^{(i)}(\nu')e^{-\nu' h} \right\} J_0(kr) \quad (1\text{-}67)$$

where $\alpha^{(1)}(\nu) \equiv \alpha(\nu)$; $\gamma^{(1)}(\nu') \equiv \gamma(\nu')$ and (1-68)

$$\alpha^{(i)}(\nu) = \frac{1}{i k_\alpha} \sum_{n=0}^{\infty} i^{-n} A_n^{(i)} P_n\left(\frac{i\nu}{k_\alpha}\right) \quad (1\text{-}69)$$

$$A_n^{(i)} = -\frac{1}{\Delta}\left[\Delta_1 a_n^{(i)} + \Delta_2 \gamma_n^{(i)}\right] \quad (1\text{-}70)$$

$$a_n^{(i)} = (2n+1)\, i^n \int_0^\infty \frac{K\,dK}{\nu} P_n\left(\frac{i\nu}{k_\alpha}\right) B^{(i)}(K) \qquad (1\text{-}71)$$

$$B^{(i)}(K) = \frac{e^{-\nu h}}{F(K)} \left[-\tilde{F}(K)\alpha^{(i-1)}(\nu) e^{-\nu h} + 4K^2\nu(2K^2-k_\beta^2)\gamma^{(i-1)}(\nu') e^{-\nu' h} \right] \qquad (1\text{-}72)$$

and similarly for the other expressions.

The term $\alpha^{(2)}(\nu)$ already involves a double integration that corresponds to a repeated Legendre transformation of the reflection coefficients. This integration cannot be carried out analytically, and furthermore the numerical techniques involve larger errors than in the case where a single integration is performed. We will not use the iterative procedure for computations, but to further develop the theory.

The iterative set of steps suggests the known method to solve functional equations. Since we are dealing with integral operators, it is possible to reduce the iterative scheme to an integral equation, in fact to a system of two linear integral equations.

The quantities to be found are $X(\nu) = \sum_{i=1}^{\infty} \alpha^{(i)}(\nu)$ and $Y(\nu') = k_\beta \sum_{i=1}^{\infty} \gamma^{(i)}(\nu')$. The definition of $\gamma^{(i)}(\nu')$ makes $k_\beta \gamma^{(i)}(\nu')$ dimensionless (see under equation (1-55). These two terms can be considered to be the magnitude of the corrections to the expressions for the point source,

to allow for the presence of the cavity; the word "magnitude" should be interpreted in the sense of equations (I-66) and (I-67). Summation over the index "i", in equations (I-69) to (I-72) and elimination of $\sum_i A^{(i)}$, $\sum_i a_n^{(i)}$, $\sum_i B^{(i)}(\kappa)$, and the like, will render the following system of integral equations with unknowns $X(\nu)$ and $Y(\nu')$.

$$X(\nu) = -\int_0^\infty \frac{\xi\, d\xi}{\mu}\left[\frac{1}{i K_\alpha}\sum_{n=0}^\infty (2n+1)\frac{\Delta_{1,n}}{\Delta_n} P_n\left(\frac{i\nu}{K_\alpha}\right) P_n\left(\frac{i\mu}{K_\alpha}\right)\right]\left\{-F(\xi)[1+X(\mu)]e^{-\mu h} + \right. \tag{I-73}$$

$$\left. + 4\xi^2\mu(2\xi^2-\kappa_\beta^2)\frac{Y(\mu')}{K_\beta} e^{-\mu' h}\right\}\frac{e^{-\mu h}}{F(\xi)} + \int_0^\infty \frac{\xi^2 d\xi}{\mu'}\left[\frac{1}{K_\alpha}\sum_{n=0}^\infty \frac{2n+1}{n(n+1)}\frac{\Delta_{2n}}{\Delta_n} P_n\left(\frac{i\nu}{K_\alpha}\right) P_n^{(1)}\left(\frac{i\mu'}{K_\beta}\right)\right]\cdot$$

$$\cdot\left\{4\mu'(2\xi^2-\kappa_\beta^2)[1+X(\mu)]e^{-\mu h} - \tilde{F}(\xi)\frac{Y(\mu')}{K_\beta} e^{-\mu' h}\right\}\frac{e^{-\mu' h}}{F(\xi)}$$

$$Y(\nu') = \int_0^\infty \frac{\xi\, d\xi}{\mu}\left[\frac{1}{K_\beta}\sum_{n=0}^\infty (2n+1) P_n\left(\frac{i\nu'}{K_\beta}\right)\sum_{j=0}^\infty (2n+4j+3)\frac{\Delta_{3,n+2j+1}}{\Delta_{n+2j+1}} P_{n+2j+1}\left(\frac{i\mu}{K_\alpha}\right)\right]\cdot \tag{I-74}$$

$$\cdot\left\{-\tilde{F}(\xi)[1+X(\mu)]e^{\mu h} + 4\xi^2\mu(2\xi^2-\kappa_\beta^2)\frac{Y(\mu')}{K_\beta} e^{-\mu' h}\right\}\frac{e^{-\mu h}}{F(\xi)} +$$

$$+ \int_0^\infty \frac{\xi^2 d\xi}{\mu'}\left[\frac{1}{i K_\beta}\sum_{n=0}^\infty (2n+1) P_n\left(\frac{i\nu'}{K_\beta}\right)\sum_{j=0}^\infty \frac{2n+4j+3}{(n+2j+1)(n+2j+2)}\frac{\Delta_{4,n+2j+1}}{\Delta_{n+2j+1}} P_{n+2j+1}^{(1)}\left(\frac{i\mu'}{K_\beta}\right)\right]\cdot$$

$$\cdot\left\{4\mu'(2\xi^2-\kappa_\beta^2)[1+X(\mu)]e^{-\mu h} - \tilde{F}(\xi)\frac{Y(\mu')}{K_\beta} e^{-\mu' h}\right\}\frac{e^{-\mu' h}}{F(\xi)}$$

where $\mu = \sqrt{\xi^2 - \kappa_\alpha^2}$, $\mu' = \sqrt{\xi^2 - \kappa_\beta^2}$.

The algebra of this system is very complex, but after a careful inspection of the integrands we can find out two of its properties. First: the kernels are products of two terms, one depending only upon the radius of the cavity, and the other only upon the depth. The intensity of the "correction terms" $X(\nu)$ and $Y(\nu')$, are given as integrals, each of them being the sum of three terms, one depending upon the point source (relative intensity 1) and the other two upon $X(\mu)$ and $Y(\mu')$ respectively. The kernels act as composite reflection coefficients because they consist of two factors, one being the known reflection coefficient of cylindrical waves at the plane surface, and the other can be regarded as reflection coefficient for cylindrical waves at the spherical surface. The way they intervene in the generation of the fields will be understood more clearly farther on when we decompose the integral equations into a set of linear equations. Second: by inspection we can realize that the unknowns can be expanded into series of orthogonal functions in the following way:

$$X(\nu) = \sum_{n=0}^{\infty} X_n P_n\left(\frac{i\nu}{\kappa_\alpha}\right) \qquad (1\text{-}75)$$

$$Y(\nu') = \sum_{n=0}^{\infty} Y_n P_n\left(\frac{i\nu'}{\kappa_\beta}\right) \qquad (1\text{-}76)$$

This very simple property enables us to replace the system of integral equations by a convenient set of linear equations and proceed to solve them by the numerical methods available in linear algebra.

Before doing the decomposition in orthogonal functions it is useful to render the system dimensionless, by the substitution $\kappa = \kappa_\alpha u$ inside the integrals. We obtain:

$$X(\nu) = -\int_0^\infty \frac{u\,du}{\sigma}\,\frac{1}{i}\sum_{n=0}^{\infty}(2n+1)\,\delta_n^1\,P_n\!\left(\frac{i\nu}{\kappa_\alpha}\right)P_n(i\sigma)\left\{-\tilde{F}(u)[1+X(\sigma)]e^{-\sigma\alpha}+\right.$$
$$\left.+\frac{4}{\sqrt{3}}u^2\sigma(2u^2-3)\,Y(\sigma')e^{-\sigma'\alpha}\right\}\frac{e^{-\sigma\alpha}}{F(u)} + \int_0^\infty \frac{u^2\,du}{\sigma'}\sum_{n=0}^{\infty}\frac{2n+1}{n(n+1)}\,\delta_n^2\,P_n\!\left(\frac{i\nu}{\kappa_\alpha}\right)P_n^{(1)}\!\left(\frac{i\sigma'}{\sqrt{3}}\right)\cdot$$
$$\cdot\left\{4\sigma'(2u^2-3)[1+X(\sigma)]e^{-\sigma\alpha} - \frac{\tilde{F}(u)}{\sqrt{3}}\,Y(\sigma')e^{-\sigma'\alpha}\right\}\frac{e^{-\sigma'\alpha}}{F(u)} \qquad (1\text{-}77)$$

$$Y(\nu') = \int_0^\infty \frac{u\,du}{\sigma}\,\frac{1}{\sqrt{3}}\sum_{n=0}^{\infty}(2n+1)\,P_n\!\left(\frac{i\nu'}{\kappa_\beta}\right)\sum_{j=0}^{\infty}(2n+4j+3)\,\delta_{n+2j+1}^3\,P_{n+2j+1}(i\sigma)\cdot$$
$$\cdot\left\{-\tilde{F}(u)[1+X(\sigma)]e^{-\sigma\alpha}+\frac{4}{\sqrt{3}}u^2\sigma(2u^2-3)\,Y(\sigma')e^{-\sigma'\alpha}\right\}\frac{e^{-\sigma\alpha}}{F(u)} +$$
$$+\int_0^\infty \frac{u^2\,du}{\sigma'}\,\frac{1}{i\sqrt{3}}\sum_{n=0}^{\infty}(2n+1)\,P_n\!\left(\frac{i\nu'}{\kappa_\beta}\right)\sum_{j=0}^{\infty}\frac{2n+4j+3}{(n+2j+1)(n+2j+2)}\,\delta_{n+2j+1}^4\,P_{n+2j+1}^{(1)}\!\left(\frac{i\sigma'}{\sqrt{3}}\right)\cdot \qquad (1\text{-}78)$$
$$\cdot\left\{4\sigma'(2u^2-3)[1+X(\sigma)]e^{-\sigma\alpha} - \frac{\tilde{F}(u)}{\sqrt{3}}\,Y(\sigma')e^{-\sigma'\alpha}\right\}\frac{e^{-\sigma'\alpha}}{F(u)}$$

Here $\delta_n^i = \frac{\Delta_{in}}{\Delta_n}$; $\sigma = \sqrt{u^2-1}$; $\sigma' = \sqrt{u^2-3}$.

Now we use formulae (1-75) and (1-76) together with the equivalent ones: $X(\sigma) = \sum_m X_m P_m(i\sigma)$, $Y(\sigma') = \sum_m Y_m P_m\!\left(\frac{i\sigma'}{\sqrt{3}}\right)$

. Their substitution in (1-77) and (1-78), the interchange of summations and integration, plus the

identification of the coefficients of the Legendre Polynomials of equal degree on both sides, leads to the linear system:

$$X_n = \delta_n' \left\{ a_{on} + \sum_m X_m a_{mn} + \sum_m Y_m b_{mn} \right\} + \delta_n^2 \left\{ c_{on} + \sum_m X_m c_{mn} + \sum_m Y_m d_{mn} \right\} \quad (1-79)$$

$$Y_n = \frac{2n+1}{i\sqrt{3}} \sum_{j=0}^{\infty} \left\{ \delta^3_{n+2j+1} \left[a_{o.\,n+2j+1} + \sum_m X_m a_{m.\,n+2j+1} + \sum_m Y_m b_{m.\,n+2j+1} \right] + \right.$$
$$\left. + \delta^4_{n+2j+1} \left[c_{o.\,n+2j+1} + \sum_m X_m c_{m.\,n+2j+1} + \sum_m Y_m d_{m.\,n+2j+1} \right] \right\} \quad (1-80)$$

Before the system can be solved, we should know the numerical value of the following integrals:

$$a_{mn} = -(2n+1)i \int_o^{\infty} \frac{u\,du}{\sigma} P_n(i\sigma) P_m(i\sigma) \frac{\tilde{F}(u)}{F(u)} e^{-2\sigma\alpha} \quad (1-81)$$

$$b_{mn} = \frac{4}{\sqrt{3}} (2n+1)i \int_o^{\infty} u^3 du\, P_n(i\sigma) P_m\left(\frac{i\sigma'}{\sqrt{3}}\right) \frac{2u^2-3}{F(u)} e^{-(\sigma+\sigma')\alpha} \quad (1-82)$$

$$c_{mn} = 4 \frac{2n+1}{n(n+1)} \int_o^{\infty} u^2 du\, P_n^{(1)}\left(\frac{i\sigma'}{\sqrt{3}}\right) P_m(i\sigma) \frac{2u^2-3}{F(u)} e^{-(\sigma+\sigma')\alpha} \quad (1-83)$$

$$d_{mn} = -\frac{1}{\sqrt{3}} \frac{2n+1}{n(n+1)} \int_o^{\infty} \frac{u^2 du}{\sigma'} P_n^{(1)}\left(\frac{i\sigma'}{\sqrt{3}}\right) P_m\left(\frac{i\sigma'}{\sqrt{3}}\right) \frac{\tilde{F}(u)}{F(u)} e^{-2\sigma'\alpha} \quad (1-84)$$

They are discussed in detail, including the numerical technique to evaluate them, in Appendix I-3.

The system (I-79), (I-80) expresses conditions in the n -space, which is associated with the representation of the field in spherical waves. There is duality between this discrete representation and the continuous representation in the k-space, which is associated with the cylindrical coordinates. The system of linear equations (I-79), (I-80) is the dual of the integral equations (I-73), (I-74); n is the dual of the wave number k; the reflection coefficient for spherical waves on the sphere δ_n^i are dual of the quantities

$$K_1(\nu, \mu, a) = \sum_{\eta} (2n+1)\delta_n' P_n\left(\frac{i\nu}{k_\alpha}\right) P_n\left(\frac{i\mu}{k_\alpha}\right)$$

and the like, which can be interpreted as reflection coefficients for cylindrical waves impinging on the sphere; and $\frac{\tilde{F}(k)}{F(k)} e^{-2\nu h}$ and the other reflection coefficients for cylindrical waves incident on the plane surface are the dual of the a_{mn}, b_{mn}, c_{mn}, d_{mn} , the reflection coefficients of spherical waves hitting the plane; and finally the intensities of the spherical waves X_n and Y_n are dual of the correction terms $X(\nu)$ and $Y(\nu')$. The different reflection coefficients come in groups of four each. They correspond to incident compressional or shear wave fields that are reflected as compressional or shear fields.

The physical interpretations of the system of linear equations (I-79), (I-80), can be given in terms of the

quantities X_n and Y_n, which represent the intensities of a multipole radiation of order "n", such as $h_n^{(1)}(k_a R) \cdot P_n(\cos\theta)$, that goes away from the walls of the cavity. They are related through the reflection coefficients δ_n^i, $(i=1,4)$, and a_{mn}, b_{mn}, etc., for spherical waves incident upon the sphere and the plane surface respectively. It is convenient to observe here, that while δ_n^i depends only upon n, a_{mn} and the like depend upon two indices to account for the fact that a spherical wave hitting the plane surface, which doesn't have the same geometry, suffers mode conversion. We will separate the field into a "primary field", the one originated by the explosion, and a "secondary field" due to later reflections from the surface of the cavity. The linear equations express an equilibrium condition. The n^{th}-component of the secondary radiation is in equilibrium not only with the primary field reflected at the plane surface, a_{on} and c_{on}, but also with all the reflected secondary fields such as $X_m a_{mn}$ and the like. The summation over the index j in the equations for Y_n, is due to the more complex mode conversion of the shear potentials (see equation (1-4). From the discussion above we can conclude that the linear equations express a condition at the cavity, due to the fields that come reflected from the plane surface.

By duality we can say that the integral equations

(I-73), (I-74) express a condition at the plane surface due to the fields that come reflected from the surface of the sphere. To state more precisely the sense of this interpretation we recall the reflection coefficients at the sphere for cylindrical waves. We define

$$K_1(\nu,\mu,a) = \sum_n (2n+1)\,\delta_n'\,P_n\left(\frac{i\nu}{\kappa_\alpha}\right)P_n\left(\frac{i\mu}{\kappa_\alpha}\right) \quad ;$$

and similar functions are introduced to denote the other three sums within the integral sign in the integral equations. The quantities $\frac{\hat{F}(\kappa)}{F(\kappa)}\,e^{-2\nu h}$ and the other three alike, are the known generalized reflection coefficients for cylindrical waves incident upon the plane surface. The wave number "k" is related to the angular parameter for oblique incidence upon the free surface. Integration over k accounts for all the possible directions of approach of the cylindrical waves. The intensity $X(\nu)$ of the component of the secondary compressional field in the direction determined by $\nu=\sqrt{\kappa^2-\kappa_\alpha^2}$ (real or complex), is given in equation (I-73) in function of the components in all directions of the primary and secondary fields that are reflected from the cavity in the direction given by ν .

A schematic representation of these dual processes, is given in figure I-3.

There is another feature to be noticed. The system of integral equations (I-73), (I-74) is exact, not being

subjected to previous approximations. It contains all the physical events, in particular the long and short wave fields. Thus it should contain the high frequency approximation of surface waves as given in the geometric optics theory developed by Keller (1960). The denominator Δ_n, given in Appendix 1-3, is the dual of the Rayleigh denominator F(k), and it is connected with surface waves existing at the surface of the cavity, as shown by Yanovskaya (1958) in the work on surface waves in a sphere. The term coming from the complex rays creeping around the sphere in Keller's theory, can be found by isolating the contribution of the pole in $\frac{1}{\Delta_n}$ when solving the integral equations (1-73), (1-74) for $X(\nu)$ and $Y(\nu')$.

Finally, we come back to the system of integral equations (1-73), (1-74) to state some of its mathematical properties. It is a system of Fredholm integral equations of the second kind, not self-adjoint. But the kernels

happen to be "polar", and it is possible to use the Hilbert-Schmidt theory to develop the solutions in terms of orthogonal functions. This is a property enjoyed by symmetric and polar kernels. (Courant and Hilbert, 1953). The integral equations are singular, both due to the infinite range of integration and to the singularities in the kernels.

THE SURFACE DISPLACEMENTS

To obtain the Rayleigh wave part of the spectra of the displacements in the expressions (I-64) and (I-65) we follow Ewing, et al, (1957) and replace $2J_p(kr)$ by $H_p^1(kr)+H_p^2(kr)$ and integrate in the complex plane deforming the contours, as shown in Figure I-4, to obtain convergent integrals. The surface wave displacements are due to the residue at the Rayleigh pole.

$$u_r = -\pi i \, \mathcal{A}(\omega) \frac{\kappa^2}{F'(\kappa)} \left\{ 4k_\beta^2 \nu_R' [1+\alpha(\nu_R)] e^{-\nu_R h} - 2k_\beta^2 (2\kappa^2 - k_\beta^2) \gamma(\nu_R') e^{-\nu_R' h} \right\} H_1^{(2)}(\kappa r) \quad \text{(I-85)}$$

$$u_z = -\pi i \, \mathcal{A}(\omega) \frac{\kappa}{F'(\kappa)} \left\{ -2k_\beta^2 (2\kappa^2 - k_\beta^2) [1+\alpha(\nu_R)] e^{-\nu_R h} + 4k_\beta^2 \kappa^2 \nu_R \gamma(\nu_R') e^{-\nu_R' h} \right\} H_0^{(2)}(\kappa r) \quad \text{(I-86)}$$

where $\nu_R = \sqrt{\kappa^2 - k_\alpha^2}$; $\nu_R' = \sqrt{\kappa^2 - k_\beta^2}$ and κ is the Rayleigh pole.

We should note here that the leading terms in $\alpha(\nu_R)$ and $\gamma(\nu_R')$ are small as $k_\alpha a \to 0$. When $k_\alpha a \to 0$, the solution converges to the one for the buried point source in the half-space.

To facilitate the numerical evaluation of the expressions above, it is convenient to transform them to a dimensionless form. We use the fact that the Rayleigh pole $\kappa = \gamma k_\beta$, where $\gamma = \frac{1}{2}\sqrt{3+\sqrt{3}} = 1.087664$.

Then $\nu_R = k_\alpha\sqrt{\gamma^2-\frac{1}{3}}$; $\nu_R' = k_\beta\sqrt{\gamma^2-1}$; $F'(\kappa) = -\frac{8\gamma}{\sqrt{3}}k_\beta^3$.

The dimensionless form of the displacements is given by:

$$u_r = \pi i\, \mathcal{A}(\omega) k_\beta^2 \frac{\gamma\sqrt{3}}{4}\left\{2\sqrt{\gamma^2-1}\left[1+\alpha(\nu_R)\right]e^{-\sqrt{\gamma^2-\frac{1}{3}}\,\alpha\sqrt{3}} - (2\gamma^2-1)k_\beta\gamma(\nu_R')e^{-\sqrt{\gamma^2-1}\,\alpha\sqrt{3}}\right\}\cdot \quad (1\text{-}87)$$

$$\cdot H_1^{(2)}(\gamma\sqrt{3}\,\alpha\frac{r}{h})$$

$$u_z = \pi i\, \mathcal{A}(\omega) k_\beta^2 \frac{\sqrt{3}}{4}\left\{-(2\gamma^2-1)\left[1+\alpha(\nu_R)\right]e^{-\sqrt{\gamma^2-\frac{1}{3}}\,\alpha\sqrt{3}} + 2\gamma^2\sqrt{\gamma^2-\frac{1}{3}}\,k_\beta\gamma(\nu_R')e^{-\sqrt{\gamma^2-1}\,\alpha\sqrt{3}}\right\}\cdot \quad (1\text{-}88)$$

$$\cdot H_0^{(2)}(\gamma\sqrt{3}\,\alpha\frac{r}{h})$$

It should be remembered here that the quantity $k_\beta\gamma(\nu_R')$ is dimensionless. The term $\mathcal{A}(\omega)$ is defined in (1-38) and is the spectrum of the source function. The quantities $u_r/(\mathcal{A}(\omega)k_\beta^2)$ and $u_z/(\mathcal{A}(\omega)k_\beta^2)$ are dimensionless.

For long ranges it is possible to use the asymptotic expressions for the Hankel functions (Ryshik and Gradstein, 1957):

$$H_p^{(2)}(z) = \sqrt{\frac{2}{\pi z}}\; e^{-i\left(z-\frac{p\pi}{2}-\frac{\pi}{4}\right)}\left[1+O(\tfrac{1}{|z|})\right]\,;\ |z|\gg p \quad (1\text{-}89)$$

The body wave part of the displacements can be obtained by evaluation of the branch line integrals over the Sommerfeld contours L_α and L_β, as described by Ewing,

et al (1957). This computation can be done also by steepest descent or stationary phase techniques (Ewing, et al, 1957). In any case, since our interest is confined to studying the effect of the cavity on the more prominent parts of the field, we will not consider the several pulses that do not exhibit a sharp character. We assume the recorder located at the free surface, and therefore, the only pulse of interest is the direct P-arrival. Evaluation of the branch line contribution over L_α, and retention of the part that is dominant in the far field, leads to

$$u_r = \frac{M_1}{r^2} e^{-ik_\alpha (r + \frac{h^2}{2r})} + \frac{N_1}{r^2} e^{-ik_\alpha (r + \frac{c_\beta h}{\sqrt{c_\alpha^2 - c_\beta^2}})} \qquad (1\text{-}90)$$

$$u_z = \frac{M_2}{r^2} e^{-ik_\alpha (r + \frac{h^2}{2r})} + \frac{N_2}{r^2} e^{-ik_\alpha (r + \frac{c_\beta h}{\sqrt{c_\alpha^2 - c_\beta^2}})} \qquad (1\text{-}91)$$

Several comparisons may be tried to examine the effect of the geometry of the medium on the propagation of waves.

In the first place, we can follow the procedure introduced by Latter, et al (1961), in relation to the decoupling theory of underground explosions. In essence, this theory shows that a tamped explosion will produce larger displacements than a similar one placed within a cavity large enough to avoid nonelastic effects (decoupled explosion). Latter, et al (1961), used a cavity in an infinite elastic medium, as a theoretical model for underground explosions. From near field measurements, they

obtained the pressure and radius of an equivalent cavity to represent the tamped explosion, and with these values they were able to compare it to the decoupled one in the far field. The introduction of a free surface changes radically the wave picture; the seismic energy is not any more confined to the P waves as in the case of the infinite space, but it separates between body and surface waves, the latter being the main feature at large distances.

We find then, that it is necessary to study two decoupling factors, one for surface and the other for body waves. The difficulty lies in the fact that we cannot use our theory to obtain the parameters of the source, from the near surface displacements. It is possible though, to estimate these values, by using the simple theory (Latter, et al, 1961), and proceed with the aid of (I-87) and (I-88) to compute the decoupling factor for surface waves, and from (I-90), (I-91) to obtain the one for body waves. The decoupling factor for surface waves, contains two factors, one depending upon the pressure and the other upon the frequency. It is independent of the distance. This factor is the same for horizontal and vertical displacements as shown at the end of this section. It is given by:

$$\frac{u}{u_h} = \frac{P}{P_h} \cdot \frac{1+\alpha(\nu_R)-\frac{2\gamma^2-1}{2\sqrt{\gamma^2-1}}K_\beta\,\gamma(\nu_R')\,e^{-(\sqrt{\gamma^2-\frac{1}{3}}+\sqrt{\gamma^2-1})\alpha\sqrt{3}}}{1+\alpha_h(\nu_R)-\frac{2\gamma^2-1}{2\sqrt{\gamma^2-1}}K_\beta\,\gamma_h(\nu_R')\,e^{-(\sqrt{\gamma^2-\frac{1}{3}}+\sqrt{\gamma^2-1})\alpha\sqrt{3}}} \qquad (I-92)$$

A second type of comparison that helps to understand the effect of the free surface, is given by the normal-

ization with respect to the displacements from a cavity in an infinite space. This can be done for both, the P and Rayleigh waves. Since the spectra of the displacements of the body waves in the infinite solid are given by:

$$u = -\frac{P(\omega)a^3}{\mu}\left(\frac{1}{R^2} + \frac{ik_\alpha}{R}\right)\cdot\frac{e^{-ik_\alpha R}}{4 - 4ik_\alpha a - 3k_\alpha^2 a^2} \qquad (1\text{-}93)$$

where $R = \sqrt{r^2 + h^2}$ and $P(\omega) = \frac{P_o}{2\pi i\omega}$, (see equation (1-38)), we find that for Rayleigh waves the normalized displacements are:

$$\frac{u_r}{u} = \frac{3}{2}\sqrt[4]{3}\sqrt{\frac{\pi\gamma k_\alpha R}{2}}\left\{2\sqrt{\gamma^2-1}\left[1+\alpha(\nu_R)\right]e^{-\sqrt{\gamma^2-\frac{1}{3}}\,\alpha\sqrt{3}} - (2\gamma^2-1)k_\beta\gamma(\nu_R')e^{-\sqrt{\gamma^2-1}\,\alpha\sqrt{3}}\right\} \qquad (1\text{-}94)$$

$$\frac{u_z}{u} = \frac{3}{2}\sqrt[4]{3}\sqrt{\frac{\pi k_\alpha R}{2\gamma}}\left\{-(2\gamma^2-1)\left[1+\alpha(\nu_R)\right]e^{-\sqrt{\gamma^2-\frac{1}{3}}\,\alpha\sqrt{3}} + 2\gamma^2\sqrt{\gamma^2-\frac{1}{3}}\,k_\beta\gamma(\nu_R')e^{-\sqrt{\gamma^2-1}\,\alpha\sqrt{3}}\right\} \qquad (1\text{-}95)$$

A third way to compare the effect of an explosion within a cavity with the point source solution which requires the same amount of energy, is to normalize the displacements, dividing the ones from a cavity in a half space by the corresponding ones from the point source in a half space. The latter can be obtained from the expressions above by letting $a \to o$ while keeping $P(\omega)a^3$ constant. The normalized values are:

$$\frac{(u_r)_{sphere}}{(u_r)_{point}} = \frac{e^{i\beta}}{1 - i\beta - 0.75\beta^2}\left\{1+\alpha(\nu_R) - \frac{2\gamma^2-1}{2\sqrt{\gamma^2-1}}\,k_\beta\gamma(\nu_R')e^{\left(\sqrt{\gamma^2-\frac{1}{3}}\,-\sqrt{\gamma^2-1}\right)\alpha\sqrt{3}}\right\} \qquad (1\text{-}96)$$

$$\frac{(u_z)_{sphere}}{(u_z)_{point}} = \frac{e^{i\beta}}{1 - i\beta - 0.75\beta^2}\left\{1+\alpha(\nu_R) - \frac{2\gamma^2\sqrt{\gamma^2-\frac{1}{3}}}{2\gamma^2-1}\,k_\beta\gamma(\nu_R')e^{\left(\sqrt{\gamma^2-\frac{1}{3}}\,-\sqrt{\gamma^2-1}\right)\alpha\sqrt{3}}\right\} \qquad (1\text{-}97)$$

Here $\beta = k_\alpha a$; $\alpha = k_\alpha h$.

They do not depend either on the source function in time, or on the distance of the receiver. The only parameters in these expressions are $k_\alpha a$ and $k_\alpha h$. The first factor, the only one hitherto considered in calculation of explosions, depends upon $k_\alpha a$. The second one is found by this theory and depends upon both, $k_\alpha a$ and $k_\alpha h$.

Since $(2\gamma^2-1)^2 - 4\gamma^2\sqrt{\gamma^2-1}\sqrt{\gamma^2-\frac{1}{3}} = 0$, we find that $\frac{2\gamma^2-1}{2\sqrt{\gamma^2-1}} = \frac{2\gamma^2\sqrt{\gamma^2-\frac{1}{3}}}{2\gamma^2-1}$, and, therefore, the second members in equations (I-96) and (I-97) are identical. The ratio of horizontal to vertical displacements is kept invariant when we pass from the point source to a spherical source, and the particles will move on an ellipse.

NUMERICAL RESULTS

The inversion of the system of equations (I-79), (I-80), was performed on the IBM 7090 computer at the Computing Center of the California Institute of Technology. Computations were carried on for several values of the cavity radius-depth ratio a/h. We chose $0.3 \leq a/h \leq 0.7$, at intervals of 0.1 ; an additional value, $a/h=0.65$, was included to provide more information. For each value of a/h, we could invert the system (I-79),(I-80), within a frequency interval that was limited by two considerations. First, the fast growth of the terms a_{mn} , b_{mn} etc. , at low frequencies, produced large round-Off errors in the inversion process. Second, the slow convergence of the exponential series for a_{mn} etc. at high frequencies, called for an increase in the number of terms of the series, beyond the capacity of the computer.

We concerned ourselves with the Rayleigh wave part of the displacements. The body wave computations are in progress, and they will be the subject of a future paper. The very low frequency Rayleigh wave displacements will also be investigated by a technique similar to Born's approximation, starting from the static displacements as initial trial.

To study the effects produced by the coupling of the cavity and the free surface upon the generation of surface waves, we made the comparisons described in the

last section.

The decoupling factor studied by Latter, et al (1961), is modified according to formula (I-92). There, following Latter's notation we labeled with an index h the terms related to the hole (the decoupled explosion), keeping unlabeled the ones referring to the tamped explosion. In order to apply this theory to the Rainier explosion, we take Latter's estimates: $a/h=0.3$ and $P/P_h = 50$. Thus, the decoupling for a cavity radius-depth ratio of 0.3 is 50. For other ratios, we have frequency dependent decoupling factors as shown in Figure I-6. A decoupling factor larger than 50 is better than the one predicted by Latter, and it is due to destructive interference of the waves. But we notice also that for a/h ratios larger than 0.6, the decoupling factor is reduced to 25 for certain frequencies, and there is a tendency towards even smaller values. For the time being we can predict a significant reduction of the decoupling factor for these cases, but we must wait for a complete picture of the behaviour at very low frequencies to give the exact amount of this effect.

The normalization with respect to a sphere in an infinite space is described by equations (I-94),(I-95). Since the ratio of the horizontal to the vertical component of the displacements of Raleigh waves is constant, and equal to $\frac{2\gamma\sqrt{\gamma^2-1}}{2\gamma^2-1}$, it is possible to consider only one of them. This normalization has the property of excluding the effect

due to the cavity alone,and therefore shows more clearly the phenomena connected to its interaction with the free surface. Unfortunately, due to the partition of seismic energy between body and surface waves that we mentioned in the previous section, the normalization becomes dependent upon the distance. From equation (I-94) we observe that it is sufficient to divide the displacements ratio by $\sqrt{\frac{R}{h}}$ to obtain a term that is independent of the distance. This term we present in Figure I-7. To see how much influence we may expect from the spectrum of the displacements from a cavity in an infinite space, we give it in Figure I-5; the factor containing the distance to the source is not included there. Since the spectrum is very smooth and nearly constant, we expect little influence upon the results. The normalized values in Figure I-7, show a marked dependence on the frequency, with holes that correspond to the large decoupling factors, and peaks that tend to increase the coupling.

Finally, it is interesting to examine the normalization of the surface wave displacements to the equivalent ones for the point source in a half space. Figures (I-8), (I-9) and (I-12) give the amplitude ratios, and (I-10),(I-11) give the phase differences. In this case the normalization is independent of the distance, and furthermore the passage to the limit when $a/h \to 0$ is simple. For instance, a small size cavity ($a/h = 0.3$), doesn't differ very much

from the point source, except at high frequencies (see Figure I-8). The changes begin to be noticed at $a/h=0.4$.

Since by this normalization we are eliminating the effect caused by the plane surface alone, after observing the similarity of Figures I-7 and I-9, we can say that the prominent features observed in the spectral ratios are due to the interaction of the two boundaries, and not to either of them separately.

In Figures (I-8),(I-9), we have used two dimensionless frequencies, in order to observe if some of the peaks or holes in the spectral ratios were mainly dependent upon either the cavity radius or the depth. What we obtained with this change of representation in the horizontal scale, was a better picture of the transition from one value of a/h to the next. Thus, the peaks near $k_\alpha a=0.68$, in Figure I-9, are shifted orderly with increasing a/h values, while in Figure I-8 this doesn't happen.

The phase is represented in degrees in Figures I-10 and I-11. It can be seen that when $a/h \to 0$, the phase difference between the point source and the spherical source goes to zero. The maxima and minima in the amplitude spectra correspond to the inflection points in the phase spectra.

In Figure I-12 we attempt to show the way the amplitude spectrum behaves for a constant frequency, when the ratio a/h is changed. The significant fact is that for

small values of a/h , the curves are almost flat and show that the spectral ratio is almost insensitive to variations in a/h , particularly for the lower frequencies.

CONCLUSIONS

By using the relationships to transform wave functions between cylindrical and spherical coordinates, in conjunction with Schwarz's technique to solve boundary value problems, we have been able to obtain a solution for an elastodynamic system with mixed boundaries, that is connected to the theory of underground explosions.

The analysis of the problem in the wave number space, leads to a dual mathematical formalism in terms of elementary waves in both systems of coordinates. These elementary waves are in dynamic equilibrium with similar ones. The equilibrium conditions are expressed either by a system of two integral equations (I-73), (I-74), or by an infinite set of linear equations, (I-79),(I-80).

Application of the results to decoupling theory, shows that for a large cavity radius-depth ratio, the decoupling factor may be significantly reduced for some frequencies.

The transition to the limiting cases is simple only in the case of the point source in a half space. This limit is obtained by letting the radius of the cavity go to zero independently of the other parameters. When the frequency is very small, the limiting case is the static field of displacements. This limit is not obvious.

PART II

PRECISION DETERMINATION OF FOCAL DEPTHS AND EPICENTERS OF EARTHQUAKES

INTRODUCTION

The problem of precision location of the hypocenter of earthquakes is becoming increasingly important. It is greatly simplified by the use of electronic computers, which make it possible to undertake rapid computation of large amounts of data, and repeat the computation for different values of the parameters involved.

Some results which may be obtained with computer techniques are:

a) Accurate determination of epicenter and depth of earthquakes, and elimination of some earthquakes from suspicion as explosions, by using focal depths as criteria.

b) More insight into the study of the earthquake mechanism by providing the distribution of the aftershocks in three dimensions.

c) Construction of accurate travel time curves for regions with uniform crust, when sufficient direct arrival data are available to determine precise hypocenters. This requires several stations (possibly temporary ones) within 150 km of the epicenter, as indicated in Figure II - 1.

d) Investigation of crustal structure in rugged regions, by interpretation of systematic deviations of travel time data.

We present an initial study of these problems specially for local shocks in California. Both the introduction of variable travel times and the use of several

crustal phases contribute to greater accuracy in depth determination in a program written for an IBM 7094 computer.

ON THE METHOD OF LEAST SQUARES

For a long time the method of least squares, as described by Jeffreys (1959), has been used to determine a "best" solution for the hypocenter of earthquakes. An initial trial for the focus is changed in such a way as to minimize the deviations of the actual time to the stations from the ones given in the tables. The deviations are called "residuals".

The changes can be obtained after forming the usual set of normal equations. The solution of the normal equation can be written in matrix notation (Bolt, 1960):

$$\begin{bmatrix} \Delta\lambda \\ \Delta\varphi \\ \Delta h \\ \Delta t_o \end{bmatrix} = \begin{bmatrix} A_1 & A_2 & \cdots & A_n \\ B_1 & B_2 & \cdots & B_n \\ C_1 & C_2 & \cdots & C_n \\ D_1 & D_2 & \cdots & D_n \end{bmatrix} \cdot \begin{bmatrix} \delta t_1 \\ \delta t_2 \\ \vdots \\ \delta t_n \end{bmatrix} \qquad (11\text{-}1)$$

where $\Delta\lambda$, $\Delta\varphi$, Δh, Δt_o, are the changes in longitude, latitude, depth and origin time, to be made in the guess. The large matrix is a function of the slopes of the travel time curves at the several distances between the epicenter and each of the stations, and δt_i is the residual at the i^{th} station.

From equation (1) we see that if the travel-times are linear, one iteration is sufficient, since the matrix

depends on the slopes, which are constants. The travel times do not deviate much from linearity except near the origin, and we can expect a fast convergence if the data are consistent, that is, if there exists a solution for which all the residuals vanish or become very small. This occurs when the travel times are very close to the true ones, and one can read accurately the arrival times of the phases. This ideal situation is not the case in practice because of errors in reading times due to the time corrections in the records, low signal to noise ratio, misidentification of the phases, etc. Thus, the case of an exact solution is unlikely and seismologists look for a minimization of the sum of the squares of the residuals. In applying the criteria of least squares we should be careful to avoid wrong "best" solutions due to systematic deviation of the true travel times from the ones that are used. For example, a thicker crust to the west of an epicenter, if not accounted for in the travel times, may result in a shift of the solution toward the east. To decrease the influence of systematic errors of this kind it is advisable to weight the stations not only on account of the quality of their instrumentation, but also according to the accuracy of that portion of the travel time curves corresponding to them. Thus, in local shocks the heaviest weights should be assigned to the stations observing the direct arrival, which is not affected by crustal thicknesses.

We noticed that in doing the weighting, the convergence to a solution is accompanied by a considerable decrease in the residuals of the stations with larger weights, together with a slower rate of decrease of the other residuals. Once the former ones decrease beyond a certain limit, the subsequent changes are determined by the latter; this effect leads to instability in a few cases.

It follows from equation (II-1) that if we want to obtain the probability distribution of the four unknowns on the left-hand side, it is necessary to know the distribution of each of the residuals and also the uncertainties in the travel times, or more precisely, in their slopes which enter into the elements of the large matrix. The problems involved in the estimation of these uncertainties will be discussed in a later paragraph.

The solution (II-1) of the system of normal equations assumes that the unknowns are normally distributed around means equal to the values the solution takes. This supposition is plausible for the coordinates of the epicenter and the origin time, but not for the depth. The reason for this is that a normal distribution for the depth will always give a finite probability for the focus being above the free surface. In fact, on repeated occasions researchers have found that the application of the least squares method gave them negative depths. We know "a priori" that the probability of a shock being

above the surface is zero. The sample space is the positive real axis and the frequency distribution should be skew symmetric. In order to continue using the least squares technique, we need to introduce instead of the depth "h", a new variable "μ" to be determined from the normal equations and such that: (a) $h = h(\mu) > o$, when $-\infty < \mu < \infty$; (b) the transformation $h = h(\mu)$ be one-one; (c) the distribution of μ be normal. The simplest way to achieve the three conditions above is to use the transformation $h = e^{\mu}$. The depth "h" then has a lognormal distribution. Its properties can be found in most texts in statistics. If $\bar{\mu}$ and σ_{μ} are the mean and standard deviation of μ , then $\bar{h} = e^{\bar{\mu}+\frac{1}{2}\sigma_{\mu}^2}$ and $\sigma_h = \bar{h}\cdot(e^{\sigma_{\mu}^2}-1)^{1/2}$. The changes to be made in the normal equations are few and simple: the quantity $\frac{\partial t}{\partial h}$ is to be replaced by $h\cdot\frac{\partial t}{\partial h}$ everywhere, and the depth for a new iteration is equal to current depth times $e^{\Delta\mu}$, where $\Delta\mu$ is the correction to μ just computed. The computation of depth thus becomes more rational without losing in simplicity. When $\sigma_{\mu} << \bar{\mu}$ the lognormal distribution approaches the normal. Other attempts to attack the problem by the techniques of linear programing are considerably more involved and arbitrary.

The accuracy and stability of the solutions are very difficult to study theoretically. However, it is rather easy to check some specific examples. This we did in three ways: (a) By direct confrontation with the data of

explosions. The discrepancies in depth for the Corona and Victorville explosions (Press, 1960) were 1 km and 3 km respectively. The corresponding errors in epicenters were 1.5 km and 2.7 km. (b) By selecting well recorded earthquakes (with seven or more stations within the range of the direct wave) and comparing the very accurate hypocenters thus determined with the ones obtained by using a uniform crustal model and raw data from distant stations only. This error in estimate is due to crustal variations and shows how important it is to correct for these variations, if accurate focal depths are desired. Some examples of this effect are shown in table No. II-1. (c) By studying the change in focus, when a unit change was made in the arrival time of each of the stations, in such a sense (plus or minus) as to produce the maximum deviation in the corrections $\Delta\lambda$, $\Delta\varphi$, Δh, or Δt_o. For the main Kern County earthquake, with a net of twelve stations, a variation of .1 sec at each produced the following results: $dh = 1.28$ km, $d\lambda = 2.7$ km and $d\varphi = 1.1$ km.

The geometry of the distribution of the stations around the epicenter also plays an important role in the confidence we may have in a given determination (Flynn, 1964). It is obvious that the best epicentral location will be that in which the stations are evenly distributed in azimuth. We can also have a good control with sufficient near stations, even if the distribution is not optimal.

As Nordquist (1962) pointed out, the precision in depth will depend on the type of wave recorded. For instance, if we have only P_2 arrivals there is no control upon depth, because a variation in depth will be compensated by a shift in origin time. If P_2 and P_n are present, there is some control, but very little. The depth can be tied down with more certainty only when the direct wave is present. In any case, due to the properties of the rays, the uncertainty is not complete. The P_2 arrivals are first within a range which depends upon the depth (see Figure II - 1). For a fixed distance, an increase in the focal depth will allow the direct wave to arrive first. Similar considerations hold for P_n and P_1.

DESCRIPTION OF THE COMPUTER PROGRAMS

In the Caltech Seismological Laboratory at Pasadena there are several programs with different degrees of sophistication, which provide determinations of hypocenters. One, written by Mr. John M. Nordquist for the Bendix G-15 computer, is designed specifically for local shocks (Nordquist, 1962). It has been extended by Mr. John K. Gardner to an IBM 7094 computer (Gardner, 1964). Another, written by Mr. Saul Shragowitz for teleseisms, has been adapted by the author to compute local shocks as well. The latter, also written for the Bendix G-15 computer, has been taken as basis for a more complete IBM 7094 program.

In the Bendix G-15 program we included accurate direction cosines for the local network of stations, and travel time tables were calculated from Press' model for the California-Nevada region (Press, 1960). This model is composed of a two layer crust with compressional velocities 6.11 km/sec and 7.66 km/sec, and 8.11 km/sec for the mantle. The thicknesses are 25 and 26 km respectively. The input to the program consists of code numbers that identify the stations, the arrival times for each station, and an initial guess for the hypocenter.

Data for each station is printed out in the following pattern after each iteration:

CODE, Δi(km), $(t_o)i$, Pi - $\Delta i/8.11$, (Residual)i

Here Δi is the distance epicenter-station, $(t_o)i$ the origin time as seen from each station, and Pi the arrival time. Following this, the machine types out the standard deviation in time, $\sigma = (\frac{1}{n} \sum (\text{Residuals})^2)^{\frac{1}{2}}$, and then it prints the next trial:

Longitude (degrees), Latitude (degrees), Depth (km), t_o(sec)

The iterations continue until the computer is stopped manually. If fifteen stations are processed, the time per iteration is 7.5 minutes. The program gives focal depths smaller than 56 km only, which is sufficient for all the cases known in California.

The program for the IBM 7094 computer is essentially

different because of the introduction of multiregional travel times for local shocks, and has considerably more capacity, speed and flexibility. It is designed to treat teleseisms and local shocks automatically in any order. A generalized flow diagram of the program is given in Figure II - 2.

All data that are to be used permanently are stored on magnetic tape and read into the memory at execution time. Thus, we have on tape a catalog with the names and locations of the seismological stations in the world that are more frequently used, a similar catalog for the local net of stations, the P and S travel times for teleseisms, the pP-P and sS-S tables, and the crustal structure in the California-Nevada region. The content of the tape can be modified and extended periodically by means of an auxiliary program.

Several options contribute to the flexibility of the program. Weights can be assigned to each station in the input cards. We consider it more flexible to weight the stations according to the user's decisions than to follow Bolt's automatic weighting method (Bolt, 1960). The shocks are processed automatically, and for each shock the iterations continue until the variation in origin time is smaller than one tenth of a second, or until the number of iterations exceeds an upper bound given at input time. To

prevent gross errors, a tolerance test is made on the residuals to eliminate those which are evidently wrong. At input time it is possible to give an initial tolerance limit, its rate of decrease per iteration, and a lower bound; thus we can control the way we reject some stations, which proves to be helpful in obtaining a good solution. If the depth is known or it is convenient to hold it fixed, there is an option to do so. Also, the printing of intermediate iterations can be skipped, but it proved useful to have them for comparison purposes. The phases that correspond to each reading are identified and their names typed out.

For local shocks we have provided multiregional travel times that take into account the variations in the properties of the crust and the upper mantle. The times are computed internally from formulas, instead of from tables. Three P-phases and three S-phases are allowed; they are either the direct arrival, the wave refracted at the Conrad discontinuity, or the one refracted at the Moho. In order to minimize the number of data cards to be handled, the input times for the several shocks to be processed can be read with a variable format to be given at execution time. This allows us to have four stations per card when only first arrivals are reported, two stations per card when more than one P-reading is present, and one station per card if there are P and S readings.

Special features for the processing of teleseisms are P and S travel times stored in the memory of the computer as two dimensional arrays. At present we have Jeffreys' European travel times (Jeffreys, 1964), but the user can replace them by more suitable ones at execution time if desired. If a pP-P or sS-S reading is included in the input card of any station, the depth of the focus will be computed according to these readings and held fixed. To this effect the corresponding Jeffreys-Bullen tables are used. If several stations have these readings, each one is used and an average of the resulting depths is taken. As in the case of the local shocks, a variable format is also given to decrease the number of cards. If only P phases exist, it is possible to enter four stations per card. If S phases are present also, a maximum of two stations per card is allowed. Since the problem of mapping the differences in structure in the whole world is much more complex than for a small region, and still unsolved, we have provided a single correction for crustal effects. Together with the time of each station it is possible to give the thickness of the crust under it, the standard being 33 km. A contrast in velocities from 6 to 8 km/sec is assumed at the base of the crust in correcting travel times for crustal thickness.

In Appendix II - 1, we give the instructions to be followed to process shocks with this program. Appendix II-2 contains the names and functions of the subroutines

which were used.

ON THE TRAVEL TIMES FOR LOCAL SHOCKS

The program for location of local shocks is designed for use in the California-Nevada region, 32^{o} - 42^{o}N, 114^{o} - 124^{o}W. This region is divided by a grid with a spacing of $\frac{1}{2}^{o}$ in latitude and longitude. Thicknesses of the two crustal layers, the velocities of compressional and shear waves in each layer and in the underlying mantle and a time correction for thickness of the sedimentary layer at the surface are assigned at each grid point, to produce a mathematical model representing approximately the true structure of the region.

To obtain the structure between an epicenter and a station, the path joining them is divided into segments of 25 km and the crustal values at the division points are computed by bilinear interpolation among the values at the four corners of the corresponding grid cell. In Table II - 2, we give some of the crustal values between Tinemaha and Pasadena as an example.

Precise formulas allowing for variations in the velocities and thicknesses of the model in computing the arrival times of the different phases become very involved and require continuous integration along the path (Bullen, 1963), together with an extremely complex use of Fermat's principle. To simplify the computation, integration along the path was replaced by summation on segments in which

velocities and thicknesses of the layers were considered constant.

The head waves and direct waves coming from below the first discontinuity are refracted at the interfaces between layers; each one of them corresponds to a least-time ray chosen among a family of rays with similar geometry. We found it easier and faster to determine directly the least-time path in a vertical section by choosing it among several possible ones, instead of using Snell's law. We compared the times of the rays obtained by shifting the points of refraction along the interfaces in steps of 12.5 km until a true minimum was obtained. We began with the points of refraction under the station, and moved them toward the epicenter to maintain convexity of the rays and minimize computing time.

Finally, we could profit from the fact that horizontal variations are small and slowly varying, and avoid the exact treatment of lateral refraction within a layer by using instead the theory of small perturbations. If V is the average velocity and v the deviation from it at a point of the path, the travel time between two points A and B is given by:

$$t = \int_A^B \frac{ds}{V+v} \qquad (II - 2)$$

where ds is the distance element along the path. We make use of the relationships:

$$\frac{\sin\theta}{V+v} = K \qquad (II - 3)$$

$$dv = \left| \text{grad } v \right| \cdot ds \cdot \cos\theta \qquad (II - 4)$$

where θ is the angle between the direction of the path and the gradient of the velocity. After elimination of θ and ds in equations (II - 2), (II - 3) and (II - 4), we obtain

$$t = \int_A^B \frac{dv}{|\text{grad } v| \cdot (1 - K^2(V+v)^2)^{1/2}(V+v)} \qquad (II - 5)$$

To the first order in v, this expression is equal to:

$$t = \frac{\Delta}{V} - \frac{1}{V^2} \int_A^B (1 - tg^2\theta)\, v\, ds \qquad (II - 6)$$

where the angle θ has been reintroduced, and ds now is the distance element along the line connecting A and B, and Δ is the total distance. In equation (II - 6) the term with a factor 1 is the correction for the change in velocity, and the one with a factor $tg^2\theta$ is the correction for the deflection of the path from a straight line. If θ is close to 90^o, v is very small, keeping the product bounded.

Two additional corrections of a general character were included in the program. The curvature of the earth is not negligible for distances between 300 and 1000 km. The difference between horizontal distances measured at the surface of the earth and at the Mohorovicic discontinuity is $\Delta - \Delta' \approx H \frac{\Delta}{R}$, where H is the thickness of the crust and

R the radius of the earth. For Δ = 1000 km and H = 40 km. $\Delta-\Delta' \approx 7$ km, which corresponds to a time error of 0.8 sec in a Pn arrival. Since this amount is large the necessity for the correction is obvious. But the effect of ellipticity is too small to be considered in any case. We used the radius of the mean sphere to compare distances along great circles. To estimate the error so produced we may consider that the distance along a meridian is given by $\Delta' \approx a\,[1 - e \sin^2\varphi\,]\, d\varphi$, to the first order in the ellipticity e. Here a is the radius at the equator and φ the the latitude. The distance computed by the program is $\Delta = a(1 - \frac{2}{3} e) d\varphi$. If we take the end points at 32° and 42°, the difference between the two calculations is $\Delta-\Delta' \approx .12$ km.

The subroutines used for the computation of the local travel times are listed in Appendix II - 2.

A SURVEY OF CRUSTAL DATA IN THE CALIFORNIA-NEVADA REGION

The California-Nevada region is a complex one with a diversity of structural features; at the same time it is rich in problems and difficult to study. In Figure II - 3 a sketch of the Geologic Provinces is given according to Oakeshott (1955).

Much work was done in the past with different geophysical techniques, but specially relevant to the computation of theoretical arrival times is the large scale program of refraction seismology launched by the

U.S.G.S. in recent years. A resume of this work is given by Pakiser (1963). We have used the information given by the U.S.G.S. as the basis for the model described in section No.II-4,complementing it with the results of the work of other authors using explosions, earthquakes, surface wave dispersion and gravimetry.

It is necessary to remark that in spite of the large amount of information gathered, a complete and accurate crustal model has not yet been developed, the information being concentrated along certain lines which are not dense enough throughout the area. Our aim was to construct a crustal model using and not contradicting the known data, simple enough to be usable by a computer, and easy to modify in the light of new information.

As the data for the S phases is scanty, we assumed a Poisson's ratio of 0.25 and obtained the velocities from the corresponding P-phases. From the U.S.G.S. we obtained the time delay due to surface sediments, the P velocities in the first two layers and the depth of the first layer. We followed Press (1960) in assigning a thickness of 26 km for the second layer and 8.11 km/sec for the deepest compressional velocity. The criterion used to continue the model to points where no direct information was available was to keep the velocities within the same geologic province, and to reflect the topography for the depth of the first layer. A correlation by least squares between

topography and depth (where the latter was known independently) gave a trend $H = 24.5 + 2.98\ h$, where h is given in km above sea level. The scatter shown in Figure II - 4 is considerable, and it is obvious that topography is not the only parameter affecting the thickness of the crust.

The Mohave desert and the Basin and Range Provinces are the more uniform features in the region. More accurate data are available here. We took a Pn velocity close to 7.8 km/sec in the Mohave desert and 7.9 km/sec for the Basin and Range Province (Pakiser and Hill, 1963). For the Mohave desert we followed Press (1960), Roller and Healy (1963), Diment, Stewart and Roller (1963). The depths of the first layer ranged from 25 to more than 30 km, increasing to the north.

In the Great Valley we took the curve given by Eaton (1963) to estimate the time delay due to the sediments. Wherever the sediments are thick, the variation of the surface time delay is rapid, and we believe that the spacing of our grid, which otherwise is satisfactory, becomes too gross and causes an exaggerated spread of local effects. This becomes evident in the San Francisco area, where on crossing the San Andreas fault to the east, the low-velocity Franciscan Formation delays the times of the direct arrivals (Hamilton, Ryall and Berg, 1964), (Tocher, 1962). In using our grid spacing we were not able to account for the totality of the effect without perturbing the other travel

times.

Very little information was available for the Peninsular Ranges, except for surface wave data from Press (1956) and Alexander (1963). In the Pacific there is a profile by Shor (1958) complemented by dispersion data from Alexander. An 8.11 Pn velocity and a decrease in crustal thickness down to 11 km are the more important facts.

In the Imperial Valley delay times were computed from seismic data by Kovach et al. (1962).

Tables II - 3 to II - 6 show the values assigned to the crust at the nodal points of the grid.

The three compressional velocities increase with depth. Recently Press and Biehler (1964, in press) showed a velocity reversal in the Sierra Nevada. Such a structure will require a revision of our computational procedures for travel times.

To test the model we computed the travel times along some of the traverses of the U.S.G.S. For the line along the coast of California (Healy, 1963) there is some apparent disagreement. The profile San Francisco to Camp Roberts fits well within 0.3 sec for the P_2 arrival, but the direct wave is about 1 sec late with respect to the theoretical times. We believe this is due to the fact that the shot point was placed offshore from San Francisco, and thus the direct wave was transmitted partly in sediment. This is reasonable, since the line lies on the west side of the

San Andreas fault and therefore Pg has a normal velocity; moreover for the Natividad quarry explosions (Hamilton, Ryall and Berg, 1964) the agreement is very good. Something similar happens when the shot point is in Santa Monica, the delay being of the same order. The profile Santa Monica-Lake Mead (Roller and Healy, 1963) has a delay of about 1 sec for Pg and P_2. The reverse fits well the direct arrival within 0.3 sec but the refracted P_2 arrival is consistently 0.6 sec early. No correction for this delay has been attempted along the structure because the Corona and Victorville quarry blasts and the nuclear explosions showed excellent agreement with the model. Also the profile from the Nevada Test Site to Kingman (Diment et al, 1961), when corrected for the difference in the location of the explosions, gave a fit within 0.3 sec.

A test of the correction for the root of the Sierra Nevada was obtained from the observation at Tinemaha of the Corona explosion (Press, 1960). The difference with the observed travel time was 0.1 sec.

LOCATION OF EXPLOSIONS

To test the advantage of the variable travel times, we redetermined the location of some chemical and atomic explosions which were well recorded within the California-Nevada region. The Corona explosions gave an excellent fit, with very small residuals. We tested the normality of

the residuals by the Kolmogorov-Smirnov test (Hoel, 1962). This test is more adequate to our purpose than the χ^2-test, because there is no need to group the observations in numbers greater than five. We will refer to it as the KS-test. We obtained $\overline{X} = 0.04$ sec, $\sigma = 0.424$ sec, Dn = 0.10, with n = 25. As $D_n^{\alpha} = 0.27$ for $\alpha = 0.05$, the hypothesis of normality is accepted at the 5% level.

No change in location from the initial (exact) trial location was found and the residuals were small for the combined Blanca and Logan nuclear explosions. The Victorville explosion, with a small set of residuals, gave a depth oscillating between 4.9 and 5.1 km.

A different experiment was performed for the nuclear explosions Hardhat, Haymaker, and Sedan. We used the Vela-Uniform set of stations up to a distance of 1000 km. The times were not corrected for crustal structure, except for the stations within the California-Nevada region, but we had very accurate readings of later phases.

In processing the Hardhat explosion, an initially assigned depth of 15.0 km was reduced to 12.1 in two iterations. When resubmitted, an initial depth of 7.0 km was corrected to 1.3 km in 3 iterations. After the third iteration the process became unstable, in the form explained in section No. 1.

The location of the Sedan explosion was not well controlled. All the readings were first arrivals, and no

direct wave was available. The final depth became stable at 7.0 km with some residuals over 1 sec.

The Haymaker explosion had the best set of readings. Two different trials gave depths of 0.2 and 0.4 km. We attribute the goodness of the solutions to the control given by the direct wave, in spite of the absence of close stations. Several P and S phases were available at each station.

Nordquist (1962) studied the computer location of the French atomic explosion in the Sahara of May 1962. With the teleseism part of our program, we repeated the determination. We are confident that our location was done under better conditions for two reasons. First, we use the European travel times which are more adequate to the region than the standard Jeffreys-Bullen tables. Second, we used the probability distribution for depth as given in section 2. In our solution, we tried to circle the point of explosion with stations in the four quadrants, and in two different trials we obtained solutions in depth of a fraction of a kilometer.

THE KERN COUNTY SERIES OF AFTERSHOCKS

The original Bendix program, with uniform travel times, proved useful in providing accurate locations for a series of shocks under special conditions. These conditions were present in the Kern County series of aftershocks (starting

July 21, 1952). They occurred in a limited area, and the ray paths to the several stations could be considered almost constant. Moreover, the number of portable stations installed in the epicentral region was enough to locate a set of some 25 aftershocks of magnitude over 4, using data from the direct waves only.

The great majority of the aftershocks were located close to the ends of the White Wolf fault. We classified them in three groups according to their location. Group A includes those on the SW end of the fault, Group C those on the NE corner and Group B those in between.

With accurate origin times of aftershocks based on data from near stations, and the arrival times to the distant stations, we were able to determine the actual travel times for each path. The differences from the travel times for our assumed model were interpreted as being due to variations in crustal structure. These differences were also used as corrections to the arrival times of the corresponding stations for other shocks which were not so widely recorded. By applying such corrections we succeeded in getting precision depths for most of the aftershocks where at least one station received the direct wave. Figure II - 6 shows the distribution of the aftershocks in a horizontal plane with the sense of motion according to Båth and Richter (1958), and Figure II - 7 shows our depth distributions of the aftershocks in a projection over a

plane perpendicular to the strike of the White Wolf fault.

Observations of Figure II - 7 shows that the tectonic activity was mostly confined to the northwestern side of the White Wolf fault. We call this region the "active block". Almost all of the aftershocks in Figure II - 6 that are on the southeastern side of the fault trace give computed hypocenters the assumed plane of the fault. The general trend of the motion of the "active block" is upward and toward the SW, as indicated by the sequence of aftershocks worked out by Båth and Richter (1958), on the basis of first motion of P waves. In Figure II - 6 there are 29 shocks having a left-hand strike-slip motion, against 9 with a right-hand motion.

Geodetic measurements (Whitten, 1955) of relative displacements agree with this indicated trend in the horizontal component, but not in the vertical. Moreover, the main shock had the characteristic of an overthrust motion (Gutenberg, 1955). It is not clear how to reconcile the overthrust dip-slip motion of the main shock to the mechanism of the strike-slip and normal dip-slip aftershocks. A theory based on a rebound effect would explain only the difference in vertical motion.

In contrast with the dominant left-hand strike-slip motion, shocks 194, 141 and adjacent ones in Figure II - 6 have right-hand strike-slip motion. Båth and Richter

conclude that they correspond to a secondary release of energy far from the main fault, and they wonder why it is not present on the southern side too. It is clear now that we should not expect this, since our new hypocenters indicate that this showed little seismic activity.

The distribution of the aftershocks within the active block is such that in the projection shown in Figure II - 7 it is easy to observe linear trends. This suggests the possibility of several major breaks rather than one. Tentative locations for the breaks are indicated in Figure II - 7 by dashed lines.

A list of the residuals at the several stations for shocks of type A and C are given in Table II - 8.

Assuming that velocities do not change horizontally, we can interpret the residuals at Tinemaha and Haiwee in terms of a deepening of the first discontinuity by some 5 km under the Sierra Nevada. This increase should be associated with the offset point where the ray begins to emerge. A similar calculation for the residuals at Berkeley, San Francisco, and Mount Hamilton suggests that the crust is some 8 km thinner at these points. In the arrivals to Barrett a residual of -.6 sec is interpreted in terms of a 4 km thinner crust. These results have been incorporated into the crustal model for the IBM 7094 program. The correction to the model in the San Francisco area has been distributed between depth and velocity variations.

For shocks in the C location the residuals at Santa Barbara are high; this effect could be due to the presence of the upper Tertiary and Quaternary sediments in the region (Reed and Hollister, 1936). We confirmed this result in the next section.

We obtained the previous results by the introduction of a crustal correction Δt_i to the travel time of the i^{th} station. The new hypocenters gave a set of residuals that were very small, but still not zero. A further step was taken to improve the correction Δt_i, adding to it a second order parameter ξ_i in such a way as to minimize the sum of the squares of the residuals for all the processed shocks. It was found that the second order corrections ξ_i were given by the average sum of the residuals of all the shocks at the i^{th} station.

The numerical values of ξ_i were small, the largest being of the order of .1 sec. Our confidence in the analysis was thus confirmed, and we therefore concluded that no further changes in the station corrections were necessary.

SHOCKS IN THE CALIFORNIA-NEVADA REGION

In order to obtain a frequency-depth distribution of shocks in California, and prove that the introduction of variable travel times is helpful in obtaining a better set of solutions, we selected five regions where the number of near stations was sufficient to guarantee good solutions. In doing this selection we also restricted ourselves to

the period 1950-63 when the number of stations and the quality of the time signals were far superior than before. The regions are shown in Figure II - 5. To be certain of the intensity of the signals and to favor the statistical significance of the results, we selected shocks with magnitudes between 4 and 5, plus a few with magnitudes between 5 and 5.6. After selecting and processing all the earthquakes we were left with 116 which gave solutions on which we could rely. A good check on the goodness of the solutions is given by the fact that each shock was run at least three times with different initial guesses for the depth, and the best result selected.

A resume containing the residuals, magnitudes and depths in these regions is given in Tables II - 14 to II -18. At the bottom of the column for each station we give the mean and standard deviation of the set of its residuals for all of the shocks in the region. The normality of the distribution of residuals is tested by the KS test. The observed parameter Dn is smaller than the critical value $Dn^{0.5}$ in all cases, and considerably smaller for most of them, and we can accept the hypothesis of normality. The means are smaller than 0.2 sec except in a few cases such as Santa Barbara for earthquakes in region 1. The occurrence of these large deviations from the travel times indicates that improvements in the assumed structure must be made. The paths concerned are not near enough to

regions where crustal structure has been investigated. The effect of these significant deviations was minimized by placing heavy weights on stations near the epicenters.

The frequency distribution of the Kern County aftershocks with depth is given in Figure II-8. Frequency values refer to the number of shocks with depth within intervals of 1 km. It is interesting to notice the decrease in activity at about 9 to 10 km, and the presence of a maximum near the surface and another near 14 to 15 km. No shocks are observed at depths greater than 20 km. The same phenomena can be observed for the distribution of the combined regions as shown in Figure II-9. Apparently the frequency distribution shows appreciable scattering, but after introducing the uncertainties in each depth determination, we end with the smoother and more representative values shown in Figure II-10. As the probability distribution for each shock is lognormal, in introducing the uncertainties the shallower shocks spread mainly downwards but the deeper ones spread in both directions.

We performed this process numerically by running averages with triangular filters that approximate the lognormal distribution. The smoothed frequency values are given by $Gm = \sum_n a_{mn} f_n$ where f_n are the original values. We chose filter coefficients $a_{mn} = \frac{5-m}{15}$, $m=0,4$. for $n=0$; $a_{mn} = \frac{4-|m|}{12}$, $m=-1,3$. for $n=1$; and $a_{mn} = \frac{3-|m|}{9}$, $m=-2,2$. for $n>1$. The cumulative distribution is not affected greatly by this smoothing. We see that 80% of the shocks happen at

depths shallower than 6 to 7 km. Since the range of magnitudes is not sufficiently narrow, it is convenient also to investigate the distribution of energy with depth. We transformed magnitude to energies by the formula $\log_{10} E = 12 + 1.8\ M$ (Richter, 1958). The result is shown in Figure II - 11, and the smoothing by the consideration of the uncertainties in depth is given in Figure II - 12. Clearly, the energy approach stresses even more the seismic importance of the upper 7 km of the crust over the deeper regions.

It is interesting to relate these results to previous investigations on the vertical extent of faulting. Byerly and De Noyer (1958), from energy considerations and assuming a constant static displacement with depth after the faulting, find a depth of 10 km for the fault break in the San Francisco earthquake of 1906. Knopoff (1958), by applying the methods of static elasticity to the study of the energy difference before and after faulting, obtained a static displacement that decreases to zero at the bottom of the fault plane, and a fault depth of 3.2 km for the San Francisco earthquake. Chinnery (1961), using dislocation theory and a rigid body displacement along the fault plane, computed a vertical extent of faulting of less than 6 km for the San Francisco earthquake. They all assumed infinite extent of the fault in the horizontal direction.

We have noticed that in the White Wolf fault, most of the Kern County aftershocks fall near the ends of the fault trace (see Figure II - 6). This accumulation of seismic activity may be due either to concentration of stresses around these places, or to a decrease in the yielding point of the material. In any case, it is reasonable (but by no means certain) to expect a similar behavior at the lower edge of the fault plane, and an increase of seismic activity there. The frequency-depth and energy depth distributions give maximum concentration of seismicity at about 5 to 6 km. We remark here that the main Kern County shock had good control for epicenter but not for depth, due to lack of near stations. If in accordance with the fact that aftershocks in the first two days lie on the fault plane, we project the main epicenter vertically on the fault plane, we find a probable depth less than 8 km (Figure II - 7) which would tend to agree with Chinnery's computation, assuming that the San Francisco earthquake represents typical behavior of the San Andreas fault.

Chinnery's assumption of constant static displacement with depth appears less plausible than Knopoff's result, but it is difficult to compare the two approaches since they are essentially different. The reasoning followed above would reject Byerly and De Noyer's result in favor of the other two.

Nevertheless, a significant amount of shocks do occur at lower depths, and evidently they are related in some way to the surface faulting. They may represent an extension of the faults to depths of the order of 17 km, with a slower rate of stress accumulation, or a different system of breaks which are triggered by the activity above.

In Figure II - 13, we compare the normalized cumulative distributions for the five regions selected. The large deviations in some are due to the fact that, when taken alone, there are an insufficient number of data points to make good statistics.

CONCLUSIONS

The determination of epicenters and depths of local shocks in regions as rugged as California can be made with an accuracy of 2 to 3 kilometers by carefully correcting the travel times to account for major sources of errors. One of the most important corrections is for variations in crustal structure. This correction can be done automatically by computing variable travel times from a suitable crustal model. The model described in section 4, part II, fits the observed travel times accurately except in isolated basins in which the thickness of sediments is large.

Nuclear explosions in the Nevada Test Site can be accurately located by using several crustal phases. For the French nuclear explosion of May 1, 1962, we obtained a better solution than previous investigations, because we used the European travel times in the teleseism part of the program. They represent that region better than the standard Jeffreys-Bullen tables.

The Kern County series of aftershocks of 1952 occurred mostly in one active block, and the depth distribution we computed shows a maximum of seismic activity at depths smaller than five kilometers.

A study of the distribution of the California shocks with depth shows that 80% of them occur at depths shallower than 6 to 7 km. This result is further confirmed

when we analyze the distribution of energies. When this result is related to the theories about extent of faulting, we are inclined to give preference to the arguments in favor of shallow penetration of fault planes in California.

REFERENCES - PART I

Blake, F. G., Spherical wave propagation in solid media, 1952 J. Acoust. Soc. Amer., 24, 211-215.

Byatt, W. J. and G. P. De Vault, Mathematical Problems 1961 in Seismology, Research Report, Sandia Corporation, Jan.

D'Yakonov, B. P., The diffraction of electromagnetic 1959 waves by a sphere located in a halfspace, Izv. Geophys. Ser., 1579-1590.

Erdelyi, A., Zur Theorie der Kugelwellen, Physica, 4, 1937 No. 2, February.

Ewing, W. M., W. S. Jardetzky and F. Press, Elastic waves 1957 in layered media, McGraw-Hill Book Co.

Grinberg, G. A., Selected problems in the theory of 1948 electric and magnetic phenomena,

Jeffreys, H., On the cause of oscillatory movement in 1931 seismograms, MNGS, 2, 407-416.

Kane, S. The propagation of Rayleigh waves past a 1962 fluid-loaded boundary, Journal of Math. and Physics, 41, No. 3, September, 179-190.

Kane, J., and J. Spence, Rayleigh wave transmission on 1963 elastic wedges, Geophysics, 28, No. 5, 715-723.

Kantorovich, L. V., and V.I. Krylov, Approximate Methods 1958 of Higher Analysis, P. Noordhoff Ltd., The Netherlands, 681 pp.

Latter, A.L., R.E. Lelevier, E.A. Martinelli and 1961 W.G. McMillan, A method of concealing underground nuclear explosions, J. Geophys. Research, 66, No. 3, 943-946.

Pekeris, C.L., The seismic surface pulse, Proc. Nat. Acad. 1955 Sci., 41, 469-470.

Ryshik, I.M. and I.S. Gradstein, Tables of Series, 1957 Products and Integrals, Veb. Deutscher Verlag der Wissenschaften, Berlin.

Sharpe, J.A., The propagation of elastic waves by
1942 explosive pressures, Geophysics, 7, 144-154, 3
311-321.

Stratton, J.A., Electromagnetic Theory, McGraw-Hill.
1941

Van der Pol, On potential and wave functions in n
1936 dimensions, Physica,6, 385-392.

Weston, V.H., Solutions of the Helmholtz equations for
1957 a class of non-separable cylindircal and
rotation coordinate systems,

REFERENCES - PART II

Alexander, S. S., Surface wave propagation in the Western
1963 United States, Doctoral Thesis, California Institute of Technology, Pasadena.

Båth, M., and C. F. Richter, Mechanism of the aftershocks of
1958 the Kern County, California earthquake of 1952, Bull. Seism. Soc. Am., 48, 133-146.

Bolt, B. A., Earthquake Epicenters, focal depths and origin
1960 times using a high-speed computer, Geophys. Journ. 3, 433-440.

Berg, J. W., et al, Seismic investigation of crustal structure
1960 in the Eastern part of the Basin and Range Province, Bull. Seism. Soc. Am., 50, 511-536.

Bullen, K. E., Introduction to the theory of Seismology,
1963 Cambridge University Press.

Byerly, P., and J. De Noyer, Energy in earthquakes as computed
1958 from geodetic observations, in Contributions in Geophysics in Honor of Beno Gutenberg, New York, Pergamon Press, 17-35.

Cameron, J. B., Earthquakes in the Northern California coastal
1961 region, Part I, Bull. Seism. Soc. Am., 51, 203-221. Part II, Bull. Seism. Soc. Am., 51, 337-354.

Cisternas, A., Precision determination of focal depths and
1961 epicenters of local shocks in California, Bull. Seism. Soc. Am., 53, 381-388.

Chinnery, M. A., The deformation of the ground around surface
1961 faults, Bull. Seism. Soc. Am., 51, 355-372

Diment, W. H., S. W. Stewart, J. C. Roller, Crustal structure
1961 from the Nevada test site to Kingman, Arizona, from Seismic and Gravity Observations, Journ. Geophys. Res., 66, 201-

Eaton, J. P., Crustal structure from San Francisco, California,
1963 to Eureka, Nevada, from seismic refraction measurements, Journ. Geophys. Res., 68, 5789-

Gardner, J. K., Doctoral Thesis, California Institute of
1964 California, Pasadena.

Gutenberg, B., Earthquakes and structure in Southern
1943 California, Bull. Geol. Soc. Am., 54, 499-526.

Gutenberg, B., Travel times from blasts in Southern
1951 a California, Bull. Seism. Soc. Am., 41, 5-

1951 b Revised travel times in Southern California, Bull. Seism. Soc. Am., 41, 143-

1952 Waves from blasts recorded in Southern California, Trans. A. G. U., 33, 427-

1953 Travel times of longitudinal waves from surface foci, Proc. Nat. Acad. of Sciences, 39, 849-853.

1955 a Wave velocities in the earth crust, Bull. Seisms. Soc. Am., Special Paper 62, 19-34.

1955 b The first motion in longitudinal and transverse waves of the main shock and the direction of slip, Bull. Div. of Mines No. 171, 165-170.

1957 Zur frage der gebirgsqurzeln, Geologischen Rundschau Bd. 46, 30-38.

Hamilton, R. M., A. Ryall and E. Berg, Crustal structure
1964 southwest of the San Andreas Fault from quarry blasts, Bull. Seism. Soc. Am., 54, 67-78.

Healy, J. H., Crustal structure along the coast of
1963 California from seismic-refraction measurements, Journ. Geophys. Res., 68, 5777-

Herrin, E., and J. Taggart, Regional variations in Pn
1962 velocity and their effect on the location of epicenters, Bull. Seism. Soc. Am., 52, 1037-1046.

Hoel, P. G., Introduction to Mathematical Statistics,
1962 3rd Ed., J. Wiley and Sons.

Jackson, W. H., S. W. Stewart, and L. C. Pakiser, Crustal
1963 structure in Eastern Colorado from seismic refraction measurements, Journ. Geophys. Res., 68, 5767-

Jeffreys, H., The Earth, 4th Ed., Cambridge Univ. Press.
1959.

Knopoff, L., Energy released in earthquakes, Geophys. Journ.,
1958 1, 44-52.

Kovach, R. L., C. R. Allen, and F. Press, Geophysical
1962 investigations in the Colorado delta region, Journ. Geophys. Res., 67, 2845-

Nordquist, J. M., 1962 A special purpose program for earthquake location with an electronic computer, Bull. Seism. Soc. Am., 52, 431-437.

1962 A note on computer determinations of the hypocenter of the Sahara explosion of May 1, 1962, Technical Report, Seismological Laboratory, Calif. Inst. of Technology, Pasadena.

Oakeshott, G. B., 1955 The Kern County earthquakes in California's geologic history, Bull. Div. of Mines No. 171, 15-22.

Pakiser, L. C., 1963 Structure of the crust and upper mantle in the Western United States, Journ. Geophys. Res., 68, 5747-

Pakiser, L. C., D. P. Hill, 1963 Crustal structure in Nevada and Southern Idaho from nuclear explosions, Journ. Geophys. Res., 68, 5557-

Press, F., 1956 Determination of crustal structure from phase velocity of Rayleigh waves, Part I: Southern California, Bull. Geol. Soc. Am., 67, 1647-

1957 Determination of crustal structure from phase velocity of Rayleigh waves, Part II: San Francisco Bay Region, Bull. Seism. Soc. Am., 47, 87-

1956 Velocity of Lg waves in California, Trans. Am. Geophys. Union, 37, 615-

1960 Crustal structure in the California-Nevada region, Journ. Geophys. Res., 65, 1039-1051.

Press, F., and S. Biehler, 1964 Inferences on crustal velocities and densities from P-delays and gravity anomalies, Journ. Geophys. Res., (in press).

Reed, R. D., 1936 Structural evolution of Southern California, AAPG, Tulsa, Okla.

Richter, C. F., 1955 Foreshocks and aftershocks, Bull. Div. of Mines No. 171, 177-197.

1958 Elementary Seismology, Freeman, San Francisco

Roller, J. C., J. H. Healy, 1963 Seismic refraction measurements of crustal structure between Santa Monica Bay and Lake Mead, Journ. Geophys. Res., 68, 5837.

Ryall, A., D. J. Stuart, Travel times and amplitudes from
1963 explosions, Nevada test site to Ordway, Colorado, Journ. Geophys. Res., 68, 5821-

Shor, G. G., Deep reflections from Southern California
1955 blasts, Trans, Am. Geophys. Union, 36, 133-

Shor, G. G., and R. W. Raitt, Seismic studies in the
1958 Southern California borderland, S10 Reference 58-70. Marine Physical Lab., Scripps Inst. of Oceanography.

Smith, S. W., A reinterpretation of phase velocity data
1962 based on the Gnome travel times curves, Bull. Seism. Soc. Am., 52, 1031-1035.

Scheidegger, A. E., A note on the techtonics of Kern County,
1959 California as evidenced by the 1952 earthquakes, Journ. Geophys. Res., 64, 1499-1501.

Tocher, D., Travel times to short distances from Blasts in
1961 Central California, (unpublished report).

Tsuboi, Ch., Crustal structure in Northern and Middle
1956 California from gravity-pendulum data, Bull. Geol. Soc. Am., 67, 1641-

Whitten, C. A., Measurements of earth movements in
1955 California, Bull. Div. of Mines No. 171, 75-80.

TABLE CAPTIONS - Part II

Table II - 1. An example of the errors involved when no crustal corrections are applied and the direct wave is not included. (See section 2, part II).

Table II - 2. Values of crustal parameters between Tinemaha and Pasadena. The distance is measured from Tinemaha. A time correction for surface sediments, the velocities of compressional waves in the first two layers, and the thickness of the first layer are given.

Table II - 3. California-Nevada Region. P velocities in the first layer at the crossing points of the grid. The longitude and latitude are given in degrees. The velocities are in km/sec.

Table II - 4. California-Nevada Region. P velocities in the second layer at the crossing points of the grid. The longitude and latitude are given in degrees. The velocities are in km/sec.

Table II - 5. California-Nevada Region. Thickness of the first layer in km, measured from a datum at 1 km above sea level. The values are given at the crossing points of the grid. The

longitude and latitude are given in degrees.

Table II - 6. California-Nevada Region. Time delay due to near surface sediments, in seconds. The values are given at the crossing points of the grid. The longitude and latitude are given in degrees.

Table II - 7. Local shocks. Station code numbers and names; A, B and C are the geocentric direction cosines; D is the height with respect to the mean sphere. The elevation is given in km, above a datum at 1 km above sea level.

Table II - 8. Time deviations from the model with horizontal layering, due to crustal variations, for shocks in the Kern County area. Regions A and C refer to Figure II - 6.

Table II - 9. Shocks in region 1 (Figure II - 5), with the trial hypocenters.

Table II - 10. Shocks in region 2 (Figure II - 5), with the trial hypocenters.

Table II - 11. Shocks in region 3 (Figure II - 5), with the trial hypocenters.

Table II - 12. Shocks in region 4 (Figure II - 5), with the trial hypocenters.

Table II - 13. Shocks in region 6 (Figure II - 5), with the trial hypocenters.

Table II - 14. Resume of the residuals for the shocks in region 1 (Figure II - 5). The residuals are in seconds and the depths in km below datum. The five rows at the bottom give the total number of residuals, the mean residual $\bar{X}$, the standard deviation σ, the critical value of the K-S test D_n^{α}, and the actual maximum deviation D_n.

Table II - 15. Same as Table II - 14 for the shocks in region 2.

Table II - 16. Same as Table II - 14 for the shocks in region 3.

Table II - 17. Same as Table II - 14 for the shocks in region 4.

Table II - 18. Same as Table II - 14 for the shocks in region 6.

TABLE NO. II - 1

No. of shocks according to Richter (1955)	Mag.	$\Delta\lambda$ (km)	$\Delta\varphi$ (km)	Δh (km)
285	5.1	-8	-8	34
155	5.8	-6.7	-8.5	68
276	5.9	-6.7	-11.4	24

TABLE II - 2

PROFILE OF CRUSTAL MODEL BETWEEN TINEMAHA AND PASADENA

DISTANCE km	CORRECTION SEDIMENTS sec	VP1 km/sec	VP2 km/sec	H km
0	0.50	6.01	7.88	29.6
25	0.46	6.00	7.87	32.2
50	0.41	6.00	7.85	35.2
75	0.40	6.00	7.85	34.8
100	0.39	5.99	7.86	33.2
125	0.41	6.01	7.86	31.3
150	0.43	6.06	7.85	29.5
175	0.44	6.10	7.85	28.6
200	0.40	6.13	7.85	28.7
225	0.36	6.17	7.84	28.6
250	0.37	6.14	7.73	27.5
275	0.37	6.11	7.62	26.6
300	0.36	6.14	7.77	27.1
325	0.35	6.20	7.96	27.9
350	0.38	6.23	8.06	27.7
373.6	0.45	6.24	8.10	27.1

TABLE II-3

COMPRESSIONAL VELOCITIES IN THE FIRST LAYER. CALIFORNIA-NEVADA REGION.

611 611 611 611 611 611 611 611 611 611 611 611 611 611 611 611 611 611 611 611 611 611	42	
611 611 611 611 611 611 611 611 611 611 611 611 611 611 611 611 611 611 611 611 611 611		
595 595 605 620 620 620 620 610 610 610 600 600 600 600 600 600 590 590 590 590 590	41	L
595 595 605 620 630 620 620 620 610 610 610 610 600 600 600 600 590 590 590 590 590		A
595 595 605 620 630 630 620 620 620 620 620 620 620 610 610 600 590 590 590 590 590	40	T
595 595 600 610 620 620 630 620 620 620 620 620 620 620 610 610 600 590 590 600 600 600		I
600 600 600 610 610 620 630 630 620 620 620 610 610 605 605 603 590 590 600 600 600	39	T
600 610 610 610 610 610 620 620 630 610 610 610 610 605 603 603 603 606 603 600 600		U
610 610 610 610 540 600 610 610 610 630 610 610 610 605 603 603 603 603 603 600 600	38	D
610 610 610 610 600 610 610 610 610 610 610 600 600 600 605 605 603 600 600 600 600		E
610 610 610 610 610 610 610 610 610 610 600 600 590 600 605 610 610 615 610 610 610	37	
610 610 610 610 610 610 610 610 610 610 600 600 590 600 605 610 611 615 615 615 615		
611 610 610 610 610 610 610 610 610 610 610 610 605 605 605 611 611 610 615 615 615	36	D
610 610 610 610 610 610 610 610 610 610 610 610 630 611 611 610 610 610 615 615 615		F
611 610 610 610 610 610 610 610 610 610 610 610 610 610 611 611 611 611 615 615 615	35	G
610 610 610 610 610 610 610 610 610 610 610 610 630 611 611 611 611 611 615 610 610		R
610 610 610 610 610 610 610 610 610 610 610 610 630 630 620 610 610 610 610 610 610	34	E
610 610 610 610 610 610 610 610 610 610 600 600 610 620 620 610 610 610 610 610 610		F
610 610 610 610 610 610 610 620 620 620 620 610 610 610 610 610 610 610 610 610 610	33	S
610 610 610 610 610 610 610 620 620 620 620 610 610 610 610 610 610 610 610 610 610		
610 610 610 610 610 610 610 620 620 620 620 620 610 610 610 610 610 610 610 610 610	32	

124 123 122 121 120 119 118 117 116 115 114

LONGITUDE DEGREES

NOTE. THE NUMBER 611 MEANS 6.11 KM/SEC.

TABLE II-4

COMPRESSIONAL VELOCITIES IN THE SECOND LAYER. CALIFORNIA-NEVADA REGION.

790	790	790	790	790	790	790	790	790	790	790	790	793	790	790	790	790	790	790	790	790	42		
790	790	790	790	790	790	790	790	790	790	790	790	793	790	790	790	790	790	790	790	790			
800	800	800	800	800	800	800	790	790	790	790	790	790	790	790	790	790	790	790	790	790	41	L	
798	798	800	785	790	785	785	790	790	790	790	790	790	790	790	790	790	790	790	790	790		A	
798	798	790	790	785	785	785	785	790	790	790	790	790	790	790	790	790	790	790	790	790	40	T	
798	798	790	790	790	785	785	785	785	780	780	790	780	770	780	790	790	790	790	790	790		I	
800	798	790	790	790	785	785	780	780	780	800	800	800	790	790	790	790	790	790	790	790	39	T	
800	800	798	790	790	790	770	785	785	785	780	800	800	800	790	770	790	790	790	790	790		U	
800	800	790	780	780	770	780	785	785	785	785	800	800	800	790	790	790	784	790	790	790	38	D	
811	811	800	800	800	800	790	790	785	785	785	788	788	790	790	790	790	790	790	790	760		E	
810	811	811	800	800	800	800	790	790	785	785	785	790	788	788	790	790	781	790	790	790	37		
811	811	811	810	800	810	810	810	800	790	785	785	790	790	790	788	788	790	781	780	780			
811	811	811	811	810	810	810	810	800	790	785	785	785	790	790	790	790	788	790	781	780	36	D	
811	811	811	811	811	810	810	810	810	800	785	785	785	790	790	780	780	780	780	780	781		E	
811	811	811	811	811	810	810	820	820	810	790	760	760	790	780	780	780	780	780	781	781	35	G	
811	811	811	811	811	811	810	820	820	820	820	810	800	790	780	780	780	780	780	750	780		R	
811	811	811	811	811	811	811	810	810	820	820	820	810	800	800	790	780	780	780	740	780	34	E	
811	811	811	811	811	811	811	811	810	810	820	820	820	810	800	790	780	780	780	780	780		E	
811	811	811	811	811	811	811	810	810	810	820	820	820	810	800	800	790	780	790	780	780	33	S .	
811	811	811	811	811	811	810	820	820	820	820	810	810	810	800	800	790	790	780	780	780			
811	811	811	811	811	811	810	820	820	820	820	810	810	810	810	800	790	790	790	780	780	32		

124 123 122 121 120 119 118 117 116 115 114

LONGITUDE DEGREES

NOTE. THE NUMBER 790 MEANS 7.90 KM/SEC.

TABLE II-5

THICKNESSES OF THE FIRST LAYER. CALIFORNIA-NEVADA REGION.

250	250	300	270	260	270	290	290	300	300	290	280	280	280	290	290	300	290	300	310	290	42			
250	250	300	270	260	270	290	290	300	300	290	280	280	280	290	290	300	290	300	310	290				
250	250	300	270	260	270	290	290	300	300	290	280	280	280	290	290	300	290	300	310	290	41	L		
250	260	270	240	250	300	300	290	290	290	290	290	290	300	300	300	300	310	330	310	300	290		A	
240	240	290	250	250	270	290	290	290	280	290	280	310	300	300	310	300	310	310	310	300	40		T	
230	260	290	250	240	240	300	300	300	310	290	280	300	302	302	302	310	310	310	300	290			I	
210	250	250	260	240	240	270	290	305	305	290	320	300	310	300	320	310	300	310	300	290	39		T	
150	230	240	250	240	240	250	270	310	310	323	320	310	310	310	290	300	280	300	300	310			U	
150	210	240	240	240	240	240	250	290	330	300	320	290	310	300	320	300	280	290	300	310	38		D	
140	150	230	240	240	270	240	240	260	320	340	290	310	310	310	300	300	250	250	250	300			E	
130	150	180	230	230	250	250	240	240	260	310	360	320	270	290	290	290	270	270	300	270	37			
120	140	150	170	240	230	260	250	240	240	260	330	280	280	250	270	290	284	270	260	270				
130	130	140	150	190	240	230	270	250	240	240	280	300	290	290	270	270	300	284	260	290	36	D		
120	120	130	140	180	220	240	230	260	240	250	290	280	270	280	290	280	300	290	284	260		E		
110	120	120	120	150	220	230	250	280	270	260	260	270	270	260	270	270	290	280	260	284	35	G		
110	110	110	120	120	180	210	210	250	350	320	270	290	360	280	280	280	240	260	260	270		R		
110	110	110	120	130	140	180	230	240	220	200	210	290	250	280	260	290	270	260	260	250	34	E		
110	110	110	120	130	130	130	210	210	210	240	250	230	260	260	280	240	270	250	240	270		E		
110	110	110	120	120	130	130	150	210	200	230	240	220	220	250	280	250	240	250	250	270	33	S		
110	110	120	120	120	120	130	130	200	200	200	210	210	210	250	270	280	250	240	240	250				
110	110	110	120	120	120	120	120	130	190	200	210	200	200	220	280	290	240	240	250	250	32			

124 123 122 121 120 119 118 117 116 115 114

LONGITUDE DEGREES

NOTE. THE NUMBER 250 MEANS 25.0 KM.

TABLE II-6

TIME DELAYS IN THE SEDIMENTARY LAYER. CALIFORNIA-NEVADA REGION.

040 040 040 040 040 040 040 040 040 040 040 040 040 040 030 030 040 040 030 030 030	42	
040 040 040 040 040 040 040 040 040 040 040 040 040 040 030 030 040 040 030 030 030		
040 040 040 040 040 040 040 040 040 040 040 040 040 040 030 030 045 040 030 030 030	41	L
040 040 040 040 040 040 040 040 040 040 040 040 040 040 030 030 030 030 030 030 030		A
040 040 040 050 060 050 040 040 040 040 040 040 040 040 040 040 030 020 020 030 030 030	40	T
040 050 050 040 080 050 050 040 040 050 050 060 060 050 040 035 015 020 030 030 030		I
010 050 050 050 100 080 050 050 050 050 050 060 040 040 030 030 015 020 030 030 030	39	T
010 010 050 050 060 080 060 050 050 040 040 050 040 030 030 030 020 020 030 030 030		U
010 010 010 050 050 120 070 050 050 050 050 040 040 030 030 030 020 020 030 030 030	38	D
010 010 010 010 075 050 050 120 080 060 050 050 060 040 030 030 030 020 030 030 030		E
010 010 010 010 050 075 050 120 070 050 040 040 040 040 040 050 020 020 015 020 030	37	
010 010 010 010 050 050 050 050 100 070 050 040 030 040 050 040 040 030 030 030 020		
010 010 010 010 010 050 050 050 060 090 060 050 030 050 030 020 020 020 020 020 020	36	D
010 010 010 010 010 010 050 060 060 090 060 040 030 020 020 020 020 020 020 020 020		E
010 010 010 010 010 010 010 050 060 050 050 040 035 025 020 020 020 020 020 020 020	35	G
010 010 010 010 010 010 010 010 050 050 050 060 040 030 020 020 020 020 020 020 020		R
010 010 010 010 010 010 010 010 010 010 010 050 050 050 040 030 020 020 020 020 020	34	E
010 010 010 010 010 010 010 010 010 010 010 010 010 010 040 040 030 040 040 040 030		E
010 010 010 010 010 010 010 010 010 010 010 010 010 010 010 040 040 040 090 040 040	33	S
010 010 010 010 010 010 010 010 010 010 010 010 010 010 040 040 040 090 100 080 040		
010 010 010 010 010 010 010 010 010 010 010 010 010 010 030 040 090 120 120 100 040	32	

124 123 122 121 120 119 118 117 116 115 114

LONGITUDE DEGREES

NOTE. THE NUMBER 040 MEANS 0.40 SEC.

TABLE II-7

CALIFORNIA-NEVADA REGION. DIRECTION COSINES OF THE LOCAL STATIONS.

CODE	NAME	A	B	C	D KM	ELEV KM	CODE	NAME	A	B	C	D KM	ELEV KM
1	PAS	-.39154	-.73109	.55874	-0.1	-0.7	33	PRS	-.42035	-.68946	.58986	-0.8	-0.7
2	MWC	-.38972	-.73122	.55985	-0.1	0.8	34	REN	-.38447	-.67095	.63404	-2.0	0.4
3	DLT	-.38682	-.73336	.55906	-0.1	-0.5	35	FER	-.42893	-.62958	.64780	-2.4	-1.0
4	RVR	-.38203	-.73780	.55650	0.0	-0.8	36	ARC	-.42486	-.62810	.65191	-2.5	-0.9
5	BBC	-.37500	-.73873	.56004	-0.1	1.1	37	SHS	-.40729	-.64208	.64950	-2.4	-0.7
6	PVR	-.39569	-.73315	.55310	0.2	-0.7	38	MIN	-.40027	-.65105	.64492	-2.3	0.5
7	SBC	-.40967	-.71779	.56297	-0.2	-0.9	39	UKI	-.42606	-.65068	.62856	-1.9	-1.0
8	FTC	-.39730	-.71986	.56917	-0.3	0.0	40	EUR	-.33904	-.69545	.63357	-2.0	1.1
9	KRC	-.40569	-.70995	.57566	-0.5	-0.3	41	NEL	-.34192	-.73851	.58111	-0.6	0.1
10	WDY	-.39266	-.71297	.58095	-0.6	-0.5	42	BCN	-.34064	-.73609	.58493	-0.7	-0.2
11	ISA	-.38838	-.71596	.58014	-0.6	-0.2	51	CHP	-.39908	-.71961	.56824	-0.3	0.6
12	ISI	-.38822	-.71581	.58043	-0.6	-0.2	52	HAV	-.38950	-.71688	.57825	-0.6	0.0
13	CLC	-.37651	-.72029	.58260	-0.7	-0.2	53	KNO	-.38978	-.71703	.57787	-0.5	0.1
14	HAI	-.37973	-.71510	.58712	-0.8	0.1	54	WRI	-.39171	-.71810	.57524	-0.5	-0.5
15	TIN	-.37839	-.70486	.59999	-1.1	0.2	55	BDI	-.39017	-.72125	.57234	-0.4	0.3
16	FRE	-.39902	-.69683	.59599	-1.0	-0.9	56	WOI	-.39201	-.72149	.57077	-0.4	0.5
17	PLM	-.37816	-.74668	.54724	0.2	0.7	57	WWI	-.39261	-.71816	.57455	-0.5	-0.4
18	BAR	-.37856	-.75361	.53737	0.4	-0.5	58	SMI	-.38913	-.71480	.58106	-0.6	1.0
19	HAY	-.36067	-.75155	.55235	0.2	-0.5	59	WDI	-.38959	-.71803	.57676	-0.5	-0.2
20	ECC	-.36323	-.75989	.53910	0.5	-1.0	60	PRI	-.38851	-.71909	.57616	-0.5	0.2
21	SNC	-.41294	-.72918	.54568	0.3	-0.7	61	CCI	-.39191	-.71852	.57457	-0.5	-0.2
22	LJC	-.38540	-.74820	.54006	0.4	-1.0	62	KEI	-.39247	-.71558	.57785	-0.6	-0.5
26	BRK	-.42241	-.66923	.61131	-1.4	-0.9	63	PKI	-.39251	-.71604	.57725	-0.5	-0.1
27	MHC	-.41814	-.67852	.60396	-1.1	0.3	64	CC2	-.39191	-.71857	.57450	-0.5	-0.2
28	PAC	-.42404	-.67388	.60504	-1.2	-0.9	65	EKI	-.40313	-.71340	.57320	-0.4	-0.3
29	SFR	-.42523	-.66868	.60996	-1.3	-0.9	66	SEI	-.40034	-.71681	.57089	-0.4	-0.5
30	SCL	-.42171	-.67619	.60410	-1.2	-1.0	67	PRR	-.38115	-.74058	.55341	0.1	-0.5
31	SCC	-.42417	-.67890	.59932	-1.1	-0.9	68	POM	-.38586	-.73465	.55802	-0.1	-0.7
32	VIN	-.41833	-.68564	.59573	-1.0	-0.7	69	CRI	-.37946	-.73640	.56012	-0.1	0.4

TABLE II - 8

RESIDUALS DUE TO CRUSTAL VARIATIONS

STATION	FROM REGION A		FROM REGION C	
	Residual Sec.	Standard Dev. Sec.	Residual Sec.	Standard Dev. Sec.
Pasadena	.01		-.07	.11
Mt. Wilson	.03	.21	.14	.26
Dalton	.11	.31	- .02	.35
Riverside	.29	.22	- .02	.36
Big Bear	.22	.31	.02	.24
Sta. Barbara	.02	.16	1.53	.18
China Lake	.76	.19	- .15	.16
Haiwee	1.59	.29	.27	.17
Tinemaha	1.67	.32	1.76	.27
Fresno	- .38	.35	---	---
Palomar	- .29	.12	- .43	.28
Barrett	- .63	.28	- .47	.22
Berkeley	-1.47	.54	---	---
Mt. Hamilton	-1.75	.34	---	---

TABLE II-9

SHOCKS IN REGION 1. TINEMAHA

DATE	LONG DEG	LAT DEG	ORIG. TIME H	M	SEC
SEP 28 1950	-118.493	37.322	11	03	24.0
JUN 16 1951	-118.660	37.000	05	52	56.0
JUN 25 1951	-117.950	35.782	19	45	41.0
JUN 26 1951	-117.950	35.812	01	26	39.0
FEB 9 1952	-117.720	36.667	08	43	30.0
JAN 21 1955	-118.333	37.150	12	20	59.0
FEB 13 1955	-118.233	36.949	00	23	03.0
JUN 10 1955	-118.682	37.500	18	26	37.0
NOV 8 1955	-118.800	37.500	02	40	52.0
JUL 11 1956	-117.932	35.766	19	22	05.7
MAR 8 1957	-117.500	35.716	13	24	57.0
JAN 5 1959	-118.050	36.150	12	36	02.2
JAN 16 1959	-117.982	36.133	00	10	06.0
JAN 19 1959	-117.966	36.183	21	46	00.0
JUN 6 1959	-118.631	37.333	16	30	46.0
AUG 4 1959	-118.650	37.350	07	40	31.8
AUG 4 1959	-118.550	37.350	07	36	59.0
AUG 4 1959	-118.650	37.466	19	12	35.2
OCT 24 1959	-118.000	35.731	15	35	15.2
JUN 5 1960	-118.600	37.500	07	47	08.0
SEP 8 1960	-118.700	37.500	18	41	36.0
JAN 28 1961	-118.050	35.767	08	12	45.5
FEB 2 1961	-118.500	37.450	00	04	15.5
FEB 2 1961	-118.500	37.450	00	07	43.0
OCT 19 1961	-117.760	35.830	05	09	43.9
SEP 16 1962	-118.044	35.755	05	36	16.0
NOV 6 1962	-119.000	37.500	11	57	16.0

TABLE II-10

SHOCKS IN REGION 2. STA BARBARA

D A T E	LONG DEG	LAT DEG	ORIG. TIME H M SEC
FEB 26 1950	-119.083	34.617	00 06 22.5
APR 15 1950	-119.617	35.750	11 56 32.0
AUG 22 1950	-119.350	34.150	22 47 58.0
DEC 14 1950	-119.167	35.050	13 56 23.0
OCT 21 1953	-119.750	34.316	16 02 38.0
NOV 17 1954	-119.117	34.500	23 03 51.0
MAY 29 1955	-119.083	34.017	16 43 34.8
MAR 3 1956	-119.233	35.083	06 24 12.0
MAR 23 1956	-119.050	35.083	21 23 26.0
JUN 4 1956	-119.133	35.167	08 33 19.0
MAR 18 1957	-119.167	34.100	18 56 27.5
AUG 9 1956	-119.800	34.366	00 08 49.0
JAN 11 1958	-119.266	34.900	23 08 45.5
JUL 14 1958	-119.482	34.349	05 25 55.0
NOV 16 1958	-119.831	34.500	09 34 04.0
JUL 1 1959	-119.050	35.200	23 49 23.0
SEP 16 1962	-119.689	34.488	18 12 35.5
JAN 9 1963	-119.103	34.921	06 04 03.9

TABLE II-11

SHOCKS IN REGION 3. PASADENA

DATE	LONG DEG	LAT DEG	ORIG. TIME H M SEC
JAN 11 1950	-118.200	33.950	21 41 35.0
SEP 22 1951	-117.333	34.113	08 22 39.0
FEB 17 1952	-117.234	34.016	12 36 58.0
AUG 23 1952	-118.216	34.500	10 09 07.0
OCT 26 1954	-117.466	33.731	16 22 26.0
MAY 15 1955	-117.466	34.083	17 03 26.0
JAN 3 1956	-117.500	33.750	00 25 49.0
OCT 4 1961	-117.751	33.853	02 21 31.6
OCT 20 1961	-117.991	33.653	19 49 50.5
OCT 20 1961	-117.979	33.660	20 07 14.5
OCT 20 1961	-117.979	33.664	21 42 40.7
OCT 20 1961	-118.012	33.671	22 35 34.2
NOV 20 1961	-117.991	33.679	08 53 34.7
APR 27 1962	-117.187	33.738	09 12 32.1

TABLE II-12

SHOCKS IN REGION 4. SAN BERNARDINO

D A T E	LONG DEG	LAT DEG	ORIG. TIME H M	SEC
JAN 13 1950	-116.482	34.017	05 07	19.2
AUG 12 1950	-116.800	34.316	02 17	16.7
AUG 28 1950	-116.782	34.300	19 45	26.0
SEP 5 1950	-116.749	33.650	19 19	56.0
OCT 16 1951	-116.981	34.167	12 42	05.0
JAN 8 1952	-116.466	33.981	06 34	28.0
SEP 11 1953	-115.632	34.050	20 50	46.0
APR 30 1954	-116.767	34.033	00 36	23.0
OCT 30 1954	-115.550	34.033	02 02	43.0
JUL 2 1955	-116.633	34.416	16 29	39.0
MAR 16 1956	-116.750	34.250	20 29	34.0
MAR 16 1956	-116.750	34.267	20 33	44.0
MAR 16 1956	-116.750	34.250	20 36	14.0
MAR 16 1956	-116.750	34.250	23 34	57.0
MAR 18 1956	-116.750	34.250	02 42	18.0
MAY 11 1956	-116.750	34.266	16 30	50.0
SEP 1 1956	-115.982	33.767	05 57	53.0
SEP 2 1956	-116.000	33.750	02 46	37.0
SEP 23 1956	-116.550	33.533	11 24	42.0
APR 2 1957	-115.931	33.700	04 22	47.0
DEC 4 1957	-116.350	34.133	02 51	43.0
DEC 12 1957	-116.167	34.267	08 00	06.0
APR 17 1959	-116.333	33.917	16 18	57.0
JUN 12 1959	-116.767	33.500	11 03	13.0
JUN 27 1959	-116.850	34.017	16 22	11.0
AUG 4 1959	-115.676	33.950	18 25	22.0
AUG 26 1959	-116.550	34.050	05 32	50.6
MAY 28 1961	-116.150	33.860	12 59	46.1
OCT 29 1962	-116.862	34.325	02 42	53.9
NOV 30 1962	-116.909	34.335	23 51	05.5
DEC 1 1962	-116.886	34.325	00 35	48.8
DEC 2 1962	-116.875	34.325	00 41	38.6

TABLE II-13

SHOCKS IN REGION 6. SAN FRANCISCO

DATE	LONG DEG	LAT DEG	ORIG. TIME H M SEC
APR 25 1954	-121.682	36.931	20 33 28.0
JUL 29 1954	-121.200	37.416	08 51 36.0
DEC 17 1954	-122.130	37.718	07 08 58.0
MAR 2 1955	-120.931	36.000	15 59 01.0
MAY 7 1955	-122.866	38.916	11 50 39.0
SEP 5 1955	-121.776	37.456	02 01 18.0
OCT 24 1955	-122.050	37.966	04 10 44.0
NOV 2 1955	-120.916	36.000	19 40 06.0
FEB 18 1956	-121.526	36.508	23 58 27.7
JUL 23 1956	-121.300	36.300	08 03 48.0
NOV 22 1956	-121.300	36.300	16 43 55.1
MAR 22 1957	-122.483	37.668	19 44 21.0
MAR 22 1957	-122.450	37.650	23 14 35.0
MAR 23 1957	-122.484	37.650	00 26 55.0
MAR 23 1957	-122.516	37.700	08 13 46.0
OCT 31 1957	-122.216	37.350	19 47 06.0
SEP 28 1957	-121.234	36.600	21 04 39.0
MAY 31 1958	-122.000	37.966	22 07 10.8
JUL 9 1958	-121.667	37.250	05 23 40.0
SEP 21 1958	-121.118	36.350	07 24 55.0
OCT 31 1958	-121.782	37.482	00 26 14.0
DEC 11 1958	-122.567	37.700	09 52 27.0
JAN 29 1959	-121.567	37.135	16 41 23.0
MAR 2 1959	-121.600	36.986	23 27 17.0
MAR 3 1959	-121.712	36.972	07 23 46.0
MAR 3 1959	-121.750	36.941	18 32 13.0
MAY 26 1959	-121.618	36.718	15 58 01.0
DEC 29 1959	-121.484	36.900	02 32 53.0
JAN 20 1960	-121.434	36.782	03 25 53.0
JAN 4 1961	-121.667	36.867	00 30 17.0
APR 9 1961	-121.300	36.683	07 23 16.0
APR 28 1961	-121.366	36.600	01 02 52.0

REGION 1. TINEMAHA

	PAS	MWC	RIV	PLM	SBC	HAI	TIN	CLC	BBC	BAR	WDY	DLT	ISA	FTC	KGR	PVR	MAG	DEPTH
June 25, 51	0.20	-0.19	0.34	0.38	0.59	0.26	-0.02	-0.25	-0.46								4.6	1.6
June 26, 51	-0.55	-0.50	0.20	0.37	0.71	-0.14	0.06	-0.03	0.03								4.4	13.5
Feb. 9, 52	-0.35	-0.12	-0.49	0.62	3.35	0.00	0.00	0.00	-0.53								4.1	1.8
Jan 21, 55	0.10	0.15	0.65	0.89			-0.18		0.42	0.47	0.80	0.33	-0.49				4.0	0.0
Feb. 13, 55	2.41		0.77	0.91	2.30	-0.03	-0.16			2.92	-0.23		-0.61	1.39	1.34		4.1	3.0
June 10, 55			1.44			0.11	-0.07				-0.21	1.16	0.30	2.00			4.0	3.0
Nov. 8, 55	-0.79	0.33	-0.10	0.35	2.74	0.01	-0.26			-0.18	-0.38		0.32	1.24	-0.55		4.2	1.2
July 11, 56	-0.77	-1.02	-0.58	-0.63	-1.06	0.27	-0.31	0.01	1.25		-0.07	-0.74	0.11	0.49	-0.01	0.17	4.2	5.6
Mar. 8, 57	-0.52	-1.12	-0.91	-1.65	1.52		-0.05	0.14	1.14	-0.72	-0.65	-1.17	0.49	0.46		0.07	4.0	3.7
Jan. 5, 59	0.24	-0.03	-0.24	0.36	2.48	0.03	-0.05	-0.16		0.12			-0.03		1.00	-0.90	4.7	0.8
Jan. 16, 59	-0.04		-0.59	0.12	1.96	0.05		-0.14		-0.02	-0.04	-0.16	0.04		0.88		4.3	0.0
Jan. 19, 59	1.01	1.44	0.71	1.12		-0.14	0.05	0.12		1.17	-0.18	3.11	0.14		1.44		4.1	5.3
June 6, 59	0.36		0.05			0.20	-0.04	-1.64			0.07	0.04	-0.27	2.53			4.0	0.1
Aug. 4, 59	-0.52	-1.09	-0.06	0.95		0.47	-0.09	-0.82		0.26	-0.74		-0.38	0.49	-0.17	0.34	5.2	5.1
Aug. 4, 59		0.22		0.18		0.12	-0.19	1.51		-0.09	0.02				0.63		4.2	5.6
Oct. 24, 59	0.65		0.26	0.59	2.13	0.23	0.14			0.89	0.27		0.30	-0.27	0.94	2.07	4.2	6.6
June 5, 60	-0.01	0.01	0.04	0.04	-0.03		0.15	-0.65		0.26	-0.37		-0.07	-0.93	0.41		5.1	0.6
Jan. 28, 61	-0.37	-0.46	-0.29	0.52	0.29		-0.24	0.28		-0.40	0.14		-0.13	0.13	0.31	0.51	5.3	3.0
Feb. 2, 61	-0.21			1.09	1.46	-0.32	0.07	-0.30		0.27	-0.91			1.20	-0.60	-1.61	5.0	3.0
Feb. 2, 61			-1.27	-0.84	1.86	-0.07	0.13	-0.31			-0.28			-0.62	-0.32	-1.00	5.2	0.3
Oct. 19, 61	-0.13	-0.03	-0.24		0.45	0.09	-0.34	0.21		-0.20	-0.10		0.18	-0.53	0.58	1.18	5.2	3.0
Sept.16, 62	0.07	-0.03	-0.50		1.32		0.00	-0.06		0.30	0.32		-0.46	0.06		0.96	4.9	4.7
Nov. 6, 62	-0.06		-0.64		1.70	0.71	0.23	-1.70		-0.63	-0.16		-0.31	1.57	0.79		4.1	5.1
N	20	15	21	18	17	18	22	18	6	16	19	7	17	15	15	10		
$\bar{x}$	0.036	-0.163	-0.069	0.298	1.396	0.103	-0.053	-0.211	0.308	0.276	-0.142	0.367	-0.051	0.613	0.445	0.179		
σ	0.702	0.625	0.616	0.698	1.087	0.230	0.153	0.692	0.703	0.835	0.383	1.316	0.317	0.982	0.631	1.053		
D_n^{α}	0.29	0.34	0.29	0.31	0.32	0.31	0.28	0.31	0.53	0.33	0.30	0.50	0.32	0.34	0.34	0.41		
D_n	0.19	0.15	0.09	0.14	0.09	0.14	0.08	0.19	0.19	0.24	0.08	0.22	0.11	0.15	0.10	0.15		

TABLE II - 14

REGION 2. SANTA BARBARA

	PAS	MWC	RVR	PLM	SBC	HAI	TIN	ISA	CLC	DLT	FTC	KRG	BAR	WDY	BBC	MAG	DEPTH
Feb. 26, 50	-0.09	-0.03	-0.31	-0.39	-0.09	0.36	0.15		-0.13							4.7	5.0
Apr. 15, 50	0.37	0.30	-0.50	-0.52	0.27	0.31	-0.31		0.36							4.6	0.1
Aug. 22, 50	0.04	0.44	1.05	1.28	-0.42	-0.35	1.39			0.01						4.2	9.8
Dec. 14, 50	-0.17	0.10	-0.63	-0.45	0.00	-1.54	-2.21		-1.93	0.02						4.4	15.0
Oct. 21, 53	1.34				0.39				-0.81	1.91	-0.22	-0.39				4.0	1.4
Nov. 17, 54	0.10	0.26	-0.84		0.10						0.04	0.21	-0.84	-1.66	-0.11	4.4	0.6
May 29, 55	-0.17	0.23	-0.02	-0.92	0.02	0.07				-0.44	-0.03	0.29	-0.66	-0.51	0.79	4.1	5.0
Mar. 3, 56	0.01	-0.05	0.02	0.67		-0.32		0.03	-0.68	0.38	0.08				-1.32	4.2	0.2
Mar. 23, 56	-0.19	-0.46	-0.29	0.04	-0.20	0.97	0.79	-0.23		0.45	0.29		0.06		-0.45	4.3	3.8
June 4, 56	0.08	-0.04	-0.38	0.23	-0.03	0.08	0.04	0.07	0.38		0.07	0.07	-0.31	-0.08	-0.57	4.0	0.8
Aug. 9, 56	-0.28	0.47	0.15	0.38	0.04		0.24	-0.62	-1.35	0.46	0.00	0.02	0.08	0.06		4.0	5.0
Mar. 18, 57	-0.36		-0.03	0.03	-0.17		-0.56	-0.61	-0.08	-0.21	0.46	0.41	-0.12	-1.66	0.50	4.7	0.5
Jan. 11, 58	-0.39	-0.07	0.07	0.20		1.20	2.63	-0.30	0.51	-0.07	-0.27	-0.10	0.23	-1.20		4.0	12.5
July 14, 58	-0.34	0.37	-0.05	-0.46	0.05			-0.98			0.19		-0.12			4.7	3.3
July 1, 59	0.05	-0.02	-0.47	-0.25	-0.13	0.37	-0.59		-0.50		0.13		-0.54	0.01		4.7	0.1
Sept. 16, 62	0.03	-0.07	-1.40		-0.46			-0.39	0.01		-0.06		-0.26	0.84		4.0	13.0
Jan. 9, 63	0.24	-0.21	0.44	1.34		1.79	2.21	-0.03	0.53		0.31	-0.05	0.10	-0.08		4.0	9.0
N	17	15	16	14	14	11	11	9	12	9	13	8	11	9	6		
$\bar{x}$	0.016	0.076	-0.199	0.084	-0.045	0.267	0.344	-0.340	-0.307	0.279	0.076	0.057	-0.216	-0.476	-0.193		
σ	0.390	0.245	0.533	0.642	0.223	0.840	1.307	0.330	0.743	0.645	0.198	0.234	0.328	0.810	0.699		
D_n^{α}	0.32	0.34	0.33	0.35	0.35	0.39	0.39	0.43	0.38	0.43	0.37	0.48	0.39	0.43	0.54		
D_n	0.24	0.19	0.13	0.13	0.12	0.18	0.17	0.13	0.13	0.28	0.11	0.10	0.11	0.15	0.14		

TABLE II - 15

REGION 3. PASADENA

	PAS	MWC	RVR	PLM	SBC	HAI	TIN	CLC	BBC	BAR	WDY	ISA	FTC	MAG	DEPTH
Jan 11, 50	-0.01	-0.05	-0.14	0.04	0.67	1.75	-0.37	-0.92						4.1	5.0
Sept.22, 51	-0.39	0.11	0.00		-0.19	-0.24	-0.23	-2.06	-0.01					4.3	5.0
Feb. 17, 52	-0.36	0.51	0.00	-0.10	0.25	-0.32	-0.12	-0.73		-0.02				4.5	15.0
Aug. 23, 52	-0.07	0.23	-0.12		1.36	0.52	0.28	0.35	0.15	1.14	1.45			5.0	15.0
Oct. 26, 54	0.04	0.20	-0.39	0.47		-0.67	0.07		0.19	-0.48		-0.09		4.1	5.6
May 15, 55	-0.10	0.02	0.08	-0.08	-0.13	-0.77			-0.04	0.32	-0.85	-0.70	-0.36	4.0	5.0
Jan. 3, 56	0.05	0.02	-0.30	-0.05	0.62	1.25	1.23		0.28	0.11	0.31	0.82	1.46	4.7	14.9
Oct. 4, 61	-0.23	-0.13	-0.12	0.59	-0.21	0.38	0.43	-0.03		-0.27	-0.06		0.32	4.1	4.3
Oct. 20, 61	0.06	-0.16	0.45	-0.42	-0.05	-0.45	-0.17	0.27		-0.01	-0.52	-0.40	-0.01	4.3	4.6
Oct. 20, 61	-0.54	0.36	-0.12	-0.51		2.16	1.83	0.34		0.36	-0.68	-0.26	0.11	4.0	6.1
Oct. 20, 61	-0.12	0.47	0.07	0.07	0.66		2.90	0.42		0.75	0.18	-0.50	0.05	4.0	7.2
Oct. 20, 61	-0.06	-0.29	-0.30	-0.40	0.55	2.53		0.54		0.29	-0.20	0.20	0.05	4.1	5.6
Nov. 20, 61	-0.21	-0.22	-0.38	-0.38	-0.78		-0.25	-0.31		0.27	-0.18	-0.37		4.0	4.3
Apr. 27, 62	0.30	-0.37	0.02	-0.19	1.63	1.84	1.17	1.42		0.18	0.41		1.69	4.1	14.5
N	14	14	14	12	12	12	12	11	5	12	10	8	8		
$\bar{x}$	-0.117	0.050	-0.089	-0.080	0.365	0.665	0.564	-0.065	0.114	0.220	-0.014	-0.162	0.414		
σ	0.209	0.267	0.214	0.328	0.661	1.140	0.974	0.877	0.121	0.410	0.627	0.449	0.695		
D_n^{α}	0.35	0.35	0.35	0.38	0.38	0.38	0.38	0.40	0.56	0.38	0.41	0.48	0.48		
D_n	0.13	0.12	0.14	0.16	0.16	0.20	0.22	0.16	0.25	0.20	0.15	0.21	0.30		

TABLE II - 16

REGION 4. SAN BERNARDINO

	PAS	MWC	RVR	PLM	SBC	HAI	TIN	CLC	DLT	BBC	BAR	WDY	KGR	FTC	ISA	Mag	Depth
Jan. 13, 50	-0.10	-0.07	0.18	0.07	2.72		0.00	0.10								4.1	0.6
Aug. 12, 50	-0.30	-0.08	-0.06		-0.08	-2.57			0.47							4.3	5.0
Aug. 28, 50	0.10	0.41	0.33	0.08	1.53	-0.19	-0.68		-0.38							4.2	15.0
Sept.5, 50	0.13	0.48	-0.29	-0.17	0.75	-0.57	-0.87		-0.76							4.8	15.0
Oct. 16, 51	0.39	0.53	0.42	0.21	1.24			0.36	0.70	-0.44						4.0	15.0
Jan. 8, 52	0.27	0.78	-0.01	-0.07		0.60	0.06	0.66	0.83	-0.06						4.4	15.0
Sept.11, 53	1.62	-0.82	-0.62				-1.31			-0.28	-0.02					4.2	2.5
Apr. 20, 54	-0.43	0.16	0.09	0.21	0.50		-0.43	-0.66	0.12	0.03	-0.24	-1.27	-0.29	0.10		4.2	5.0
Oct. 31, 54			0.12	-0.47	2.11	1.68			-0.14	0.20	0.31	-0.33	1.88		0.06	4.6	0.6
July 2, 55	-0.09	-0.07	-0.13	-0.07					0.01	0.21	0.02	-0.45	-0.24	-0.52		4.2	0.1
Mar. 16, 56	-0.31	0.36	-0.06		0.45	0.53	0.46		0.17	-0.26	0.12	-0.97		-0.09	-0.39	4.8	0.6
Mar. 16, 56	-0.09	-0.01	0.29	0.05	1.89				0.00	-0.64	0.27	0.17		2.02		4.0	4.3
Mar. 16, 56	-0.01	0.07	0.25	-0.28	0.74	1.55			0.17	-0.48	0.35	-0.28		-0.80	1.32	4.0	6.0
Mar. 16, 56	-0.06	-0.00	-0.24	-0.02	0.82	-0.27	1.39		0.12	-0.15	0.10	0.20		-0.69	-0.09	4.4	0.1
Mar. 18, 56	-0.07	-0.33	0.36	0.16	-0.51	1.62	-1.12		0.02	-0.30	-0.30			-2.02		4.0	1.1
May 11, 56	-0.35	-0.07	0.11	0.08	-0.46	-1.35	-1.38	-1.72		0.20	-0.24			-1.17		4.7	6.0
Sept. 1, 56	0.78	0.16	-0.30	0.31				0.84	-1.18	-0.13	-0.36					4.0	1.7
Sept. 2, 56	2.39	1.26	0.34	-0.30	-1.39		2.49	-0.27	0.50	-0.35	0.06	-0.65				4.2	14.0
Sept.23, 56	-1.13		-0.51	0.56			0.75	-1.12	-0.50	0.25	-0.36	0.99	0.11	-0.36	-0.70	4.3	6.4
Apr. 2, 57	1.30		-0.16	0.34			1.28	-0.80	-0.14	-0.07	-0.30					4.1	6.0
Dec. 4, 57	-0.47	0.12	-0.13	-0.14	-1.79						-1.10		1.09	2.18		4.3	5.0
Dec. 12, 57	0.84	1.36	-0.02	-0.01	1.63		0.73	1.47			0.82	0.22			0.52	4.4	15.0
Apr. 17, 59	0.92	0.77		0.60			-0.83		-0.11		-0.68					4.2	16.9
June 12, 59	-0.86	0.85	0.00	0.43	-0.41	0.67	1.53		-0.33		-0.33	-0.54			-0.34	4.0	0.0
June 27, 59	-0.04	1.32	-0.01	0.08				0.46			-0.14	-0.32			-0.83	4.0	6.2
Aug. 4, 59	0.27	0.44	-0.29	-0.07			-0.52				-0.02	-1.52				4.1	15.1
Aug. 26, 59	-0.23	0.27	-0.06	0.17			-1.61	-2.00			-0.61	-2.26	-1.76		-1.62	4.3	7.1
May 28, 61	-1.10			0.10	1.88		-1.09	-1.51			-0.10	-2.23	-1.25		-1.83	4.4	10.6
Oct. 29, 62	-0.13		-0.29	-0.47	1.32			0.44			0.62	-0.41	-0.70	-0.24	-0.54	4.8	8.6
Nov. 30, 62	0.17		-0.10	-0.67	0.45	0.95		-0.40			0.41	-0.74	-0.54	-0.46	-0.88	4.3	7.0
Dec. 1, 62	-0.01		0.03	-0.07	-0.23	0.91	0.27	-0.06			1.32	-0.63	-0.16	-0.47	-0.55	4.3	9.6
Dec. 2, 62	-0.12		0.11	-0.07	2.18	1.08	1.17				1.06			0.51		4.4	6.6
N	31	24	30	29	22	14	21	16	19	16	26	18	10	14	13		
$\bar{x}$	0.106	0.329	-0.022	0.020	0.697	0.331	0.015	-0.263	-0.023	-0.142	0.025	-0.612	-0.186	-0.144	-0.452		
σ	0.724	0.519	0.250	0.286	1.159	1.170	1.110	0.953	0.473	0.263	0.524	0.803	1.000	1.078	0.792		
D_n^{α}	0.24	0.27	0.24	0.25	0.28	0.35	0.29	0.33	0.30	0.33	0.26	0.31	0.41	0.35	0.37		
D_n	0.19	0.13	0.07	0.10	0.07	0.14	0.13	0.09	0.13	0.11	0.12	0.12	0.19	0.20	0.14		

TABLE II - 17

REGION 6. SAN FRANCISCO

	BRK	MHC	PAC	SFB	MIN	FRE	REN	SHS	VIN	MAG	DEPTH
Apr. 25, 54	0.02	0.01	-1.96	0.07		0.08	0.62	-0.06		5.3	5.0
July 29, 54	0.22	0.14	-0.38	-0.19	-0.30		0.76	2.60		4.2	0.2
Dec. 17, 54	0.04	0.04	-0.02			-1.15		-2.19		4.5	0.4
May 7, 55	0.09	-0.03	-0.16		-0.26	0.19	1.77	0.25		4.6	0.4
Sept.5, 55	0.34	0.02	0.04	-0.46	-0.63	-0.99	0.13	-1.47		5.5	5.1
Oct. 24, 55	0.34	-0.13	0.17	-0.38	0.00	0.02	2.00	0.38		5.4	5.6
Nov. 2, 55	-0.36	0.10	0.28	-0.56	2.20	0.01	1.23	0.51		5.2	15.0
Feb. 18, 56	-0.18	0.01	0.11		2.06	0.29		1.94		4.2	4.1
July 23, 56	0.45	-0.10	-0.08	0.54	1.71	-1.82				4.7	0.1
Nov. 22, 56	-0.05	-0.02	0.28	1.37	1.80	-0.26		1.33		4.2	1.5
Mar. 22, 57	0.03	-0.09	0.05		-1.07	-0.16	0.64	-2.35		5.3	3.1
Mar. 22, 57	-0.02	-0.17	-0.03	0.04	-0.76	-0.45	1.97	-2.05		4.4	5.4
Mar. 23, 57	0.10	-0.16	0.12	-0.09	-0.39	1.31	3.21	-0.01		4.0	7.0
Mar. 23, 57	-0.01	-0.04	-0.06		-0.55	0.90	2.64	2.21		4.2	15.0
Sept.28, 57	-0.30	0.02	0.26	-0.21		0.02	1.68	1.50		4.5	1.1
Oct. 31, 57	-0.27	-0.08	0.02	0.08		0.52		2.50		4.1	5.0
May 31, 58	0.03	0.31		-0.02		-0.11	1.83	0.07		4.1	5.0
July 9, 58	-0.03	-0.04	0.02	0.00	-0.08	-1.10	3.20	-0.01		4.1	6.9
Sept.21, 58	-0.51	0.08	0.35	1.00	1.06	0.01				4.6	0.2
Oct. 31, 58	-0.02	0.28	-0.22	0.22		-1.02		2.55		4.2	1.2
Dec. 11, 58	0.17	-0.25	0.21	-0.08	-1.36	-0.23	-0.08	-2.17		4.7	10.3
Jan. 29, 59	-0.07	-0.01	0.02	0.02	0.84	-2.51		2.19		4.3	5.0
Mar. 2, 59	-0.34	0.09	0.29	0.44	1.07	-0.78	1.81		0.03	5.3	12.8
Mar. 3, 59	-0.61	0.13	0.10	0.44	1.18	-0.24	2.60		0.01	4.4	10.6
Mar. 3, 59	-0.29	0.00	0.15	0.83		-0.20			-0.01	4.0	12.1
May 26, 59	-0.34	0.01	0.07	-0.33	2.96	0.27			-0.08	4.6	11.8
Dec. 29, 59	0.06	-0.08	0.11	-0.51	1.26	-0.01			-0.09	4.7	12.5
Jan. 20, 60	-0.73	-0.42	-0.30	-0.56	-0.81	0.24	0.42	-0.07		5.0	6.4
Jan. 4, 61	0.40	-0.02	0.11	0.60	2.40	1.15			-0.28	4.1	15.5
Apr. 9, 61	0.34	0.02	-0.29	-0.23	0.39	-0.06	0.11	1.40	-0.17	5.6	4.8
Apr. 28, 61		0.32	-0.15	-0.13	0.27	-0.15	2.71		-0.03	4.2	0.3
N	30	31	30	26	24	30	19	22	8		
$\bar{X}$	-0.050	-0.002	-0.029	0.073	0.541	-0.208	1.539	0.411	-0.077		
σ	0.292	0.149	0.402	0.482	1.193	0.782	1.030	1.611	0.097		
D_n^{α}	0.24	0.24	0.24	0.27	0.27	0.24	0.30	0.28	0.48		
D_n	0.11	0.15	0.18	0.13	0.13	0.17	0.14	0.12	0.14		

TABLE II - 18

APPENDIX I-1

It is necessary to transform $-\frac{\partial \Delta}{\partial r}$ to spherical coordinates. We denote by $\Delta^{(1)}$ the first term in the sum (I-2), so $\Delta^{(1)} = \sum_{n=0}^{\infty} C_n h_n^{(1)}(k_\beta R) P_n(\cos\theta)$.

We have:

$$-\frac{\partial \Delta^{(1)}}{\partial r} = -\sum_{n=0}^{\infty} \left(\sin\theta \frac{\partial}{\partial R} + \frac{\cos\theta}{R}\frac{\partial}{\partial \theta}\right) C_n h_n^{(1)}(k_\beta R) P_n(\cos\theta) \quad (I-1a)$$

This expression can be changed by the introduction of the known relations (Morse and Feshbach, 1953):

$$(2n+1)\sin\theta\ P_n(\cos\theta) = \frac{\partial}{\partial \theta}\left[P_{n-1}(\cos\theta) - P_{n+1}(\cos\theta)\right] \quad (I-1b)$$

$$(2n+1)\cos\theta \frac{\partial P_n(\cos\theta)}{\partial \theta} = \frac{\partial}{\partial \theta}\left[n P_{n+1}(\cos\theta) + (n+1) P_{n-1}(\cos\theta)\right] \quad (I-1c)$$

$$(2n+1)\frac{d}{dk_\beta R} h_n^{(1)}(k_\beta R) = n h_{n-1}^{(1)}(k_\beta R) - (n+1) h_{n+1}^{(1)}(k_\beta R) \quad (I-1d)$$

$$(2n+1)\frac{h_n^{(1)}(k_\beta R)}{k_\beta R} = h_{n-1}^{(1)}(k_\beta R) + h_{n+1}(k_\beta R) \quad (I-1e)$$

They remain true even in the case n = o, if we remember that $P_{-1}(z) = P_0(z)$, and $h_{-1}^{(1)}(z) = i h_0^{(1)}(z)$.

After replacing in (I-1a) and making the convenient simplifications we arrive to:

$$-\frac{\partial \Delta^{(1)}}{\partial r} = -k_\beta \frac{\partial}{\partial \theta} \sum_{n=0}^{\infty} \frac{C_n}{2n+1}\left[h_{n+1}^{(1)}(k_\beta R) P_{n+1}(\cos\theta) + h_{n-1}^{(1)}(k_\beta R) P_{n-1}(\cos\theta)\right] \quad (I-1f)$$

and a similar result is obtained for $\frac{\partial \Delta^{(2)}}{\partial r}$.

Noticing that for n = o only the first term in the sum contributes, and after rearranging terms, one finally has:

$$-\frac{\partial \Delta}{\partial r} = \sum_{n=1}^{\infty} \left[\Gamma_n h_n^{(1)}(k_\beta R) + \Delta_n h_n^{(2)}(k_\beta R) \right] \frac{\partial P_n(\cos\theta)}{\partial \theta} \qquad (1\text{-}1g)$$

where

$$\Gamma_n = -k_\beta \left[\frac{C_{n+1}}{2n+3} + \frac{C_{n-1}}{2n-1} \right]$$

$$\Delta_n = -k_\beta \left[\frac{D_{n+1}}{2n+3} + \frac{D_{n-1}}{2n-1} \right] \qquad (1\text{-}1h)$$

$n = 1, 2, 3, \ldots\ldots$

APPENDIX I - 2

To prove the uniform convergence of the development (I-45) in bounded regions of the ν-plane, we note that:

$$e^{-\nu z} J_0(kr) = \frac{1}{2\pi}\int_{-\pi}^{\pi} e^{ikr\cos\phi - \nu z}\, d\phi = \frac{1}{2\pi}\int_{-\pi}^{\pi} e^{ik_\alpha R\cos\gamma}\, d\phi \qquad (I\text{-}2a)$$

where

$$\cos\gamma = \cos\alpha\cos\theta + \sin\alpha\sin\theta\cos\phi \qquad (I\text{-}2b)$$

and

$$\sin\alpha = \frac{k}{k_\alpha} \qquad (I\text{-}2c)$$

The development

$$e^{ik_\alpha R\cos\gamma} = \sum i^n (2n+1) j_n(k_\alpha R) P_n(\cos\gamma) \qquad (I\text{-}2d)$$

is uniformly convergent in the finite ν-plane, because it can be derived from the substitution of the Neumann series for $(\frac{1}{2}z)^{n+\frac{1}{2}} = \sum_p \frac{(n+\frac{1}{2}+2p)\Gamma(n+\frac{1}{2}+p)}{p!} J_{n+\frac{1}{2}+2p}(z)$ in the development of e^{z}. Both developments are uniformly and absolutely convergent in bounded regions; therefore, it is permissible to reorder the terms, obtaining (I-2d). Since (I-2d) is uniformly convergent, term by term, integration is permitted inside the region of convergence. It is easy to show that:

$$\frac{1}{2\pi}\int_{-\pi}^{\pi} P_n(\cos\gamma)\, d\phi = P_n(\cos\theta) P_n\left(\frac{i\nu}{k_\alpha}\right) \qquad (I\text{-}2e)$$

and combining (I-2a) and (I-2d) with this result, we conclude that equation (I-45) is uniformly convergent in the finite ν-plane.

APPENDIX I-3

To find the response of the cavity to the field reflected from the free surface, it is necessary to evaluate the integrals:

$$a_{mn}(\alpha) = -(2n+1)\,i \int_0^\infty \frac{u\,du}{\sqrt{u^2-1}}\, P_n\left(i\sqrt{u^2-1}\right) P_m\left(i\sqrt{u^2-1}\right) \frac{\tilde{F}(u)}{F(u)}\, e^{-2\alpha\sqrt{u^2-1}} \qquad (I\text{-}3a)$$

$$b_{mn}(\alpha) = \frac{4}{\sqrt{3}}(2n+1)\,i \int_0^\infty u^3\,du\, P_n\left(i\sqrt{u^2-1}\right) P_m\left(i\sqrt{\frac{u^2-3}{3}}\right) \frac{2u^2-3}{F(u)}\, e^{-\alpha\left(\sqrt{u^2-1}+\sqrt{u^2-3}\right)} \qquad (I\text{-}3b)$$

$$c_{mn}(\alpha) = 4\,\frac{2n+1}{n(n+1)} \int_0^\infty u^2\,du\, P_n^{(1)}\left(i\sqrt{\frac{u^2-3}{3}}\right) P_m\left(i\sqrt{u^2-1}\right) \frac{2u^2-3}{F(u)}\, e^{-\alpha\left(\sqrt{u^2-1}+\sqrt{u^2-3}\right)} \qquad (I\text{-}3c)$$

$$d_{mn}(\alpha) = -\frac{1}{\sqrt{3}}\,\frac{2n+1}{n(n+1)} \int_0^\infty \frac{u^2\,du}{\sqrt{u^2-3}}\, P_n^{(1)}\left(i\sqrt{\frac{u^2-3}{3}}\right) P_m\left(i\sqrt{\frac{u^2-3}{3}}\right) \frac{\tilde{F}(u)}{F(u)}\, e^{-2\alpha\sqrt{u^2-3}} \qquad (I\text{-}3d)$$

The integrals (I-3c) and (I-3d) can be expressed in a simpler way, to avoid the associated Legendre functions of order 1. This is done with the help of the relationship:

$$u\,P_n^{(1)}\left(i\sqrt{\frac{u^2-3}{3}}\right) = \frac{n(n+1)}{2n+1}\left[P_{n+1}\left(i\sqrt{\frac{u^2-3}{3}}\right) - P_{n-1}\left(i\sqrt{\frac{u^2-3}{3}}\right)\right] \qquad (I\text{-}3e)$$

Then we find that $c_{mn}(\alpha) = 4\sqrt{3}\left(c^*_{m\,n+1} - c^*_{m\,n-1}\right)$;

and $d_{mn}(\alpha) = d^*_{m\,n-1} - d^*_{m\,n+1}$, where

$$c^{*}_{mn}(\alpha) = \int_0^\infty u\,du\; P_n\left(i\sqrt{\tfrac{u^2-3}{3}}\right) P_m\left(i\sqrt{u^2-1}\right) \frac{2u^2-3}{F(u)} e^{-\alpha\left(\sqrt{u^2-1}+\sqrt{u^2-3}\right)} \quad (1\text{-}3f)$$

$$d^{*}_{mn}(\alpha) = \int_0^\infty \frac{u\,du}{\sqrt{u^2-3}} P_n\left(i\sqrt{\tfrac{u^2-3}{3}}\right) P_m\left(i\sqrt{\tfrac{u^2-3}{3}}\right) \frac{\tilde{F}(u)}{F(u)} e^{-2\alpha\sqrt{u^2-3}} \quad (1\text{-}3g)$$

The quantities (1-3a), (1-3b), (1-3f), (1-3g), are generalized Legendre transforms of the four non-analytic reflection coefficients for cylindrical compressional or shear waves that are reflected at the plane surface as compressional or shear waves.

Since $\alpha = k_\alpha h$ is not going to be a large number, the exponentials in the integrands are going to be smooth, non oscillating functions of u, in the range of integration. This condition is equivalent to say that we will consider large wavelength only.

The integrals which we consider, have the Rayleigh pole as the only singularity. The values $u=1$ and $u=3$ in (1-3a) and (1-3g) are removable singularities, which can be eliminated by $\frac{u\,du}{\sqrt{u^2-1}} = d\sqrt{u^2-1}$, and $\frac{u\,du}{\sqrt{u^2-3}} = d\sqrt{u^2-3}$, and the use of Stieltjes' method of integration.

The contribution near the Rayleigh pole was evaluated by expansion of the integrands in Laurent series around $u = u_R$, and direct integration, using Cauchy's principal

value. The integration was symmetric with respect to the pole to avoid numerical errors. If $G(u)$ stands for any of the integrands:

$$G(u) = \frac{A}{u-u_R} + B + C(u-u_R) + \frac{1}{6} D (u-u_R)^2 + O[(u-u_R)^3]$$

then

$$\int_{u_R-\varepsilon}^{u_R+\varepsilon} G(u)\,du = -\pi i A + 2B\varepsilon + \frac{1}{9} D\varepsilon^3 + O(\varepsilon^5)$$

To the right of the Rayleigh pole, the integrands are either real or pure imaginary according to the order of the Legendre polynomials. They have a maximum near $u = n+m+\frac{1}{2}$, for small values of α . The main contribution comes from this region.

The integrals should be computed for arbitrary values of α . We use a modification of the saddle point method, that was formulated by Kane (unpublished) to deal with integrals of this kind when the value of the parameter is small. The integrands consists of two factors; an exponential and an algebraic term. The interval of integration is divided into two parts by a point at the right of all the singularities of the algebraic term. We chose the dividing point to be $u=2$ for the first three integrals and $u=2.3$ for α^*_{mn} . In the first portion of the interval the exponential term is developed in

Taylor series around the origin; and in the second portion the exponential factor is retained for convergence's sake, but the algebraic term is expanded in Laurent series. For the first portion we have:

$$\int_0^2 d(\sqrt{u^2-1})\, P_m(i\sqrt{u^2-1})\, P_n(i\sqrt{u^2-1})\, \frac{\tilde{F}}{F} \sum_{k=0}^{\infty} \frac{(-2\alpha\sqrt{u^2-1})^k}{k!} = \sum_{k=0}^{\infty} S1_{nmk}\, \alpha^k \qquad (1\text{-}3h)$$

$$\int_0^2 u^3 du\, P_n(i\sqrt{u^2-1})\, P_m\left(i\sqrt{\frac{u^2-3}{3}}\right) \frac{2u^2-3}{F(u)} \sum_{k=0}^{\infty} \frac{(-\alpha)^k(\sqrt{u^2-1}+\sqrt{u^2-3})^k}{k!} = \sum_{k=0}^{\infty} S2_{nmk}\alpha^k \qquad (1\text{-}3i)$$

$$\int_0^2 u\, du\, P_n\left(i\sqrt{\frac{u^2-3}{3}}\right) P_m(i\sqrt{u^2-1})\, \frac{2u^2-3}{F(u)} \sum_{k=0}^{\infty} \frac{(-\alpha)^k(\sqrt{u^2-1}+\sqrt{u^2-3})^k}{k!} = \sum_{k=0}^{\infty} S3_{nmk}\alpha^k \qquad (1\text{-}3j)$$

$$\int_0^{2.3} d(\sqrt{u^2-3})\, P_n\left(i\sqrt{\frac{u^2-3}{3}}\right) P_m\left(i\sqrt{\frac{u^2-3}{3}}\right) \frac{\tilde{F}}{F} \sum_{k=0}^{\infty} \frac{(-2\alpha\sqrt{u^2-3})^k}{k!} = \sum_{k=0}^{\infty} S4_{nmk}\alpha^k \qquad (1\text{-}3k)$$

The integrals $S1_{mnk}$, etc. are computed by means of the trapezoidad rule. The number of divisions was increased with the order of the Legendre polynomials, to account for the oscillations. The programing is discussed in Appendix I-5.

For the second portion of the interval, after the algebraic part is developed in Laurent series, term by term integration is possible, and the integrals can be

evaluated exactly in terms of the incomplete exponential integral $E_n(x) = \int_x^\infty \frac{e^{-u}du}{u^n}$. We put

$$\tilde{a}^{\,2}_{mn} = \int_o^\infty \frac{u\,du}{\sqrt{u^2-1}}\, P_n(i\sqrt{u^2-1})P_m(i\sqrt{u^2-1})\frac{\tilde{E}}{E}\, e^{-2\alpha\sqrt{u^2-1}} \quad , \text{ and}$$

similarly for the other integrals. The series expansion we arrive to, is as follows:

$$\tilde{a}^{\,2}_{mn} = i^{m+n}\sum_{p=o}^{\infty} R1_{nmp}\,(2\alpha)^{2p-n-m-3}\,E_{2p-m-n-2}(2\alpha\sqrt{3}) \qquad (1\text{-}31)$$

$$\tilde{b}^{\,2}_{mn} = \frac{i^{m+n}}{(\sqrt{3})^m}\sum_{p=o}^{\infty} R2_{nmp}\,\alpha^{2p-n-m-4}\,E_{2p-m-n-3}(\sqrt{1+\sqrt{3}}\,\alpha) \qquad (1\text{-}3m)$$

$$\tilde{c}^{\,2}_{mn} = \frac{i^{m+n}}{(\sqrt{3})^n}\sum_{p=o}^{\infty} R3_{nmp}\,\alpha^{2p-n-m-2}\,E_{2p-m-n-1}(\sqrt{1+\sqrt{3}}\,\alpha) \qquad (1\text{-}3n)$$

$$\tilde{d}^{\,2}_{mn} = \left(\frac{i}{\sqrt{3}}\right)^{m+n}\sum_{p=o}^{\infty} R4_{nmp}\,\alpha^{2p-m-n-3}\,E_{2p-m-n-2}(2\alpha\cdot 1.513275) \qquad (1\text{-}3o)$$

The quantities $R1_{mnp}$, and the others, are real and can be computed directly. They are put in magnetic tape together with the S_s to be used for the computations.

APPENDIX I-4

The system of equations (I-50), (I-51) can be solved after the evaluation of five 2 x 2 determinants. If we place $A = L_1 h_n^{(1)}(K_\alpha a)$; $B = n(n+1) L_2 h_n^{(1)}(K_\beta a)$; $C = L_2 h_n^{(1)}(K_\alpha a)$ $D = L_3 h_n^{(1)}(K_\beta a)$; $a = Re\, A$; $b = Re\, B$; etc. the determinants are:

$$\Delta_n = \begin{vmatrix} A & B \\ C & D \end{vmatrix} \quad ; \quad \Delta_{1n} = \begin{vmatrix} a & B \\ e & D \end{vmatrix} \quad ; \quad \Delta_{2n} = \begin{vmatrix} b & B \\ d & D \end{vmatrix} \qquad (I-4a)$$

$$\Delta_{3n} = \begin{vmatrix} A & a \\ C & e \end{vmatrix} \quad ; \quad \Delta_{4n} = \begin{vmatrix} A & b \\ C & d \end{vmatrix}$$

All of this determinants will be modified to avoid numerical errors due to the loss of the first order terms, that cancel identically. The determinants Δ_{2n} and Δ_{3n} are formally simpler, and after some straightforward computation we have

$$\Delta_{3n} = i\left[\frac{4[n(n+1)-2]}{a^3} - \frac{2K_\beta^2}{a}\right]\left[n_n(K_\alpha a)\frac{d}{da} j_n(K_\alpha a) - j_n(K_\alpha a)\frac{d}{da} n_n(K_\alpha a)\right] = \qquad (I-4b)$$

$$= -\frac{i}{K_\alpha a^2}\left[\frac{4[n(n+1)-2]}{a^3} - \frac{2K_\beta^2}{a}\right]$$

$$\Delta_{2n} = n(n+1) i\left[\frac{4[n(n+1)-2]}{a^3} - \frac{2K_\beta^2}{a}\right]\left[n_n(K_\beta a)\frac{d}{da} j_n(K_\beta a) - j_n(K_\beta a)\frac{d}{da} n_n(K_\beta a)\right] =$$

$$= -\frac{n(n+1) i}{K_\beta a^2}\left[\frac{4[n(n+1)-2]}{a^3} - \frac{2K_\beta^2}{a}\right] \qquad (I-4c)$$

where we have use the properties of the Wronskian to simplify the expressions.

The evaluation of Δ_η is more involved. The operators L_1, L_2 etc. include terms like $\frac{h_n^{(1)}(k_\alpha a)}{a}$ and $\frac{d}{da} h_n^{(1)}(k_\alpha a)$. We transform these terms by the relationships:

$$(2n+1)\frac{h_n^{(1)}(k_\alpha a)}{k_\alpha a} = h_{n-1}^{(1)}(k_\alpha a) + h_{n+1}^{(1)}(k_\alpha a) \qquad (1\text{-}4d)$$

and

$$(2n+1)\frac{d}{dk_\alpha a} h_n^{(1)}(k_\alpha a) = n\, h_{n-1}^{(1)}(k_\alpha a) - (n+1)\, h_{n+1}^{(1)}(k_\alpha a) \qquad (1\text{-}4e)$$

After the transformation is done, the determinant can be evaluated directly and yields:

$$\begin{aligned}\Delta_n = \frac{k_\alpha^2 k_\beta^2}{(2n-1)(2n+1)(2n+3)} \Big[& 4n(n-1)(n+2)\, h_{n-2}^{(1)}(k_\alpha a) h_{n+2}^{(1)}(k_\beta a) + 4(n-1)(n+1)\cdot(n+2)\cdot \\ & \cdot h_{n+2}^{(1)}(k_\alpha a)\, h_{n-2}^{(1)}(k_\beta a) - 2(n-1)(n+1)(4n+5)\, h_n^{(1)}(k_\alpha a) h_{n-2}^{(1)}(k_\beta a) - \\ & - 2n(n+2)(4n-1) h_n^{(1)}(k_\alpha a) h_{n+2}^{(1)}(k_\beta a) + 2n(n-1) h_{n-2}^{(1)}(k_\alpha a) h_n^{(1)}(k_\beta a) - \\ & - 2(n+1)(n+2) h_{n+2}^{(1)}(k_\alpha a) h_n^{(1)}(k_\beta a) + 5(2n+1) h_n^{(1)}(k_\alpha a) h_n^{(1)}(k_\beta a) \Big]\end{aligned} \qquad (1\text{-}4f)$$

The determinant Δ_{1n} can be obtained by the same formula, replacing $h_n^{(1)}(k_\alpha a)$ by $j_n(k_\alpha a)$; Δ_{4n}, replacing $h_n^{(1)}(k_\beta a)$ by $j_n(k_\beta a)$.

Then

$$A_n = -\frac{1}{\Delta_n}\left[\Delta_{1n}\, a_n + \Delta_{2n}\, \gamma_n\right] \qquad (1\text{-}4g)$$

$$\Gamma_n = -\frac{1}{\Delta_n}\left[\Delta_{3n}\, a_n + \Delta_{4n}\, \gamma_n\right] \qquad (1\text{-}4h)$$

For small values of z, it is known that $h_n^{(1)}(z) \sim \frac{(2n-1)!!}{i\, z^{n+1}}$ and $j_n(z) \sim \frac{z^n}{(2n+1)!!}$. Since a_n and γ_n depend only upon $k_\alpha h$, we can see that for small values of $k_\alpha a$, A_n and Γ_n are of the order $O[(k_\alpha a)^{2n-1}]$, because $\Delta_n \sim O[(k_\alpha a)^{-(2n+4)}]$ and $\Delta_{1n} \sim \Delta_{2n} \sim \Delta_{3n} \sim \Delta_{4n} \sim$ $\sim O[(k_\alpha a)^{-5}]$. But for $n=1$ we have $\Delta_{11} \sim \Delta_{21} \sim \Delta_{31} \sim \Delta_{41} \sim$ $\sim O[(k_\alpha a)^{-3}]$, $\Delta_n \sim O[(k_\alpha a)^{-6}]$. Then A_1 and Γ_1 are of the order $O[(k_\alpha a)^3]$.

APPENDIX I-5

The problem of the numerical analysis of the system (I-79), (I-80), together with the evaluation of the integrals a_{mn}, b_{mn}, etc. that are used in it, presents several delicate points that are discussed together with the programing for the IBM 7090 digital computer at the California Institute of Technology Computing Center.

In the first place, it was shown in Appendix I-3 how to decompose each of the integrals a_{mn}, etc., into two series: a power series in α, with complex coefficients SI_{mnk}, etc., and a Laurent series in α, but with coefficients that are products of real constants RI_{mnk}, etc., and incomplete exponential integrals. These developments are valid for any positive α, because the integrands do not cross singularities for $0<\alpha<\infty$. The only restriction we thus have is given by the rate of convergence. Since it is impossible to put all the coefficients of the series inside the memory of the computer, we are bound to count the developments at certain points that are convenient for the range of values of α we are interested in. We decided to take 15 terms for the power series, and 25 for the Laurent series. With this limitation, we find empirically that we have to restrict α to the interval (0.25, 1.6).

The computation of the coefficients SI_{mnk} , etc., is done by the trapezoidal rule and using Stieltjes' method of integration to avoid the singularities at the branch points. The integration was done numerically because of the complexity of the integrands. The program entitled "Program to compute the integrals of the Rayleigh functions" performs these integrations in two parts. The first is the evaluation of the part due to Cauchy's principal value, and it is seen in the flow chart under the heading "Residue at the Rayleigh pole". The second is the use of the trapezoidal rule for the integration in the remaining part of the interval. After the computation is finished, the values of the 4 three-dimensional complex matrices SI_{mnk} , etc., are written in magnetic tape. The real matrices RI_{mnk} , etc., are read from cards into the body of the computer and then written into the same tape that is then ready to be used in the main program.

The numerical integration described above was done with different interval sizes, to decrease the errors. The interval (o,2) in the real u-axis, was divided into 8 parts each one subdivided in equal segments. The number of divisions was increased near the branch points $u = 1$ and $u = \sqrt{3}$, to account for the steepness of the

functions. The accuracy of the integration was verified by increasing by a factor of 2 the number of intervals in the computation. The test cases gave a precision of 4 to 6 significant figures, depending upon the order of the Legendre polynomials.

The main program consist of three different computational blocks. (a) Computation of the reflection coefficients $\delta_n^i(\omega, a)$. (b) Calculation of the integrals a_{mn} etc., the reflection coefficients of spherical waves at a plane surface, from the value $\alpha = \kappa_\alpha h$, and the matrices $SI_{mn\kappa}$, $RI_{mn\kappa}$, etc., and (c) Formation of the linear equations (I-79), (I-80), and inversion of the system by Jordan's method to obtain the coefficients X_n and Y_n .

Appendix No. II - 1

INSTRUCTIONS FOR USING THE HYPOCENTER LOCATION PROGRAM FOR LOCAL SHOCKS AND TELESEISMS

The Program is contained in the deck labeled HYPO a, for FORTRAN version II, and HYPO b, for FORTRAN version IV.

Several options are possible. We can process a teleseism or a local shock. If it is a teleseism, the Program accepts only P phases, or P and S phases. If it is a local shock we can have first arrivals only, more than one P phase, or P and S phases together. The depth can be held fixed. Also, we can skip part of the printing in intermediate iterations. If a new station is not in the catalog, we can enter it as an "extra station". For each shock these should be introduced after the other stations. Each shock begins with an initial card containing general information. Then come the others with the station codes and the times of the phases. At the end of all the shocks there must be a card with a zero in columns 50 and 51, to end the computation.

The first six cards after the * DATA card are common to all the shocks. The content of these cards is shown in Figure 1. They can be changed if the user wants to alter some of the input formats, or some parameters of the computation. If any such change is made, it must be reported here.

EXPLANATION OF DATA CARDS
(See Figures 1 and 2)

Card No.	Col.	Explanation
1		Contains the headings of the output sheets
	1-12	LOCAL SHOCK (2A6)
	13-24	TELESEISM (2A6)
2		Contains the names of the phases that are used for the solution.
	1-6	P1P2PN (3A2) the P phases for local shocks.
	7-9	OFF (A3) if some phase is rejected by the Program.
	10-15	S1S2SN (3A2) S phases for local shocks.
	16-18	PS (2A1) P and S phases for teleseisms.
3		Contains the two formats for the read in of the station codes and travel times of local shocks.
	1-30	(2(13,F 2,2, 5FS.0F10.0)); read with the format (5A6) for local shocks with more than one P phase.
	31-60	(13, F2. 2, 12F5.0); read with the format (5A6) for local shocks where P and S phases are available.
4		Contains two formats for the read in of station data, codes and travel times of teleseisms, and local shocks where only the first arrival is available.

Card No.	Col.	Explanation
	1-30	(4(I3,F2.2,2F5.0,F3.1,F2.0)); read with the format (5A6) for teleseisms and local shocks where only the first arrival is available.
	31-60	(2(I3,F2.2,4F5.0,3F5.0)); read with format (5A6) for teleseisms where P and S readings exists.
5	1-54	(A6,I4,F4.1,I3,F4.1,F3.1,F2.2,6(F2.0,F4.0), 2F5.0,F5.0) read with format (9A6); for "extra stations", that is, stations that are not in the catalog.
6		Contains the initial tolerance limit for the size of the residuals, the maximum permissible number of iterations, the final tolerance limit, and the factor by which the tolerance limit is decreased. The tolerance limit is multiplied by that factor after each iteration and is kept at least equal to the final tolerance limit.
	1-4	10.0 (F4.1) tolerance limit (initial).
	5-6	03 (I2) maximum number of iterations
	7-10	2.0 (F4.1) tolerance limit.
	11-14	F4.1 Factor.
7		First card of the first shock processed. Contains general information concerning the shock.

Card No.	Col.	Explanation
	1-20	(4A5) contains the date of the shock and some other identification, such as the region, etc.
	21-28	(F8.0) Guess in longitude (in degrees), GLAM, it is positive to the east of Greenwich and negative to the west.
	29-35	(F7.0) Guess in latitude (in degrees), GPHI, positive to the north of the equator, negative to the south.
	36-41	(F6.0) Guess in depth (in km), GDEPTH, datum is sea level for teleseisms, and +1 km for local shocks.
	42-44	(F3.0) Guess origin time (minutes), GORIG,
	45-49	(F5.0) Guess origin time (seconds), GORIGS.
	50-51	(I2) The number of stations, N.
	52-53	(I2) The number of these stations that are in the catalog, NEX. If all of the stations are in the catalog, this number is equal to the previous one.
	54-55	(I2) Reference time (hours), I01. The travel times and origin times are counted with this as zero.
	56-57	(I2) Reference time (minutes), I02.
	58	(I1) Test for typing intermediate iterations, JTYPE

Card No. | Col. | Explanation

59 (11) Test for keeping a constant depth. JFIX. If JFIX=0: don't fix the depth of the shock. If JFIX=1: keep the depth fixed at the value of the guess.

60 (11) Test for teleseisms, NTELE. If NTELE=0: the shock is local. If NTELE=1, the shock is a teleseism.

61 (11) Test for the phases available. NPHASE.

If	NPHASE	LOCAL	TELESEISM
	0	only one P phase	one P phase
	1	more than one P phase	P and S phases
	2	P and S phases	----------

8 and following
Contain codes and travel times of the shock according to thefformats in cards 3, 4, or 5.

At the end of all the shocks, there must be a card similar to card No. 7, with a zero in the place of the number of stations (two zeros in columns 50 and 51).

The reference time is the zero to which all the times are referred to. It should be an exact minute.

Next we explain the formats for the different options.

Cols. | Format | Explanation

TELESEISMS

a) First Arrival Only.

Col.	Format	Explanation
		It is possible to put four stations per card.
1-3	(I3)	Code No. of the station in the catalog, INDEX.
4-5	(F2.2)	Weight assigned to each station, W. $0 \leq W < 1$
6-10	(F5.0)	Arrival time (minutes), PM.
11-15	(F5.0)	Arrival time (seconds), PS.
16-18	(F3.1)	pP-P time (in seconds), PPMP.
19-20	(F2.0)	Crustal thickness at the station (in km), CD. Usually 33 km.
21-40		Same thing for next station.
41-60		" " " " "
61-80		" " " " "
		b) If P and S Phases Are Present.
		Two stations per card are possible.
1-3	(I3)	Station code.
4-5	(F2.2)	Weight.
6-10	(F5.0)	P time (minutes).
11-15	(F5.0)	P time (seconds).
16-20	(F5.0)	S time (minutes), SM.
21-25	(F5.0)	S time (seconds), SS.
26-30	(F5.0)	pP-P time (seconds).
31-35	(F5.0)	sS-S time (seconds), SSMS.
36-40	(F5.0)	Crustal thickness (km). Usually 33 km.
41-80		Same format for the next station.
		LOCAL SHOCKS
		c) If Only the First Arrival is Known.

Col.	Format	Explanation
		The listing is the same as in case a) for teleseisms.
		The places for PPMP and CD are left in blank.
	d)	d) If More Than One P Phase Is Available.
		Up to three P phases can be used. Two stations can be put on one card.
1-3	(I3)	Station code.
4-5	(F2.2)	Weight.
6-10	(F5.0)	First P time (minutes), PM.
11-15	(F5.0)	First P time (seconds), PS.
16-20	(F5.0)	Second P time (minutes), PM2.
21-25	(F5.0)	Second P time (seconds), PS2.
26-30	(F5.0)	Third P time (minutes), PM3.
31-40	(F10.0)	Third P time (seconds), PS3.
41-80		Same format for next station.
		e) If P and S phases are present.
		Three P and three S phases can be used. Only one station per card is possible.
1-3	(I3)	Station code.
4-5	(F2.2)	Weight.
6-10	(F5.0)	First P time (minutes), PM.
11-15	(F5.0)	First P time (seconds), PS.
16-20	(F5.0)	Second P time (minutes), PM2.
21-25	(F5.0)	Second P time (seconds), PS2.
26-30	(F5.0)	Third P time (minutes), PM3.

Col.	Format	Explanation
31-35	(F5.0)	Third P time (seconds), PS3.
36-40	(F5.0)	First S time (minutes), SM.
41-45	(F5.0)	First S time (seconds), SS.
46-50	(F5.0)	Second S time (minutes), SM2.
51-55	(F5.0)	Second S time (seconds), SS2.
56-60	(F5.0)	Third S time (minutes), SM3.
61-65	(F5.0)	Third S time (seconds), SS3.

f) Extra Stations.

If a station is not in the catalog, it can be entered as an "extra station". The cards for the extra stations go after all the cards of stations that are in the catalog, for a given shock. It is possible to enter one station per card.

1-6	(A6)	Name of the station.
7-10	(I4)	Longitude of the station (degrees).
11-14	(F4.1)	Longitude of the station (minutes), without the sign.
15-17	(I3)	Latitude of the station (degrees).
18-21	(F3.1)	Latitude of the station (minutes), without the sign.
22-24	(F3.1)	Elevation of the station (km), above datum.
25-26	(F2.2)	Weight. $0 \leq W < 1$.
27-28	(F2.0)	First P time (minutes, PM.
29-32	(F4.0)	First P time (seconds), PS.

Col.	Format	Explanation
33-34	(F2.0)	First S time (minutes), SM.
35-38	(F4.0)	First S time (seconds), SS.
39-40	(F2.0)	Second P time (minutes), PM2.
41-44	(F4.0)	Second P time (seconds), PS2.
45-46	(F2.0)	Second S time (minutes), SM2.
47-50	(F4.0)	Second S time (seconds), SS2.
51-52	(F2.0)	Third P time (minutes), PM3.
53-56	(F4.0)	Third P time (seconds), PS3.
57-58	(F2.0)	Third S time (minutes), SM3.
59-62	(F4.0)	Third S time (seconds), SS3.
63-67	(F5.0)	pP-P time (seconds), PPMP.
68-72	(F5.0)	sS-S time (seconds), SSMS.
73-77	(F5.0)	Crustal thickness (km), CD.

Some examples of the way to punch the data cards are shown in Figure 2. An example of the input for a Teleseism is shown in Figure 3. The explanation of the quantities is given in the text. The geographic latitude and longitude are denoted by PHI and LAMBDA respectively. The horizontal distance is called DELTA. The errors are the standard deviations of the solutions of the normal equations and they do not involve the data which is rejected by the Program.

APPENDIX II-2

SUBROUTINES FOR HYPOCENTER LOCATION PROGRAM

1. SUBROUTINE PPP(DEPTH,Z,S,K)

Computes the depth of a teleseism from pP-P and sS-S readings. The Jeffreys-Bullen tables are used, and the depths are obtained by linear interpolation.

Input: In COMMON:

DELTA :distance epicenter-station (Km.).

K :for pP-P K=0, for sS-S K=1.

PPTIME(I,J):pP-P time tables.

SSTIME(I,J):sS-S time tables.

PPDEL(I) :distance intervals in pP-P tables.(degree)

SSDEL(I) :distance intervals in sS-S tables.(degree)

In the arguments of the subroutine:

S :pP-P or sS-S times (sec).

Output:

Z :number of pP-P or sS-S readings.

DEPTH :calculated average depth (Km).

2. SUBROUTINE PTIME(DEPTH,D1,D2,PT,DD,DH,ELEV,K)

Computes the times of P and S phases for teleseisms from the Jeffreys-Bullen tables.The times are corrected for ellipticity.

Input: In COMMON:

DELTA :distance epicenter-station (Km).

K : for P phases K=0, for S phases K=1.

TIMEP(I,J) : Jeffreys-Bullen P tables.

TIMES(I,J) : Jeffreys-Bullen S tables.

In the arguments of the subroutine:

ELEV : elevation of the station (Km).

DEPTH : depth of the focus (Km).

D1 : elevation of the mean sphere at the station (Km).

D2 : elevation of the mean sphere at the epicenter (Km).

Output:

DD : $\delta t/\delta\Delta$, variation of the travel time with distance (sec/Km).

DH : $\delta t/\delta h$, variation of the travel time with the depth of the focus (sec/Km).

PT : travel time of the P or S phase (sec).

3. SUBROUTINE VECTOR(AM,PHI,A,B,C,D)

Input:

AM : longitude (radians).

PHI : latitude (radians).

Output:

A,B,C : geocentric direction cosines.

D : elevation of the mean sphere (Km).

4. SUBROUTINE DISTAN(A1,B1,C1,A2,B2,C2,DELTA,DDDLAM, DDDPHI)

Computes the distance epicenter-station and the partial derivatives with respect to the longitude and latitude of the epicenter.

Input:

A1,B1,C1, :direction cosines of the station.

A2,B2,C2 :direction cosines of the epicenter.

Output:

DELTA :distance epicenter-station (Km).

DDDLAM :$\delta\Delta/\delta\lambda$ (Km/radian).

DDDPHI :$\delta\Delta/\delta\varphi$ (Km/radian).

5. SUBROUTINE AZIMTH(A1,A2,A3,B1,B2,B3,AZI,DELTA)

Input:

A1,A2,A3 :direction cosines of the stations.

B1,B2,B3 :direction cosines of the epicenter.

DELTA :distance epicenter-station (Km).

Output:

AZI :azimuth of the line epicenter-station at the epicenter (radians).

6. SUBROUTINE CHOOSE(XLAM,PHI,A,B,C,DELTA,L,DUMMY)

Selects the crustal values for Local shocks, at various points between the epicenter and the station.

Input: In COMMON:

CRUST(I,J,K) :crustal values at the grid crossings in the California-Nevada region.

In the arguments of the subroutine:

XLAM : longitude of the epicenter (degrees).

PHI : latitude of the epicenter (degrees).

A,B,C : direction cosines of the station.

DELTA : distance epicenter-station (Km).

Output: In COMMON:

VPATH(I,J) : crustal values at the L+2 points that divide the distance DELTA. DELTA is divided into L segments of 25 Km. and a last segment, called DUMMY, smaller than 25 Km.

In the arguments of the subroutine:

L : the largest integer contained in $\frac{DELTA}{25}$.

DUMMY : DELTA-25.L (Km).

7. SUBROUTINE MTP1(ELEV,DTP1DD,DTP1DH,VP1,VP2,VP3,DUMMY, L)

Computes the travel time of the direct arrival in an irregular crust, and the derivatives with respect to the distance and the depth.

Input: In COMMON:

VPATH(I,J) : crustal values along the path.

DELTA : distance epicenter-station. (Km).

H : depth of the focus, below the datum (Km).

K : for P phases K=1, for S phases K=4.

In the arguments of the subroutine:

ELEV :elevation of the station (Km).

VP1,VP2,VP3 :mean velocities (P or S) in the layers (Km/sec).

DUMMY :DELTA-25.L (Km).

L :largest integer contained in DELTA/25.

Output:

TP1 :travel time of the direct wave (sec). (in COMMON).

DTP1DD :$\delta t/\delta\Delta$ at the epicenter (sec/Km).

DTP1DH :$\delta t/\delta h$ at the epicenter (sec/Km).

8. SUBROUTINE MTP2(ELEV,TP2,DTP2DD,DTP2DH,VP1,VP2,DUMMY, L)

Computes the travel time of the first refracted arrival in an irregular crust.

Input: In COMMON:

VPATH(I,J) :crustal values along the path.

DELTA :distance epicenter-station.(Km).

H :depth of the focus below the datum (Km).

K :for P phases K=1, for Sphases K=4.

In the arguments of the subroutine:

ELEV :elevation of the station (Km).

VP1,VP2 :mean velocities (P or S) in the layers (Km/sec).

DUMMY :DELTA-25.L (Km).

L :largest integer contained in DELTA/25.

Output:

TP2 : travel time of the first refracted arrival (sec).

DTP2DD : $\delta t/\delta \Delta$ at the epicenter (sec/Km).

DTP2DH : $\delta t/\delta h$ at the epicenter (sec/Km).

9. SUBROUTINE MTPN(ELEV,TPN,DTPNDD,DTPNDH,VP1,VP2,VPN, DUMMY,L)

Computes the arrival time of the second refracted arrival in an irregular crust.

Input: In COMMON:

VPATH(I,J) : crustal values along the path.

DELTA : distance epicenter-station (Km).

H : depth of the focus (Km).

K : for P phases K=1, for S phases K=4.

In the arguments of the subroutine:

ELEV : elevation of the station (Km).

VP1,VP2,VPN : mean velocities (P or S) in the layers (Km/sec).

DUMMY : DELTA-25.L (Km).

L : largest integer contained in DELTA/25.

Output:

TPN : travel time of the second refracted arrival (sec).

DTPNDD : $\delta t/\delta \Delta$ at the epicenter (sec/Km).

DTPNDH : $\delta t/\delta h$ at the epicenter (sec/Km).

10. SUBROUTINE DETERM(A,B,C,D,E,F,G,H,T,U,P,Q,R,S,X,Y,Z,V)

Solves the equation:

$$\begin{bmatrix} A & B & C & D \\ B & E & F & G \\ C & F & H & T \\ D & G & T & U \end{bmatrix} \begin{bmatrix} X \\ Y \\ Z \\ V \end{bmatrix} = \begin{bmatrix} P \\ Q \\ R \\ S \end{bmatrix}$$

by Gauss elimination technique.

Output:

X :correction in latitude, $\Delta\varphi$ (radians).

Y :correction in longitude, $\Delta\lambda$ (radians).

Z :correction in depth, Δh (Km).

V :correction in origin time, Δt_o (sec).

11. SUBROUTINE SNOREQ(DTDPHI,DTDLAM,DTDH,RES,W,A,B,C,D,E,F,G,H,T,U,P,Q,R,S,WC,WN)

Forms the normal equations.

Input:

DTDPHI :$(\delta t/\delta\varphi)_i$ at the i^{th} station (sec/radian).

DTDLAM :$(\delta t/\delta\lambda)_i$ at the i^{th} station (sec/radian).

DTDH :$(\delta t/\delta h)_i$ at the i^{th} station (sec/Km).

RES :$(\text{residual})_i$ at the i^{th} station (sec).

Output:

$A=\sum (\delta t/\delta\varphi)_i^2\omega_i^2$; $B=\sum (\delta t/\delta\varphi)_i(\delta t/\delta\lambda)_i\omega_i^2$;

$C=\sum (\delta t/\delta\varphi)_i(\delta t/\delta h)_i\omega_i^2$; $D=\sum (\delta t/\delta\varphi)_i\omega_i^2$;

$E=\sum (\delta t/\delta\lambda)_i^2\omega_i^2$; $F=\sum (\delta t/\delta\lambda)_i(\delta t/\delta h)_i\omega_i^2$;

$G=\sum (\delta t/\delta\lambda)_i\omega_i^2$; $H=\sum (\delta t/\delta h)_i^2\omega_i^2$;

$T=\sum(\delta t/\delta h)_i\omega_i^2$; $U=\sum\omega_i^2$; $P=\sum(\delta t/\delta\varphi)_i Res_i\omega_i^2$;

$Q=\sum(\delta t/\delta\lambda)_i Res_i\omega_i^2$; $R=\sum(\delta t/\delta h)_i Res_i\omega_i^2$;

$S=\sum Res_i\omega_i^2$; $WC=\sum(Res_i)^2\omega_i^2$; $WN=\sum 1$.

12. SUBROUTINE STANDR(A,B,C,D,E,F,G,H,T,U,DX,DY,DZ,DV)

Computes the values DX,DY,DZ,DV, that are used to estimate the standard deviations of the solution of the normal equations.

If

$$\mathfrak{N} = \begin{bmatrix} A & B & C & D \\ B & E & F & G \\ C & F & H & T \\ D & G & T & U \end{bmatrix}$$

then $DX=(\mathfrak{N}^{-1})_{11}$, $DY=(\mathfrak{N}^{-1})_{22}$, $DZ=(\mathfrak{N}^{-1})_{33}$, $DV=(\mathfrak{N}^{-1})_{44}$

FIGURE CAPTIONS - Part I

Figure I - 1. Geometry of the problem.

Figure I - 2. Contour of integration for the integral representations of the field. Branch points and branch cuts are not shown. The indentation is at the Rayleigh pole κ.

Figure I - 3. Schematic representation of the waves that must be in equilibrium according to the linear equations (I-79), (I-80); and the integral equations (I-73), (I-74). Only one of the reflected waves is shown. (a) Spherical coordinates n-space. (b) Cylindrical coordinates, k-space. Equilibrium is achieved through the reflection coefficients δ_n^1 in case (a), and through $(\tilde{F}(k)/F(k))\cdot e^{-2\nu h}$ in case (b).

Figure I - 4. Paths of integration in the complex k-plane, to compute the surface wave contribution from the branch line integrals.

Figure I - 5. Behavior of the body waves from a spherical cavity in an infinite solid.

Figure I - 6. Decoupling factor for Rayleigh waves. The numbers in the figure indicate the ratio of the cavity radius to its depth.

Figure I - 7. Normalization of Rayleigh waves to a sphere in an infinite space. The numbers in the figure indicate the ratio of the cavity radius to its depth.

Figure I - 8. Rayleigh waves from a cavity in a half space, normalized to the Rayleigh waves from a point source in a half space. The numbers in the figure indicate the ratio of the radius of the cavity to its depth.

Figure I - 9. Same as Figure I-8, but the independent variable is $k_\alpha a$ instead of $k_\alpha h$.

Figure I - 10. Phase of the Rayleigh wave displacements from a cavity in a half space, minus the phase of the Rayleigh wave displacements from the point source is a half space. The phase is given in degrees. The numbers in the figure indicate the ratio of the radius of the cavity to the depth.

Figure I - 11. Same as Figure I - 10, but the independent variable is $k_\alpha a$ instead of $k_\alpha h$.

Figure I - 12. Amplitude of the displacements normalized to the point source in a half space. The independent variable is a/h the ratio of the cavity radius to its depth. The numbers in the figure indicate the values of the dimensionless frequency $k_\alpha h$.

Figure I - 13. Contours utilized for numerical evaluation of the integrals A_{on} and C_{on}.

Figure I - 14. Values of $(-1)^n A_{on}(\alpha)\alpha^{n+3}$. Only the real part is given.

Figure I - 15. Values of $(-1)^{n-1} C_{on}(\alpha)\alpha^{n+3}$. Only the real part is given.

Figure I - 16. Flow diagram for the program to compute the integrals given in equations (I-81) to (I-84).

Figure I - 17. Flow diagram for the program to solve the system of linear equations (I-79), (I-80).

FIGURE CAPTIONS - Part II

Figure II - 1. First arrival as a function of distance and depth of the focus, for a simple crustal model with parallel plane boundaries (Press, 1960).

Figure II - 2. Simplified flow diagram for the IBM 7094 hypocenter location program.

Figure II - 3. California-Nevada region, as used in the computation of local shocks. The different geologic provinces are limited by dotted lines. The grid lines are $\frac{1}{2}^{o}$ apart.

Figure II - 4. Correlation between topography and thickness of the crust. The negative elevations correspond to points below sea level. All values are given in km.

Figure II - 5. Regions in which shocks were selected for the period 1950 on, to study statistical frequency-depth relationships. Well located shocks in region 5 were few and they were not included in the results.

Figure II - 6. Horizontal distribution of the epicenters of the Kern County aftershocks. The sense of motion is taken from Båth and Richter (1955), the lower ones are slanted and give the depths in km.

Figure II - 7. Vertical cross section showing the distribution of the aftershocks in depth. The dashed lines indicate possible breaks north of the main fault. The depth of the main shock is uncertain, and it could well be shallower than 8 km.

Figure II - 8. Frequency and cumulative distribution of the Kern County shocks with depth. For the frequency distribution divide the vertical scale by 10.

Figure II - 9. Frequency and cumulative distribution for the combined regions of Figure II - 5. For the frequency distribution, divide the vertical scale by 5.

Figure II - 10. Frequency and cumulative distribution for the combined regions of Figure II - 5, when the uncertainties in depth are taken into account by smoothing the histograms of Figure II - 9, according to section Part II. Divide the vertical scale by 5, for the frequency distribution.

Figure II - 11. Frequency and cumulative distribution for the energy of the combined regions of Figure II - 5.

Figure II - 12. Frequency and cumulative distribution for the energy of the combined regions of Figure II - 5.

Figure II - 13. Normalized cumulative distributions for the several regions in Figure II - 5. They refer to the total number of shocks in each region.

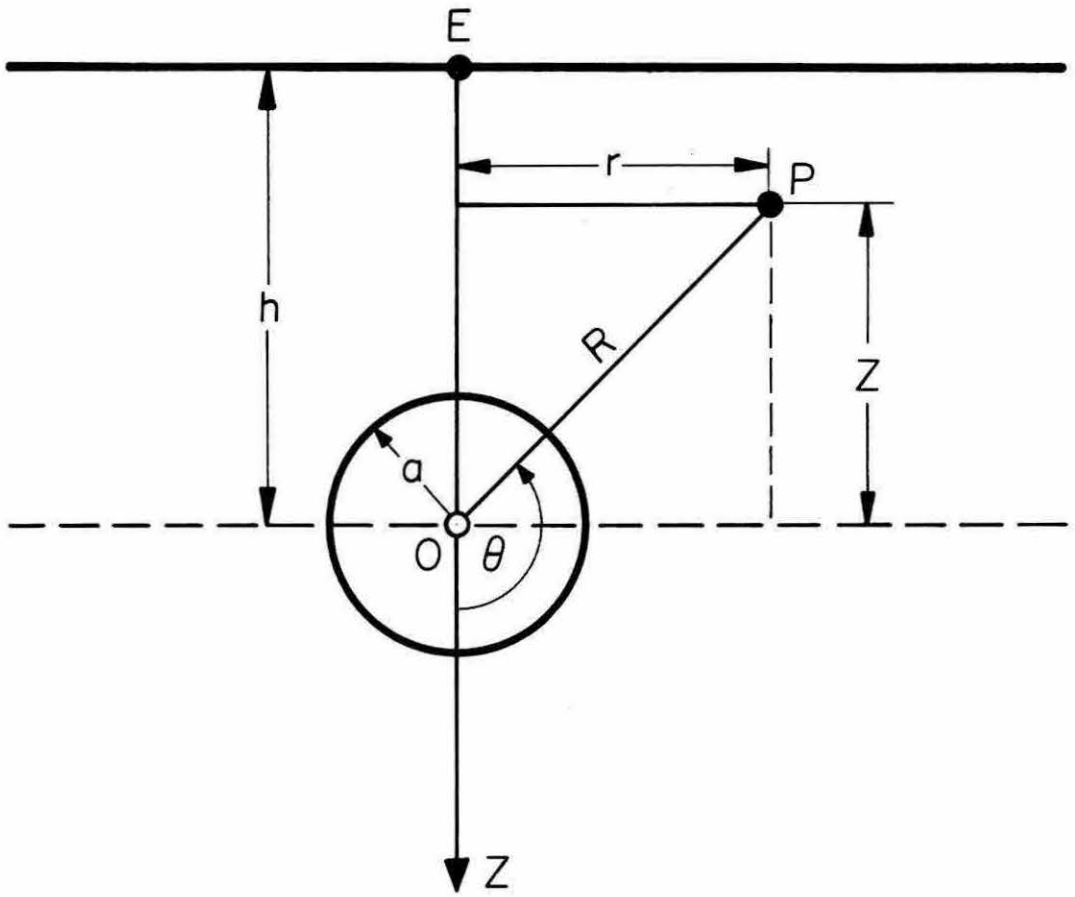

Figure I-1

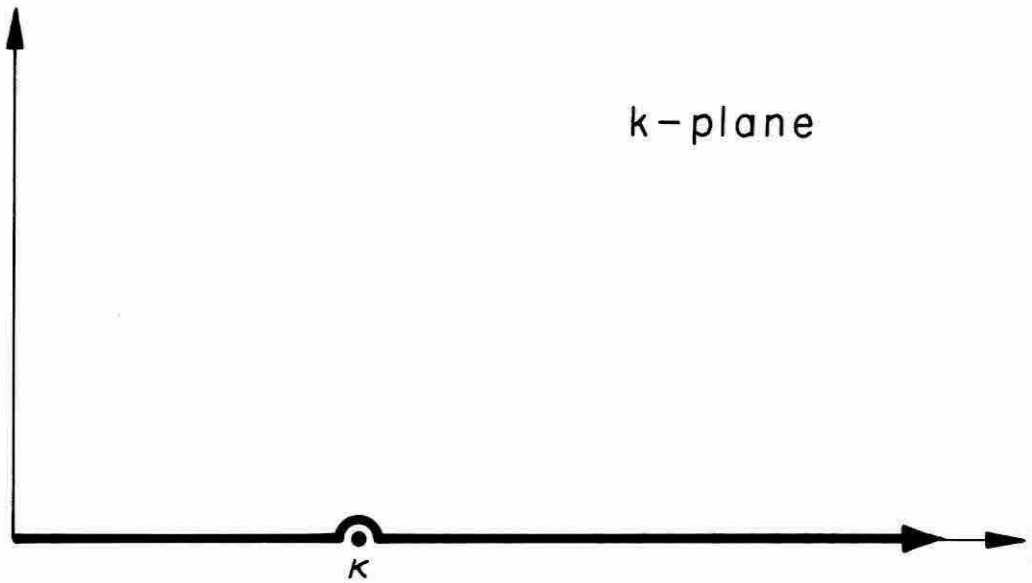

Figure 1-2

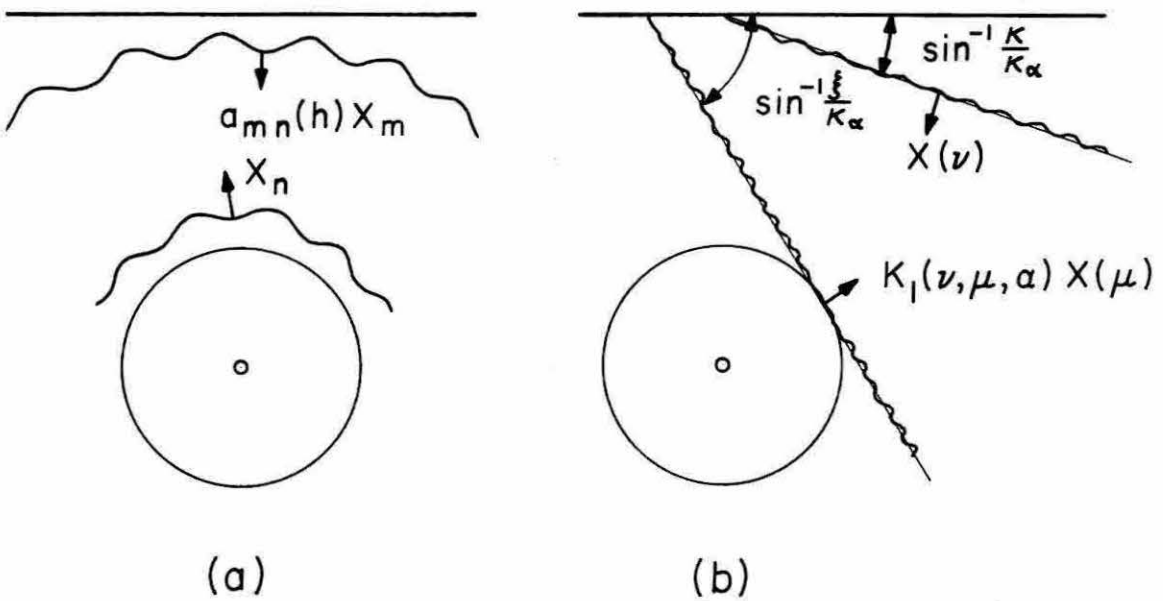
$a_{mn}(h)X_m$
X_n
(a)
$\sin^{-1}\frac{\kappa}{\kappa_\alpha}$
$\sin^{-1}\frac{\xi}{\kappa_\alpha}$
$X(\nu)$
$K_1(\nu,\mu,\alpha)\,X(\mu)$
(b)

Figure I-3

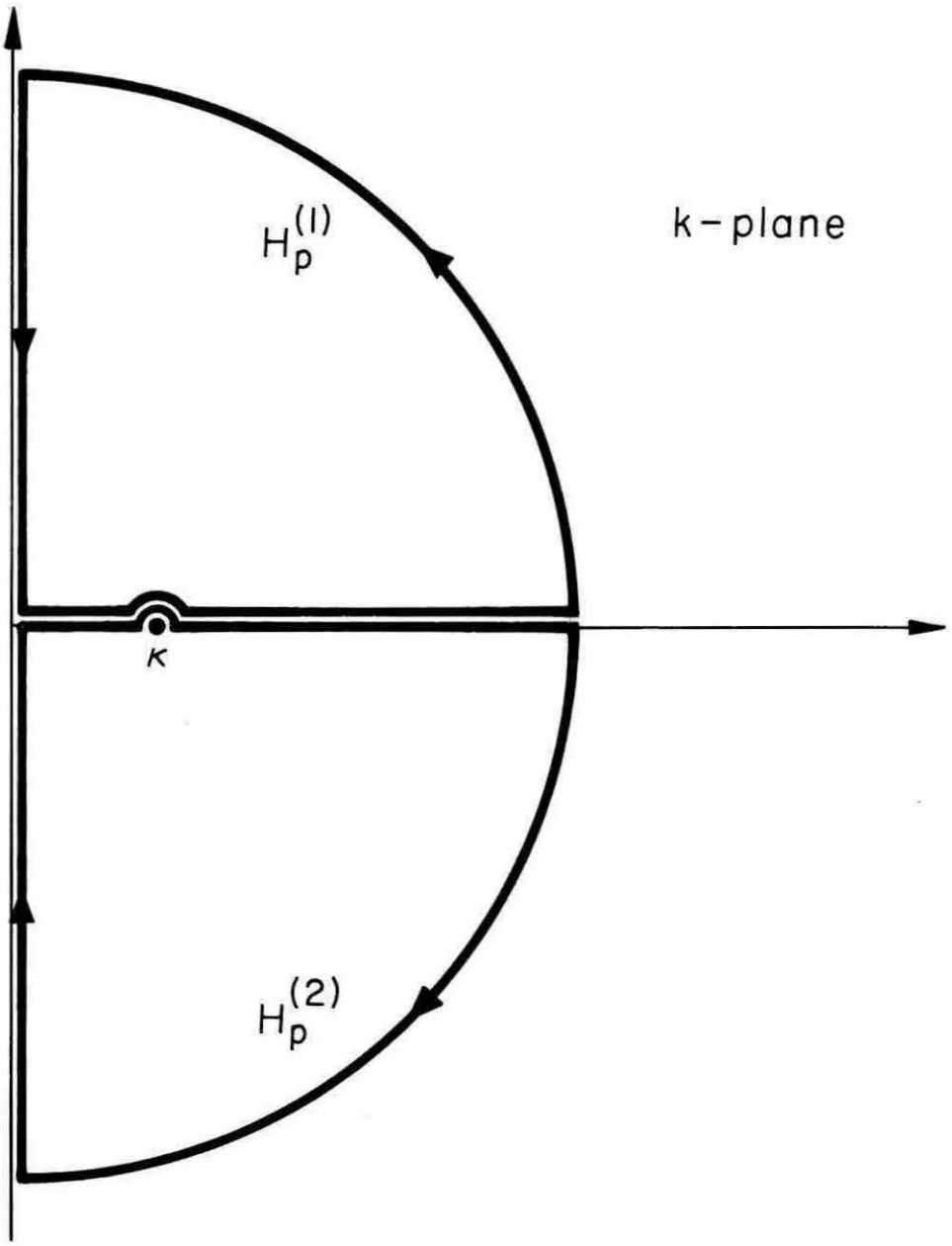

Figure 1-4

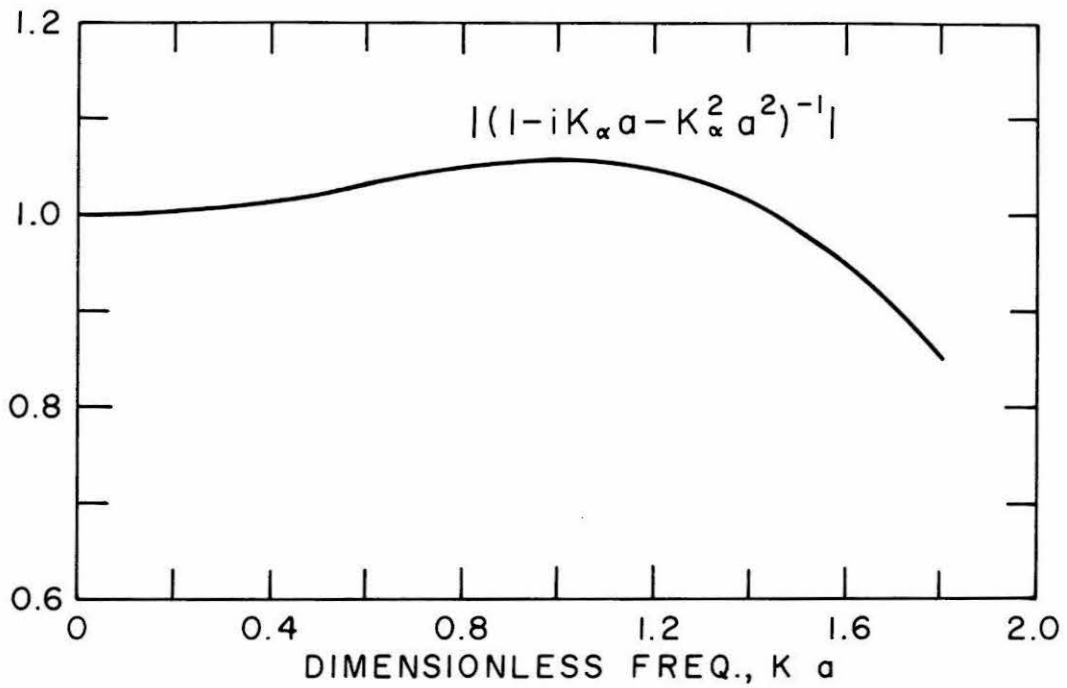
1.2
1.0
0.8
0.6
$|(1-iK_\alpha a-K_\alpha^2 a^2)^{-1}|$
0
0.4
0.8
1.2
1.6
2.0
DIMENSIONLESS FREQ., K a

Figure I-5

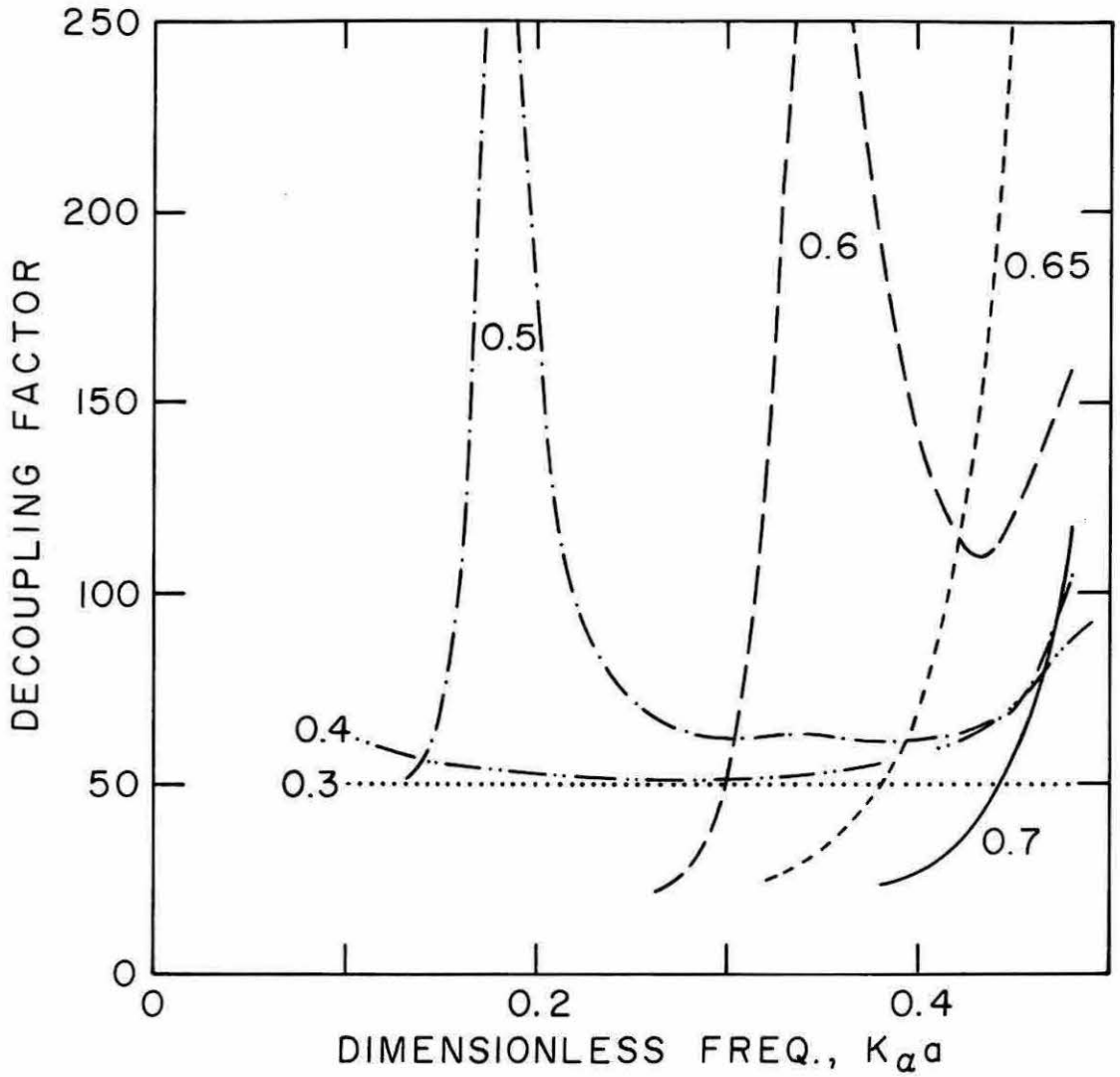
250
200
150
100
50
0
DECOUPLING FACTOR
0
0.2
0.4
DIMENSIONLESS FREQ., $K_a a$
0.3
0.4
0.5
0.6
0.65
0.7

Figure 1-6

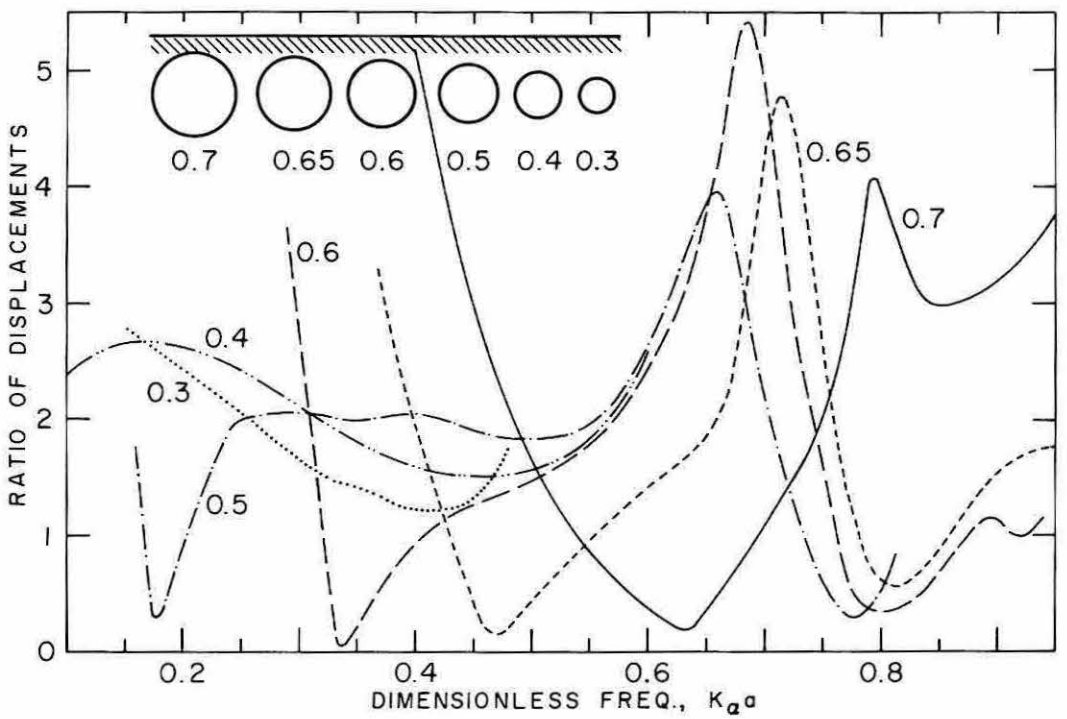
0.7
0.65
0.6
0.5
0.4
0.3
0.6
0.4
0.3
0.5
0.65
0.7
RATIO OF DISPLACEMENTS
0
1
2
3
4
5
0.2
0.4
0.6
0.8
DIMENSIONLESS FREQ., $K_a a$

Figure I-7

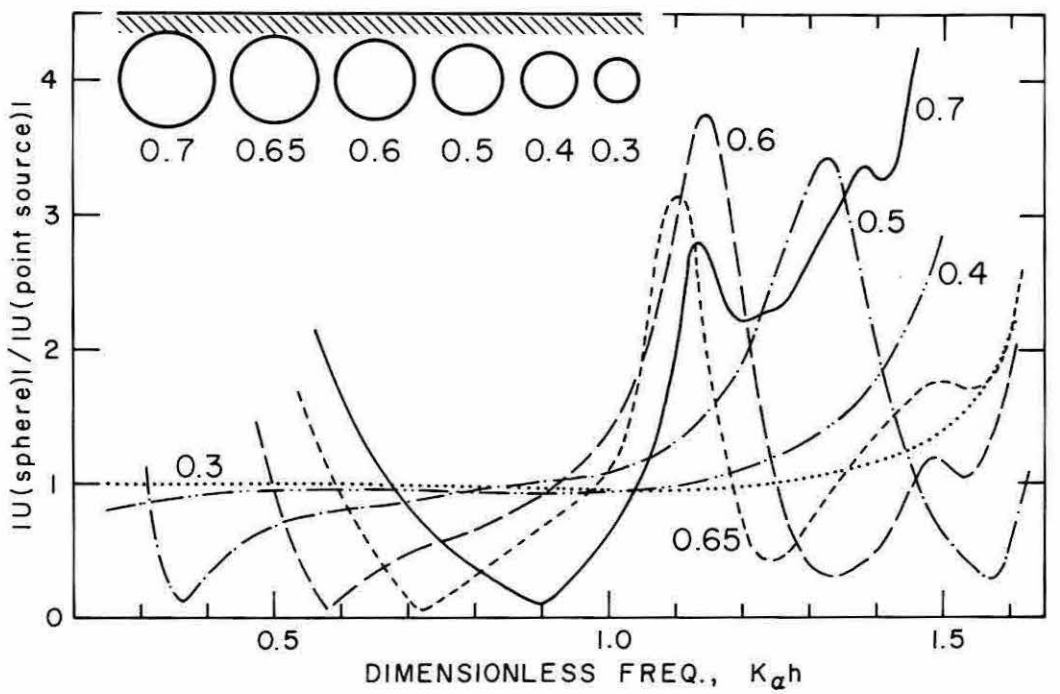
0.7
0.65
0.6
0.5
0.4
0.3
0.7
0.6
0.5
0.4
0.3
0.65
|U(sphere)| / |U(point source)|
0
1
2
3
4
0.5
1.0
1.5
DIMENSIONLESS FREQ., $K_a h$

Figure I-8

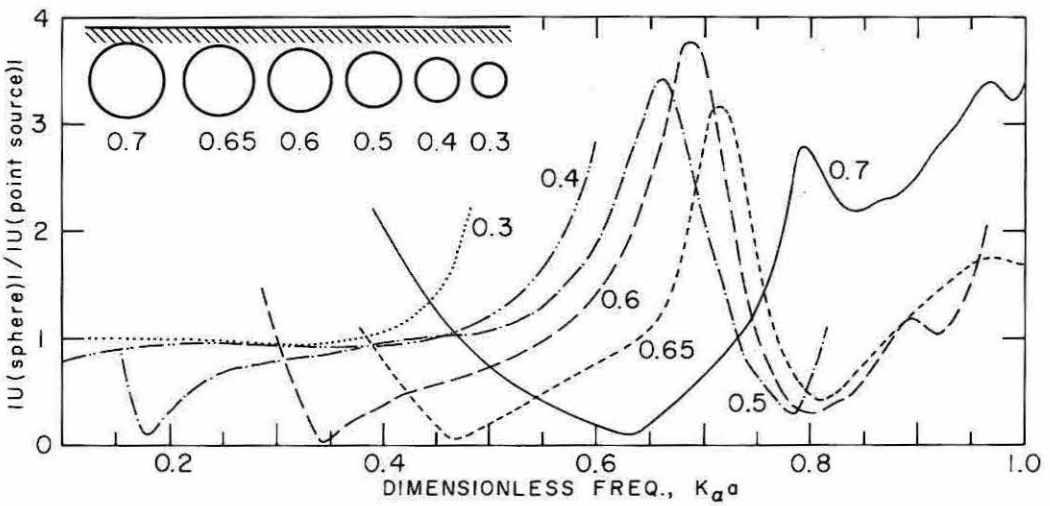
4
3
2
1
0
|U(sphere)| / |U(point source)|
0.7
0.65
0.6
0.5
0.4
0.3
0.4
0.3
0.6
0.65
0.7
0.5
0.2
0.4
0.6
0.8
1.0
DIMENSIONLESS FREQ., $K_a a$

Figure 1-9

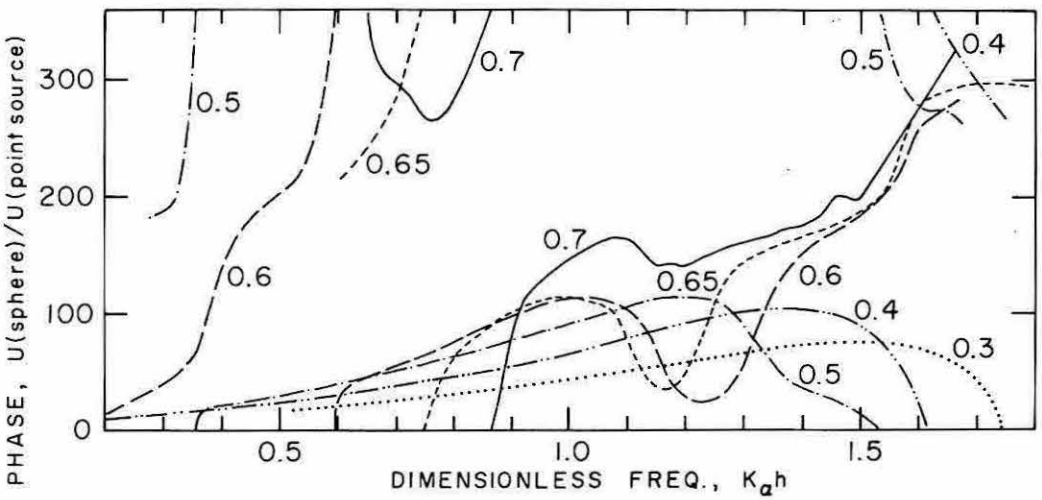
PHASE, U(sphere)/U(point source)
300
200
100
0
0.5
1.0
1.5
DIMENSIONLESS FREQ., $K_a h$
0.5
0.7
0.65
0.6
0.7
0.65
0.6
0.5
0.4
0.4
0.3
0.5

Figure 1-10

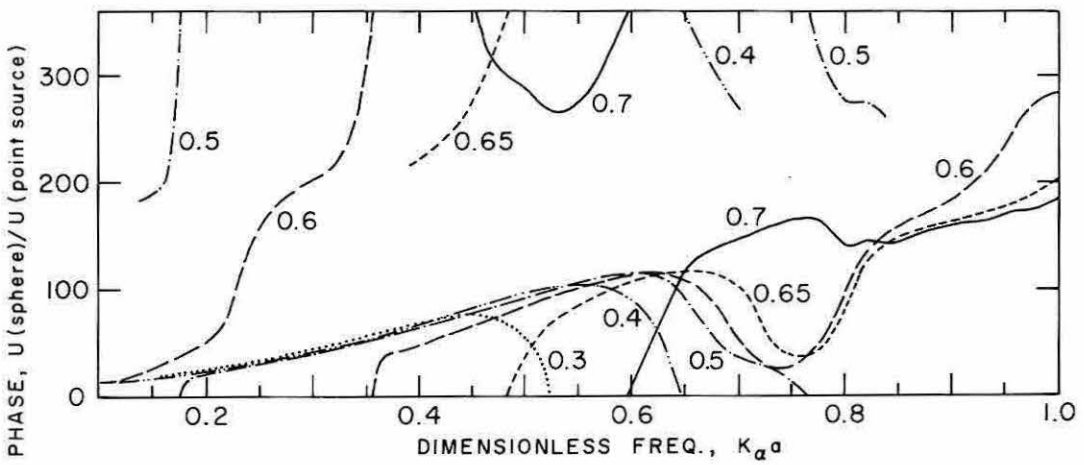
PHASE, U (sphere)/U (point source)
300
200
100
0
0.2
0.4
0.6
0.8
1.0
DIMENSIONLESS FREQ., $K_a a$
0.5
0.6
0.65
0.7
0.4
0.5
0.6
0.7
0.65
0.4
0.3
0.5

Figure I-11

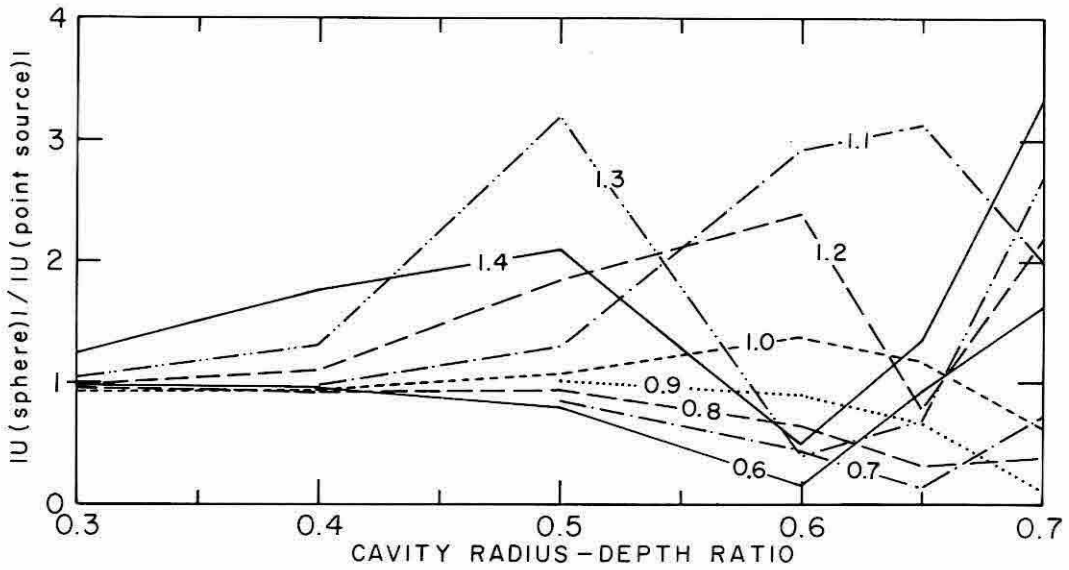
|U (sphere)| / |U (point source)|
4
3
2
1
0
0.3
0.4
0.5
0.6
0.7
CAVITY RADIUS-DEPTH RATIO
1.4
1.3
1.1
1.2
1.0
0.9
0.8
0.6
0.7

Figure 1-12

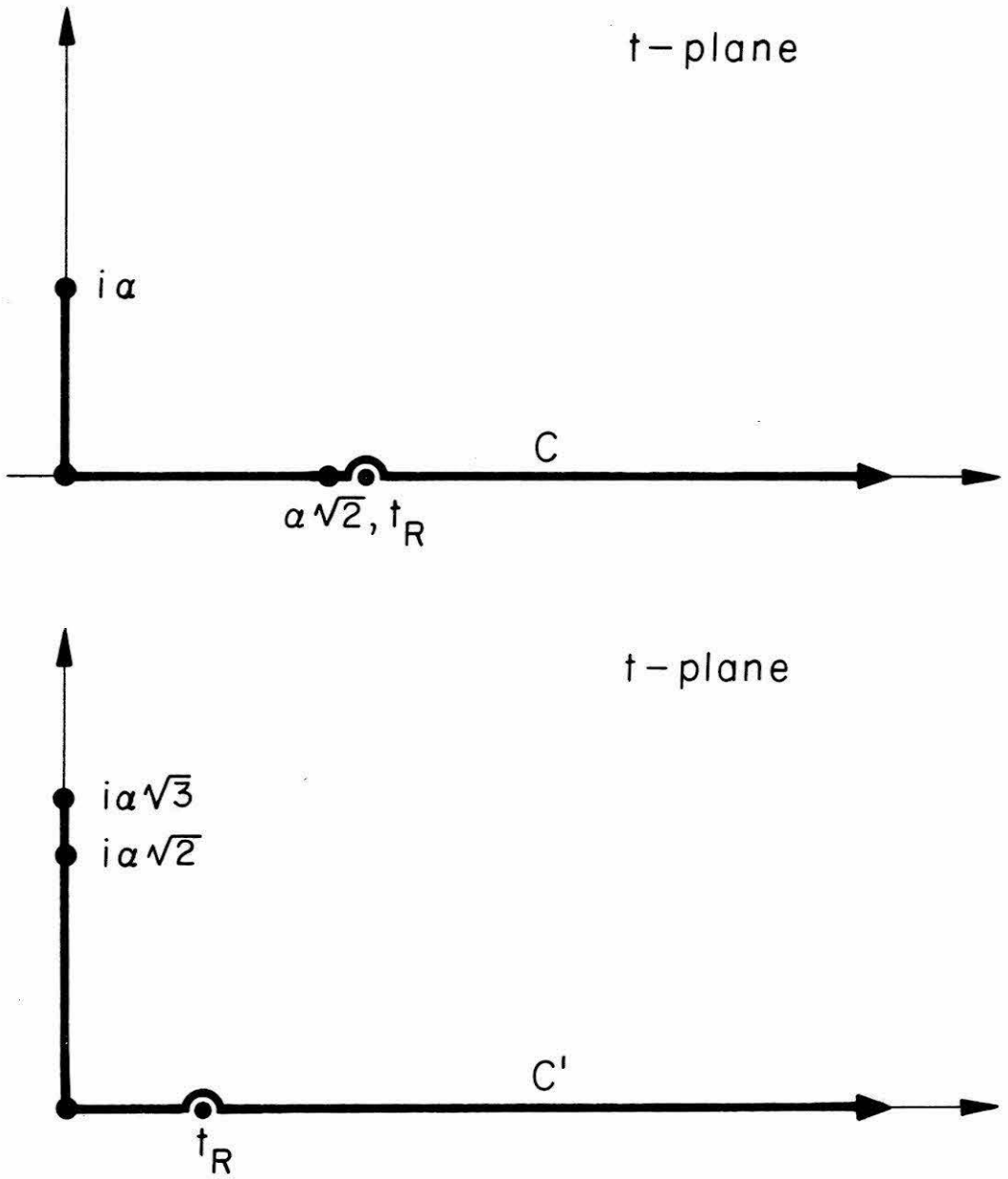

Figure I-13

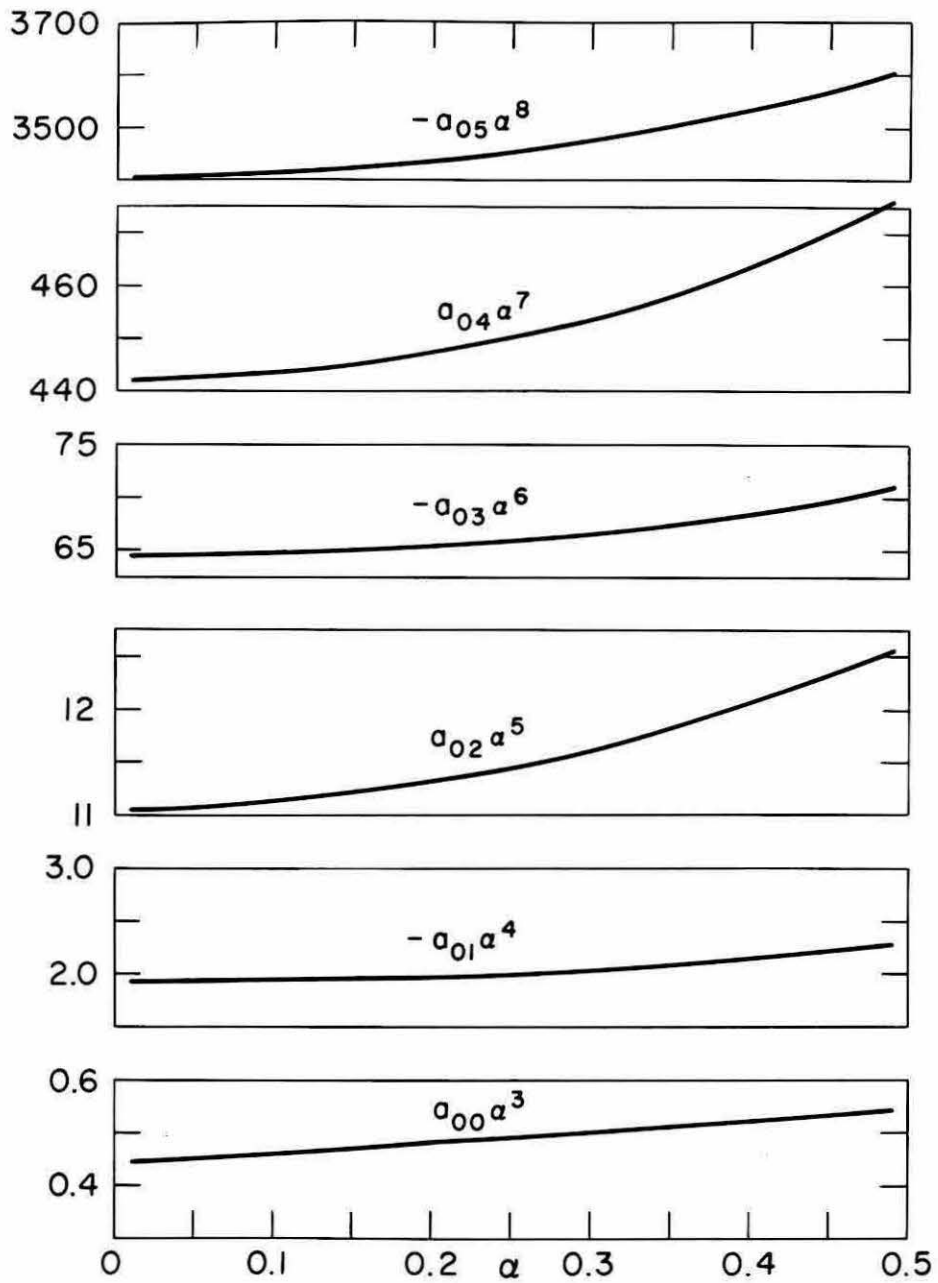
3700
3500
$-a_{05}\alpha^8$
460
440
$a_{04}\alpha^7$
75
65
$-a_{03}\alpha^6$
12
11
$a_{02}\alpha^5$
3.0
2.0
$-a_{01}\alpha^4$
0.6
0.4
$a_{00}\alpha^3$
0
0.1
0.2
α
0.3
0.4
0.5

Figure 1-14

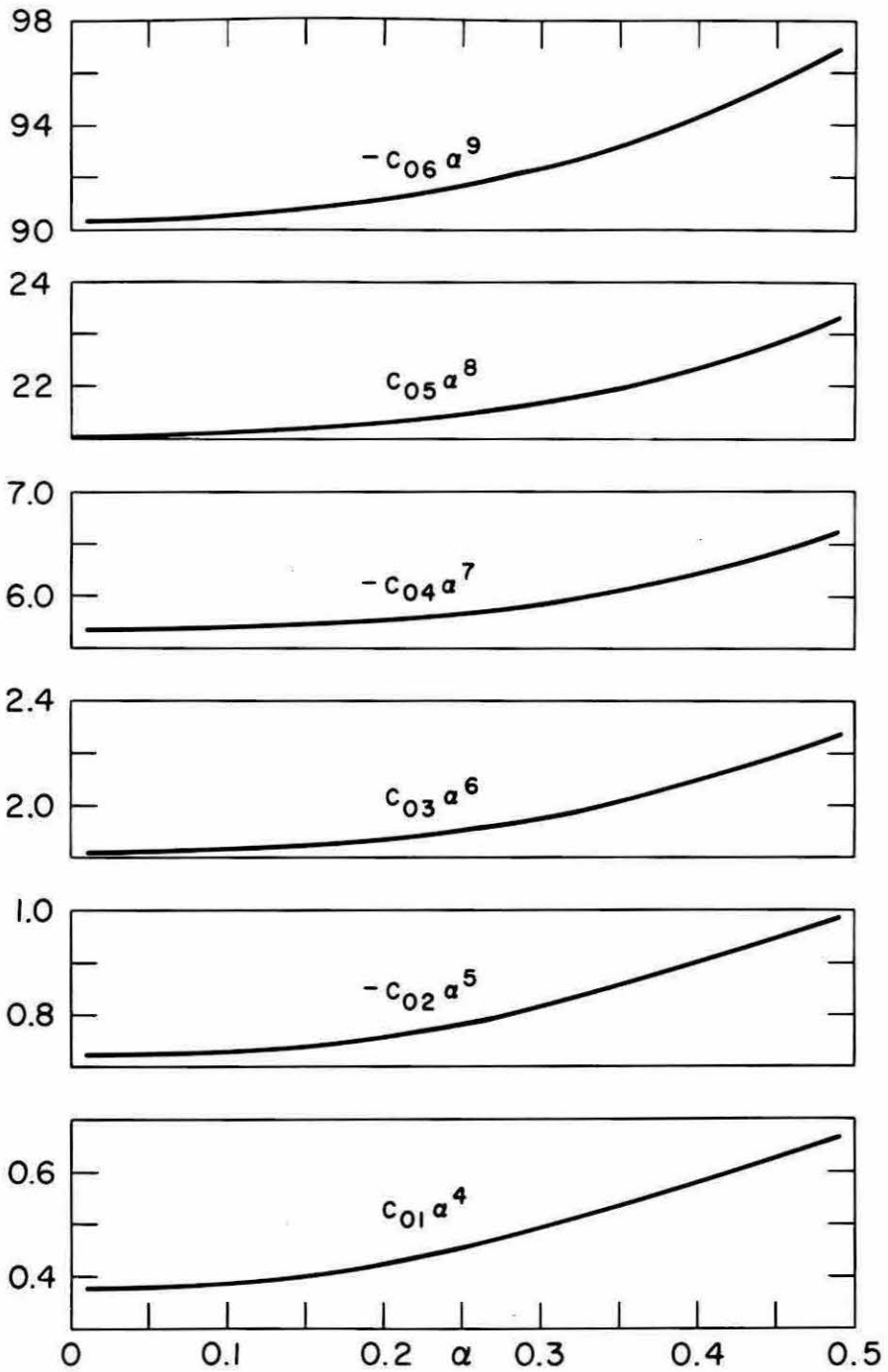
98
94
90
$-c_{06}\alpha^9$
24
22
$c_{05}\alpha^8$
7.0
6.0
$-c_{04}\alpha^7$
2.4
2.0
$c_{03}\alpha^6$
1.0
0.8
$-c_{02}\alpha^5$
0.6
0.4
$c_{01}\alpha^4$
0
0.1
0.2
α
0.3
0.4
0.5

Figure 1-15

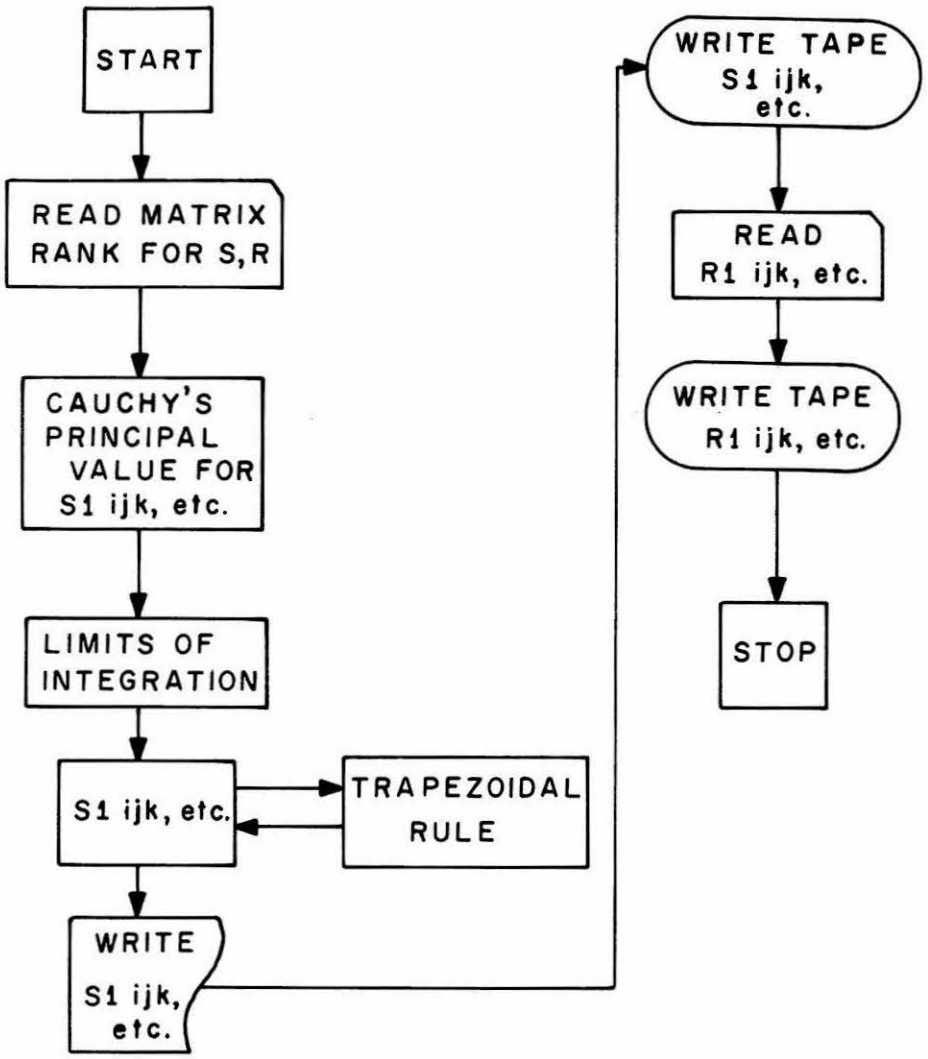
START
READ MATRIX RANK FOR S,R
CAUCHY'S PRINCIPAL VALUE FOR S1 ijk, etc.
LIMITS OF INTEGRATION
S1 ijk, etc.
TRAPEZOIDAL RULE
WRITE S1 ijk, etc.
WRITE TAPE S1 ijk, etc.
READ R1 ijk, etc.
WRITE TAPE R1 ijk, etc.
STOP

Figure I-16

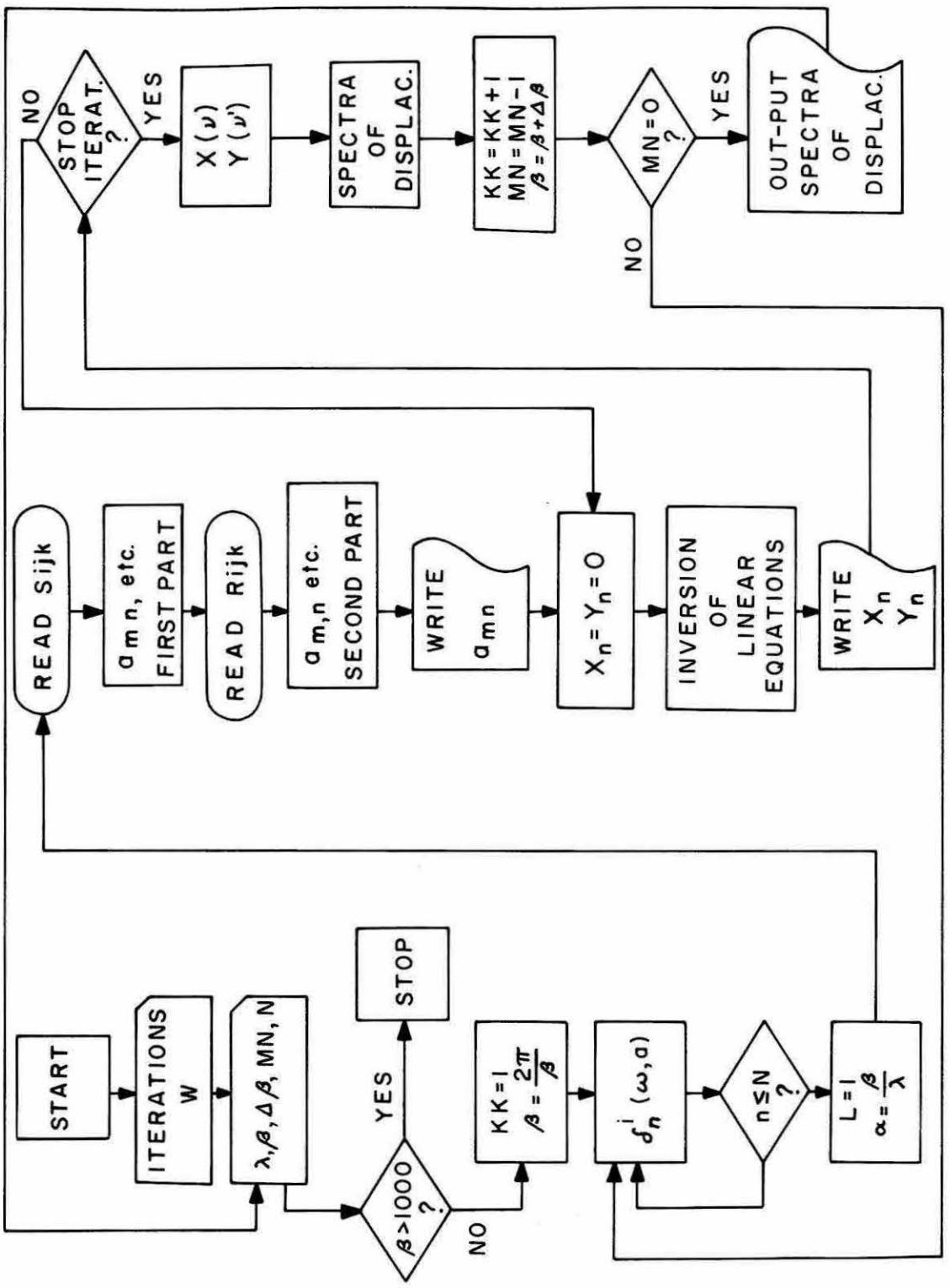
START
ITERATIONS W
λ, β, Δβ, MN, N
β>1000 ?
YES
STOP
NO
KK=1
β = 2π/β
$\delta_n^i(\omega,\alpha)$
n≤N ?
L=1
α = β/λ
READ Sijk
a_{mn}, etc. FIRST PART
READ Rijk
$a_{m,n}$ etc. SECOND PART
WRITE a_{mn}
$X_n = Y_n = 0$
INVERSION OF LINEAR EQUATIONS
WRITE X_n Y_n
STOP ITERAT. ?
NO
YES
X(ν) Y(ν')
SPECTRA OF DISPLAC.
KK=KK+1
MN=MN-1
β=β+Δβ
MN=0 ?
YES
NO
OUT-PUT SPECTRA OF DISPLAC.

Figure I-17

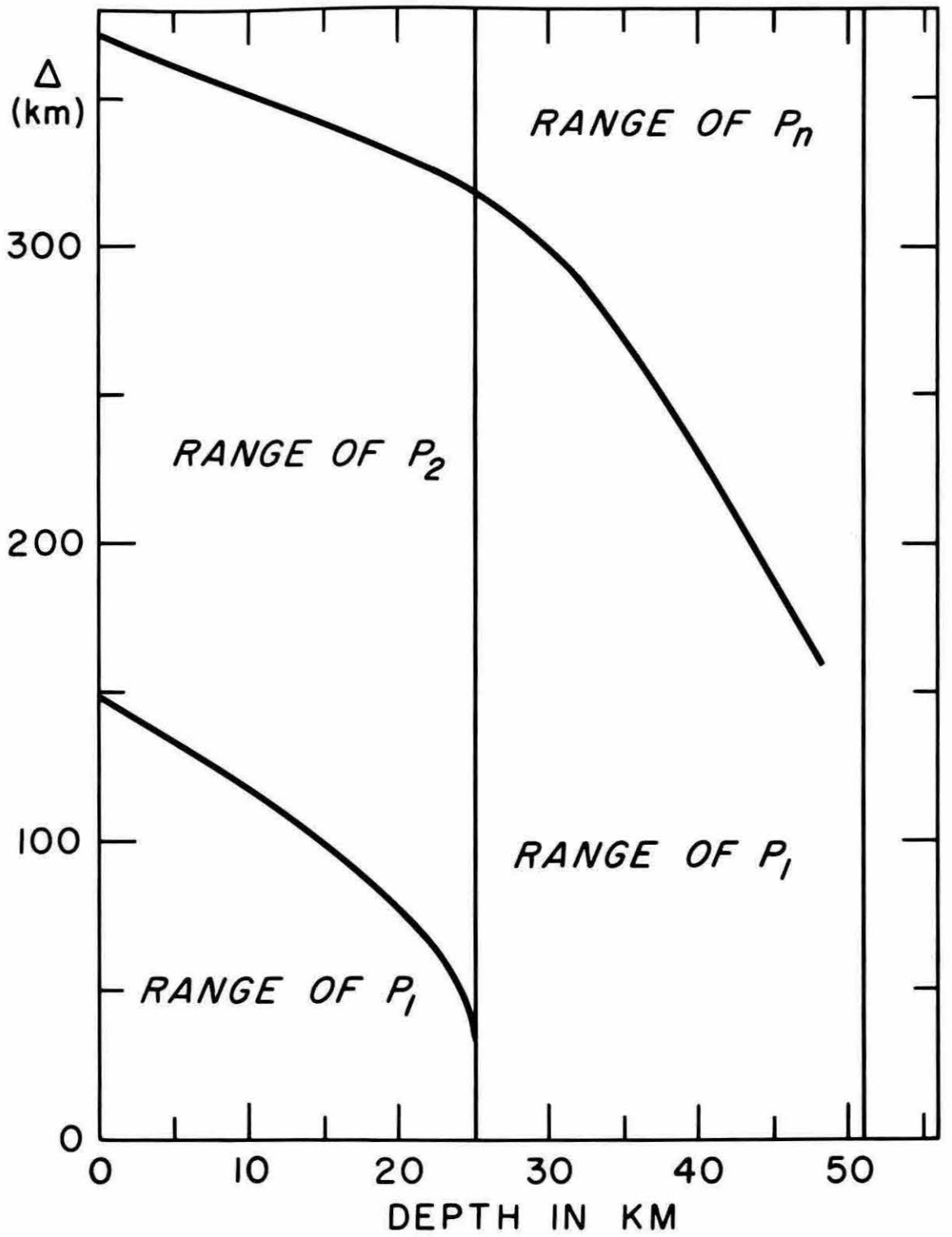
Δ
(km)
300
200
100
0
RANGE OF P_n
RANGE OF P_2
RANGE OF P_1
RANGE OF P_1
0
10
20
30
40
50
DEPTH IN KM

Figure II-1

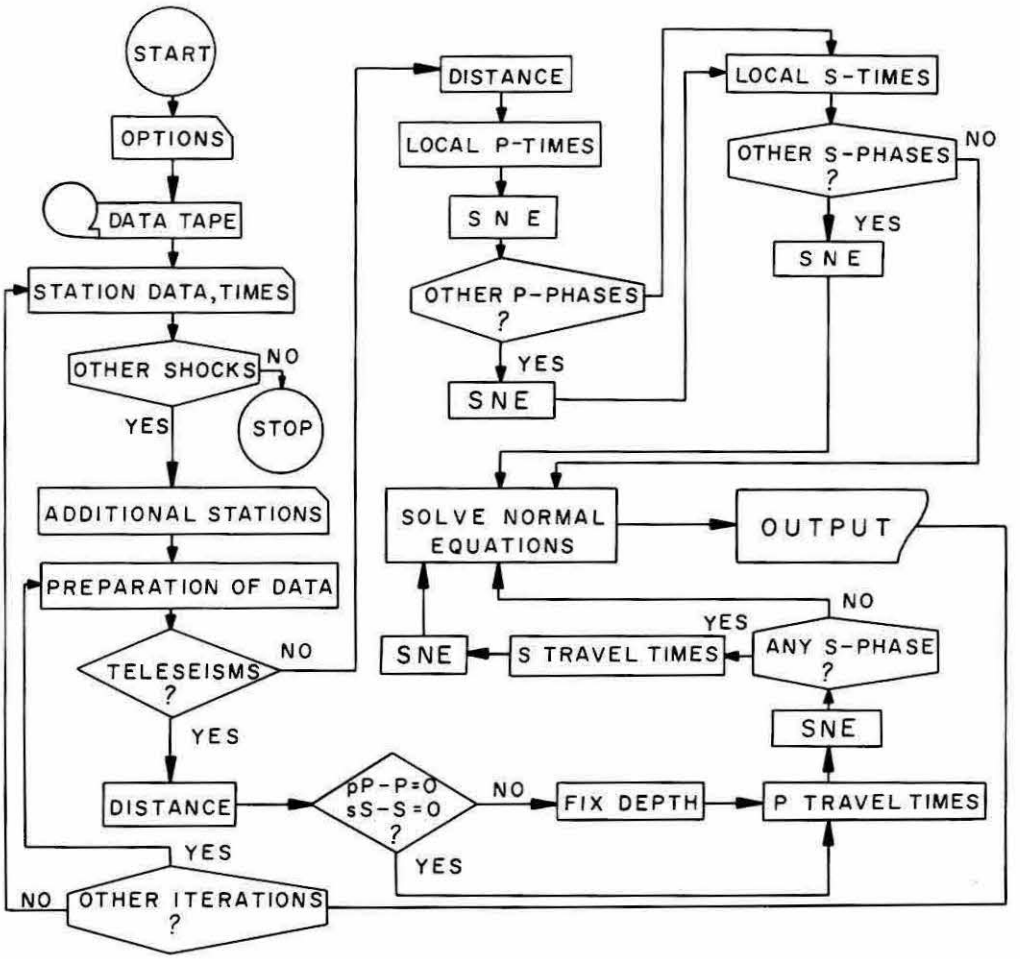

SNE: SET COEFFICIENTS OF NORMAL EQUATIONS

Figure II-2

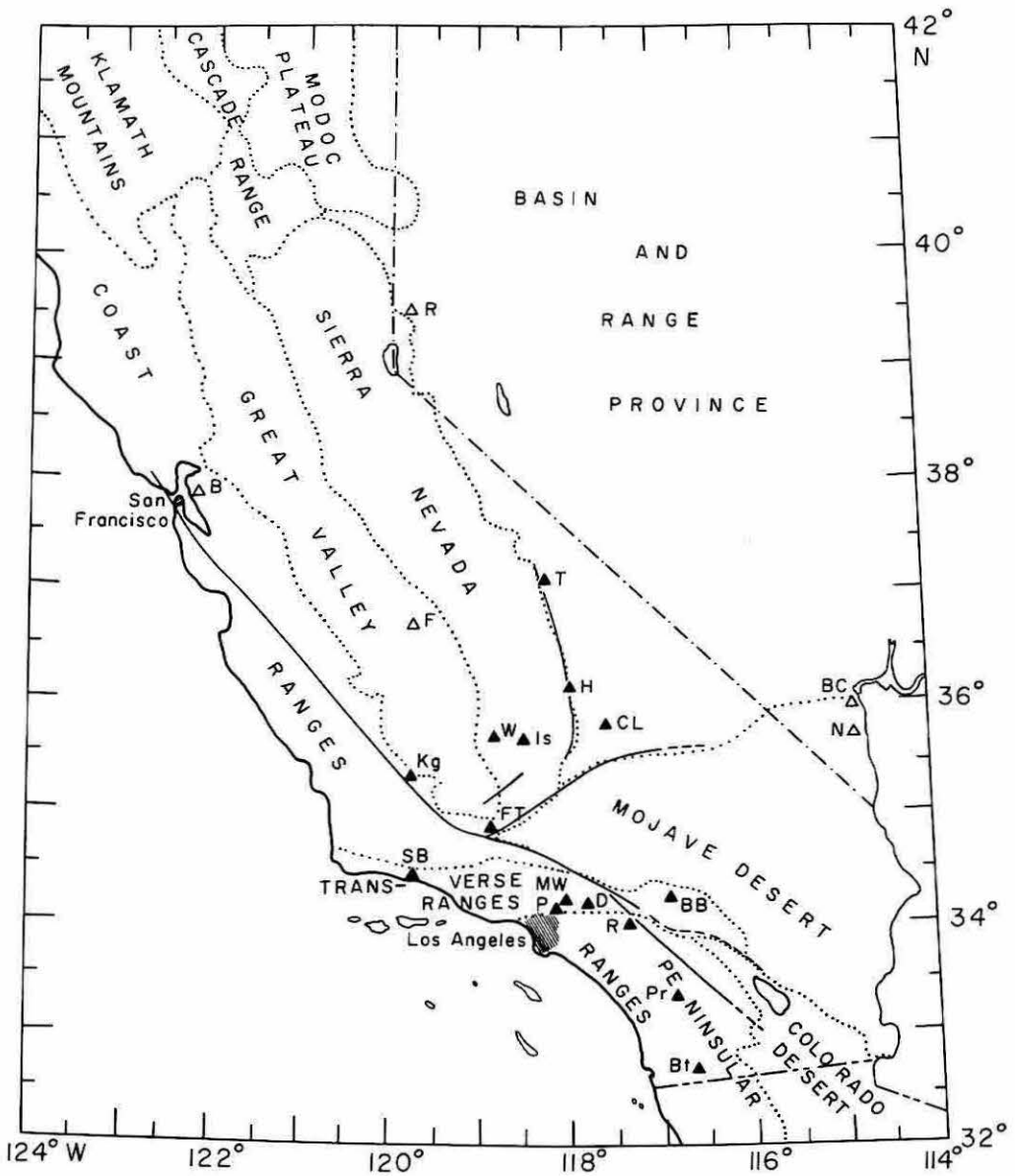
42° N
40°
38°
36°
34°
32°
124° W
122°
120°
118°
116°
114°
KLAMATH MOUNTAINS
CASCADE RANGE
MODOC PLATEAU
BASIN AND RANGE PROVINCE
COAST RANGES
SIERRA NEVADA
GREAT VALLEY
San Francisco
B
R
F
T
H
W
Is
CL
Kg
FT
BC
N
SB
TRANS-VERSE RANGES
MW
P
D
R
BB
Los Angeles
PENINSULAR RANGES
Pr
Bt
MOJAVE DESERT
COLORADO DESERT

Figure II-3

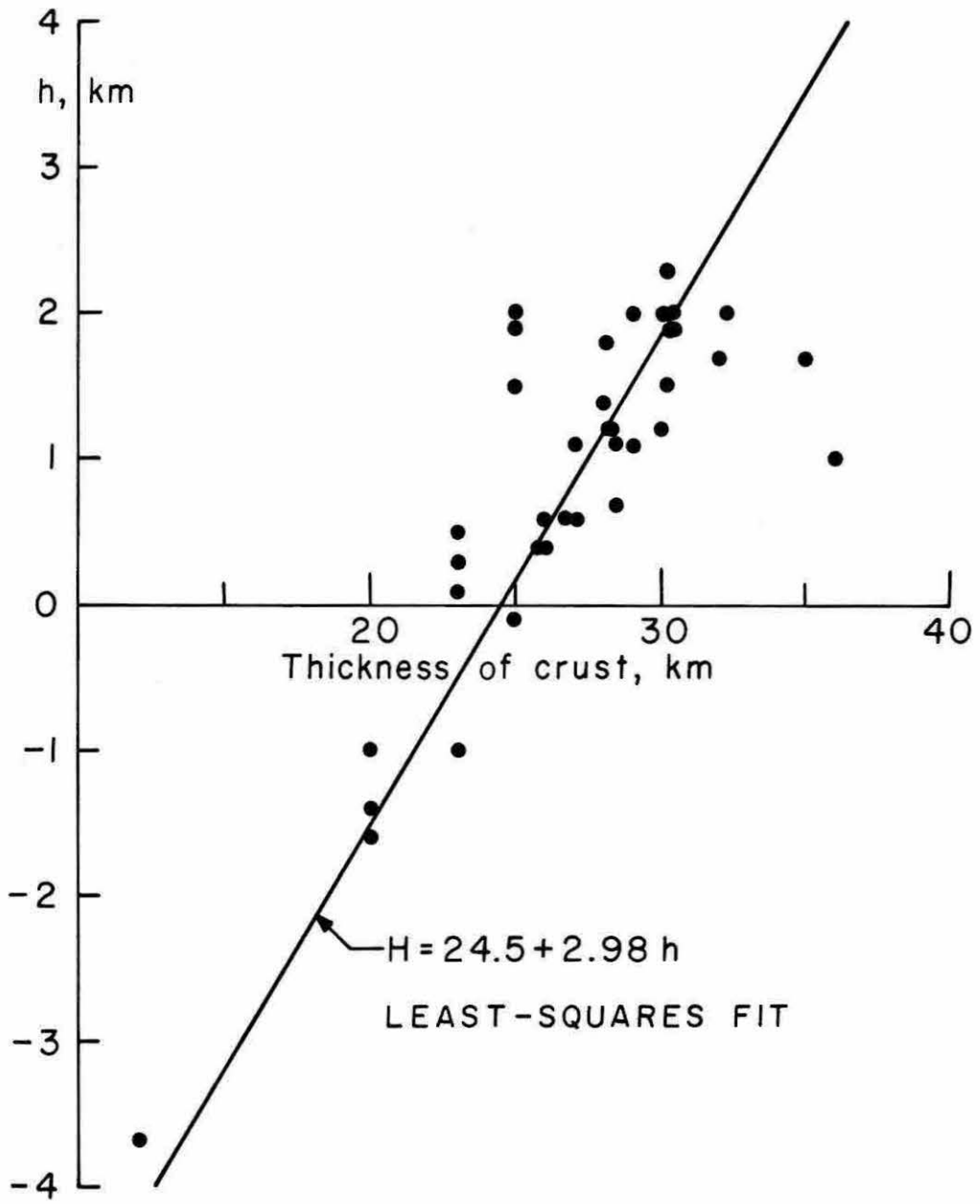
4
h, km
3
2
1
0
-1
-2
-3
-4
20
30
40
Thickness of crust, km
H = 24.5 + 2.98 h
LEAST-SQUARES FIT

Figure II-4

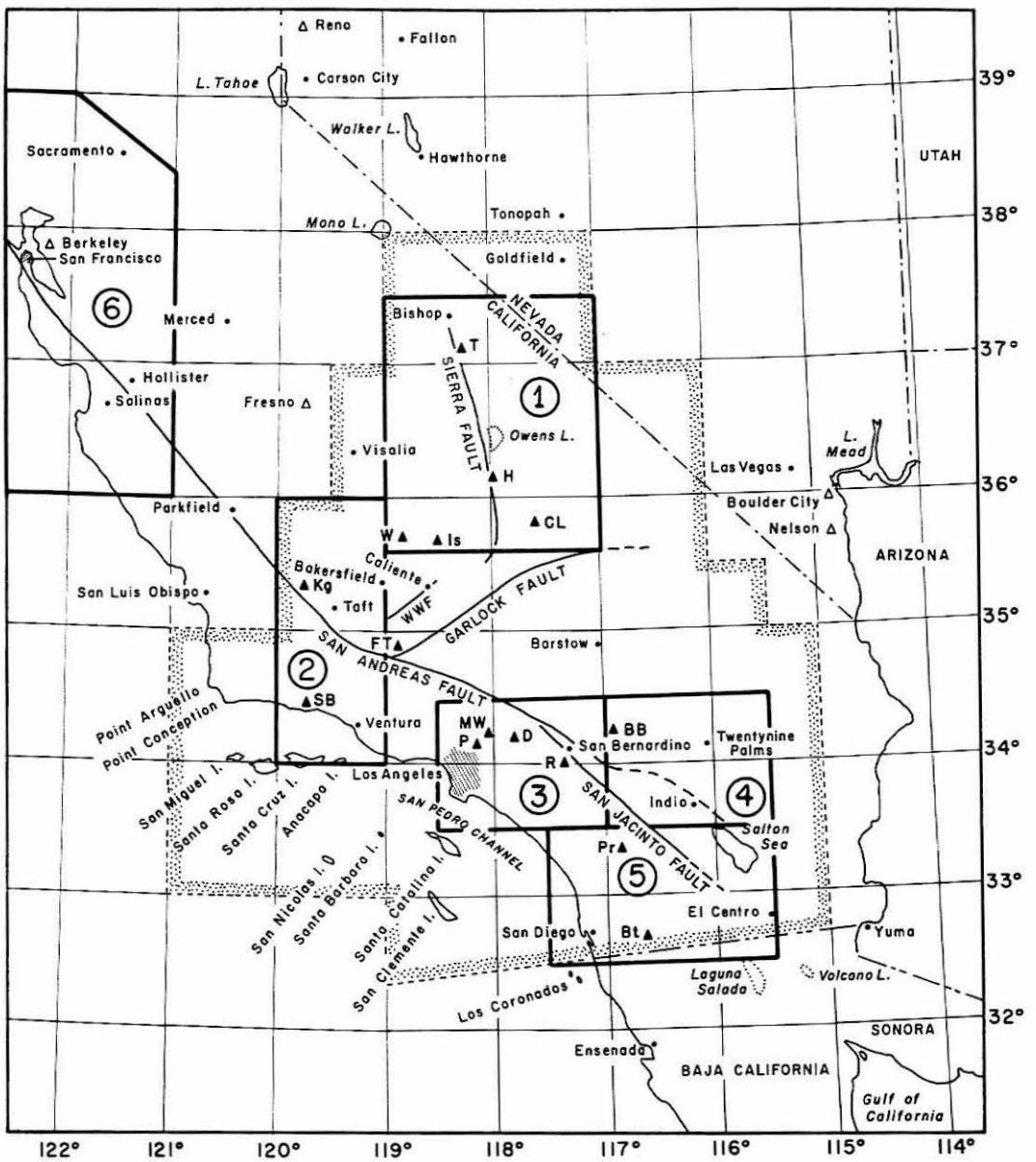
Reno
Fallon
L. Tahoe
Carson City
Walker L.
Hawthorne
Sacramento
UTAH
Mono L.
Tonopah
Berkeley
San Francisco
Goldfield
NEVADA
CALIFORNIA
Bishop
T
Merced
Hollister
Salinas
Fresno
SIERRA FAULT
Owens L.
Visalia
H
Las Vegas
L. Mead
Parkfield
W
Is
CL
Boulder City
Nelson
ARIZONA
Bakersfield
Kg
Caliente
San Luis Obispo
Taft
WWF
GARLOCK FAULT
FT
Barstow
SAN ANDREAS FAULT
SB
Ventura
Point Arguello
Point Conception
MW
P
D
BB
San Bernardino
Twentynine Palms
R
Los Angeles
San Miguel I.
Santa Rosa I.
Santa Cruz I.
Anacapa I.
SAN PEDRO CHANNEL
Indio
SAN JACINTO FAULT
Salton Sea
Pr
San Nicolas I.
Santa Barbara I.
Santa Catalina I.
San Clemente I.
El Centro
San Diego
Bt
Yuma
Laguna Salada
Volcano L.
Los Coronados
SONORA
Ensenada
BAJA CALIFORNIA
Gulf of California
39°
38°
37°
36°
35°
34°
33°
32°
122°
121°
120°
119°
118°
117°
116°
115°
114°

Figure 11-5

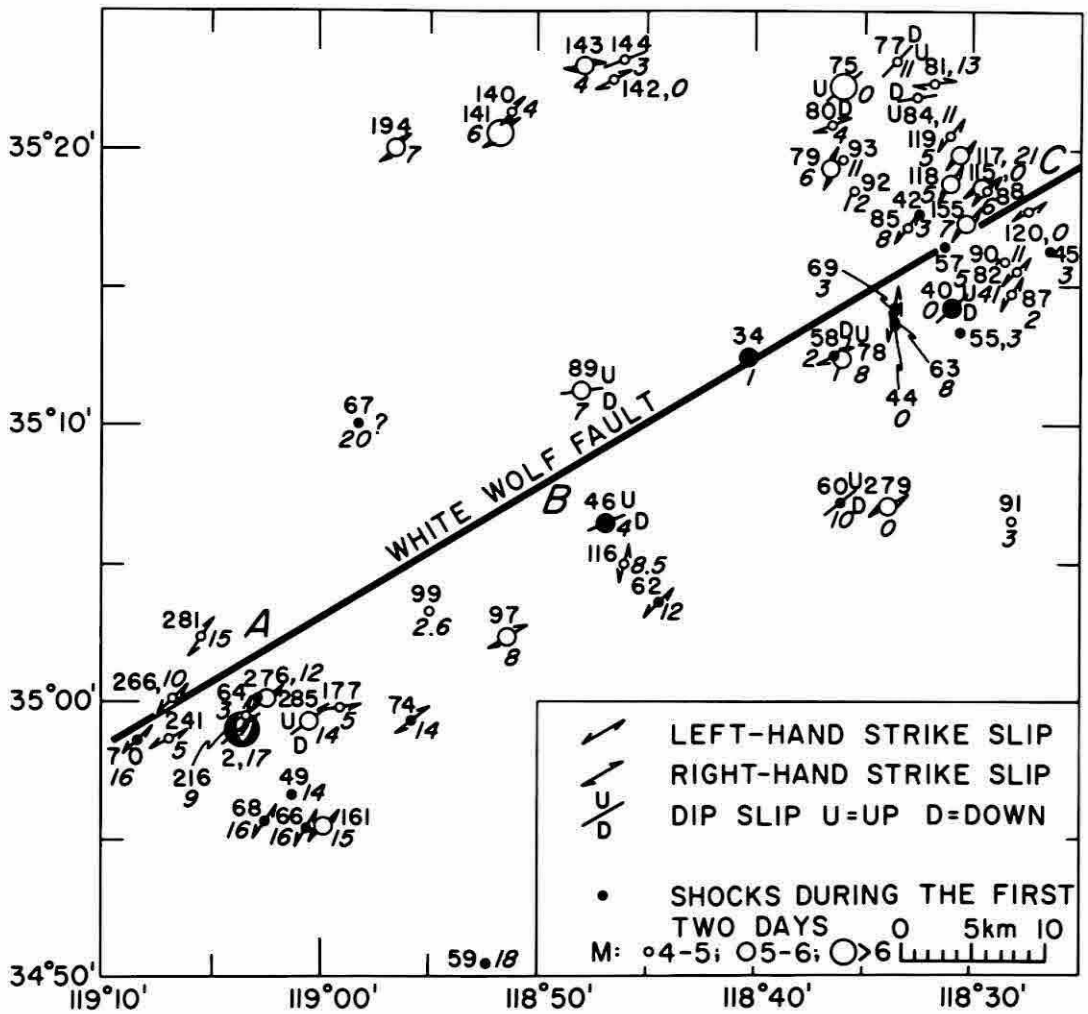
35°20'
35°10'
35°00'
34°50'
119°10'
119°00'
118°50'
118°40'
118°30'
WHITE WOLF FAULT
A
B
C
LEFT-HAND STRIKE SLIP
RIGHT-HAND STRIKE SLIP
DIP SLIP U=UP D=DOWN
SHOCKS DURING THE FIRST TWO DAYS
M: ○4-5; ○5-6; ◯>6
0 5km 10

Figure 11-6

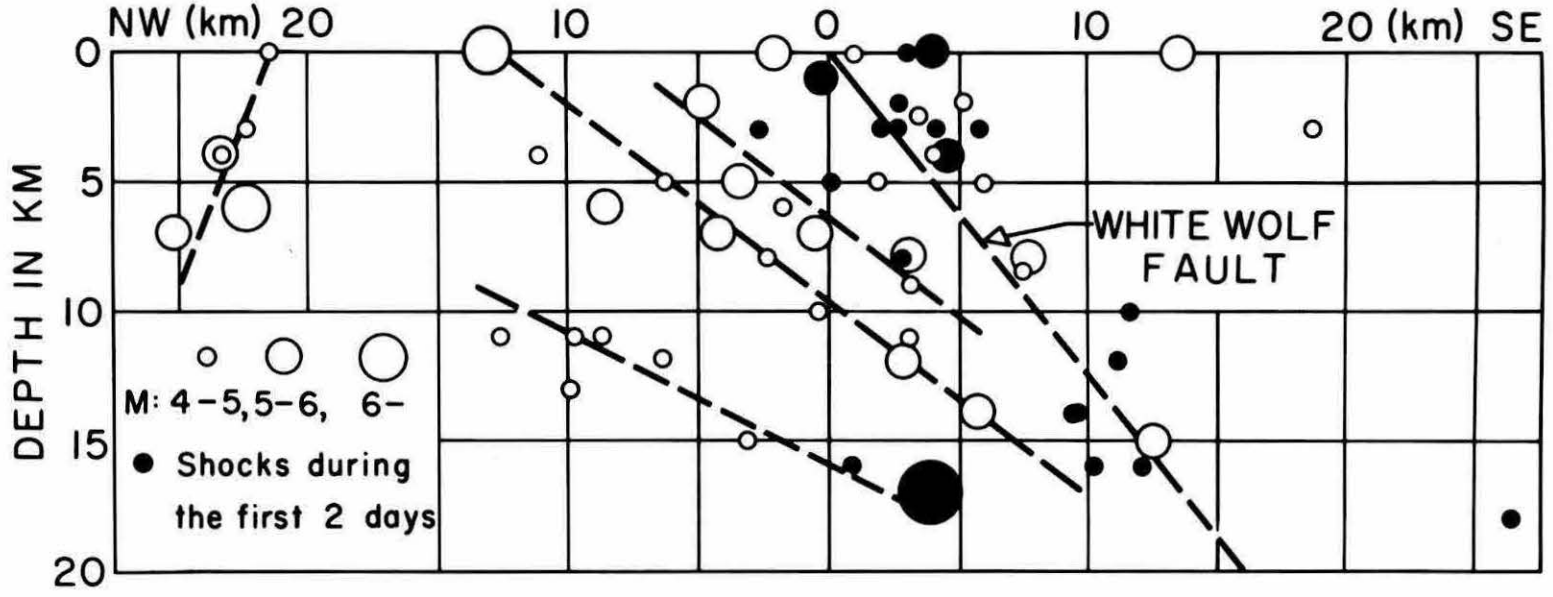
NW (km) 20
10
0
10
20 (km) SE
DEPTH IN KM
0
5
10
15
20
WHITE WOLF
FAULT
M: 4-5, 5-6, 6-
Shocks during
the first 2 days

Figure II-7

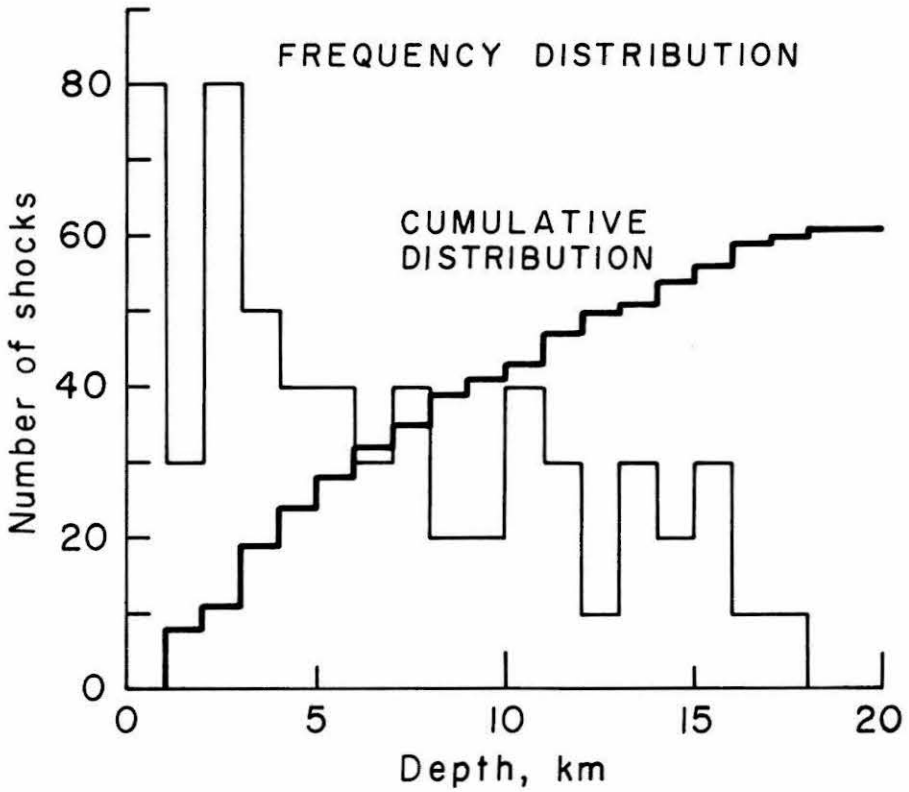
FREQUENCY DISTRIBUTION
CUMULATIVE
DISTRIBUTION
Number of shocks
80
60
40
20
0
0
5
10
15
20
Depth, km

Figure 11-8

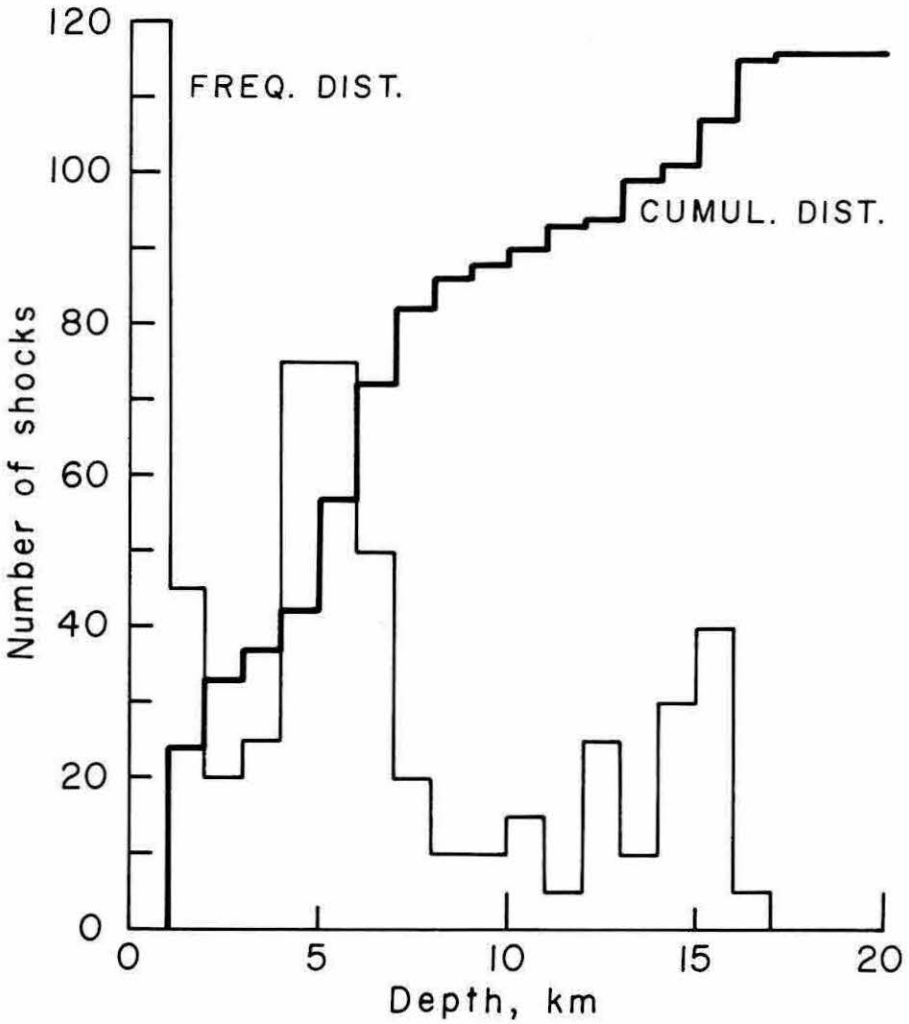
120
100
80
60
40
20
0
Number of shocks
FREQ. DIST.
CUMUL. DIST.
0
5
10
15
20
Depth, km

Figure 11-9

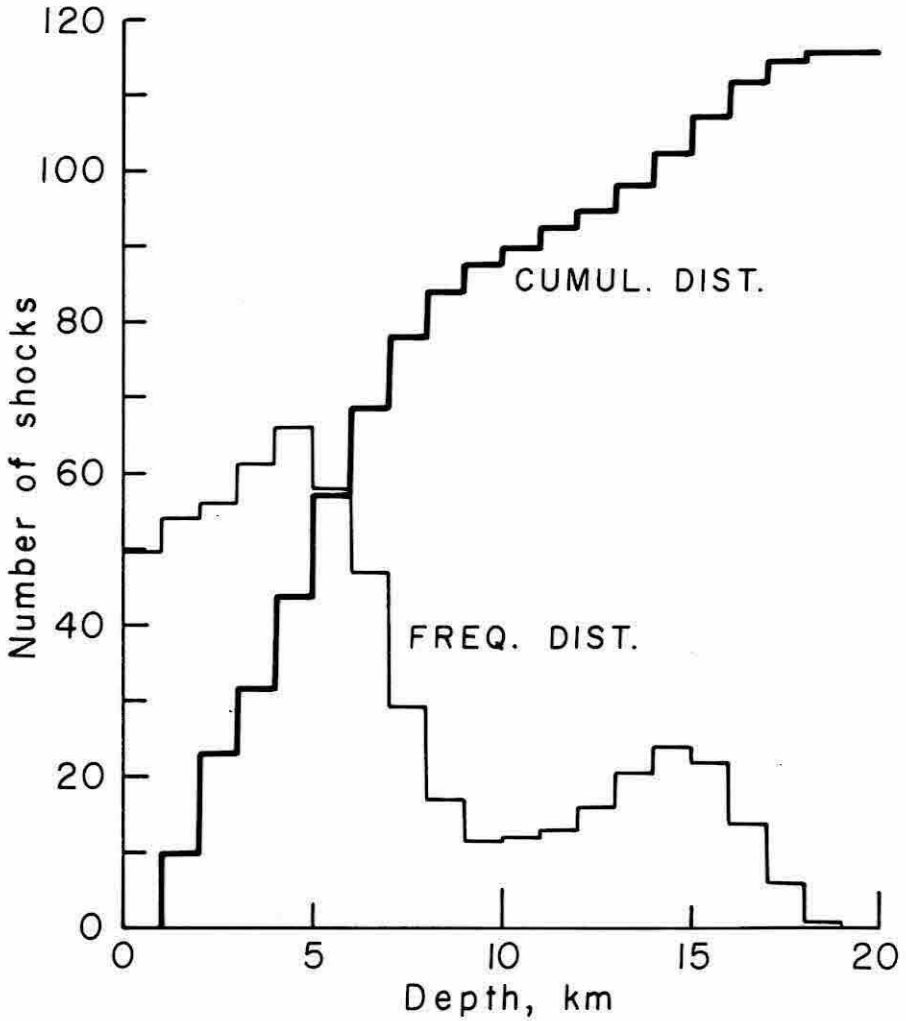
120
100
80
60
40
20
0
Number of shocks
CUMUL. DIST.
FREQ. DIST.
0
5
10
15
20
Depth, km

Figure 11-10

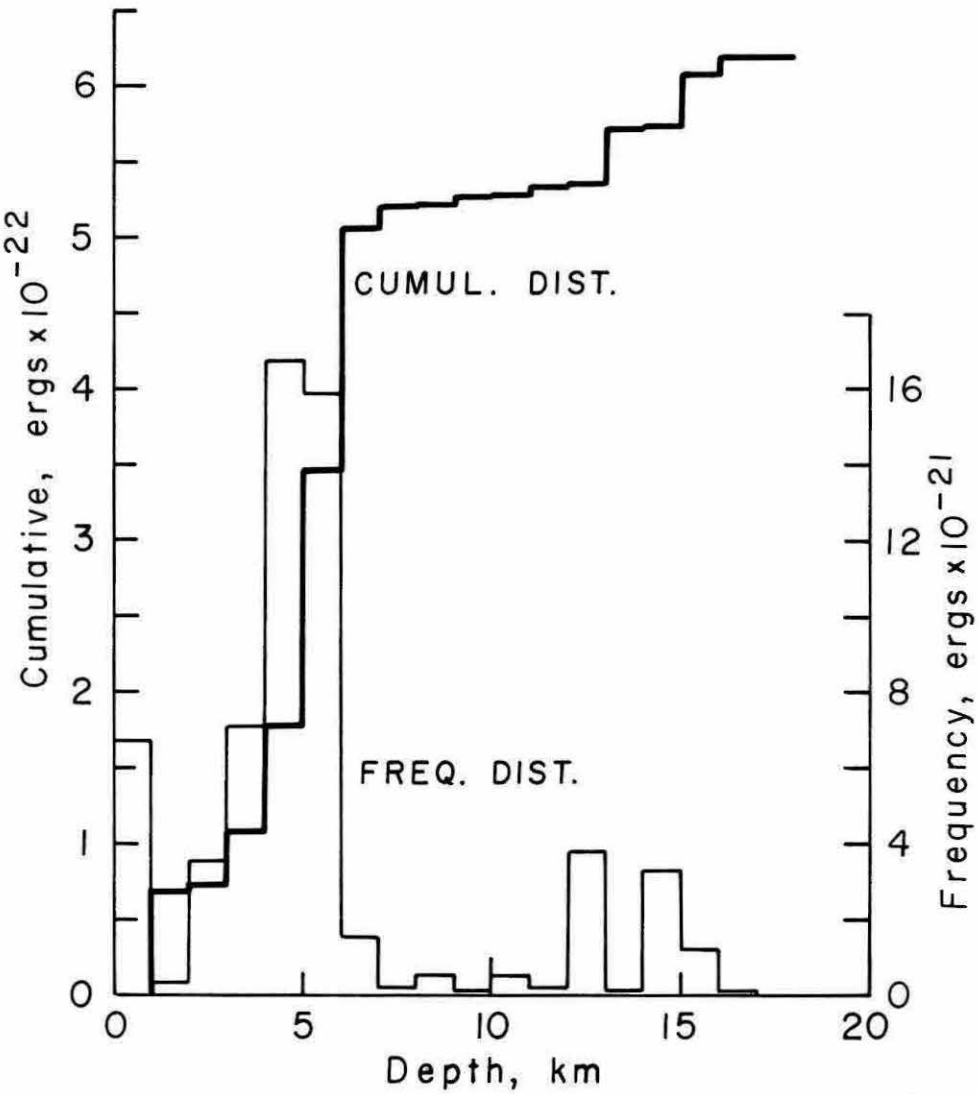
Cumulative, ergs x 10^-22
Frequency, ergs x 10^-21
CUMUL. DIST.
FREQ. DIST.
Depth, km
0
1
2
3
4
5
6
0
4
8
12
16
0
5
10
15
20

Figure II-11

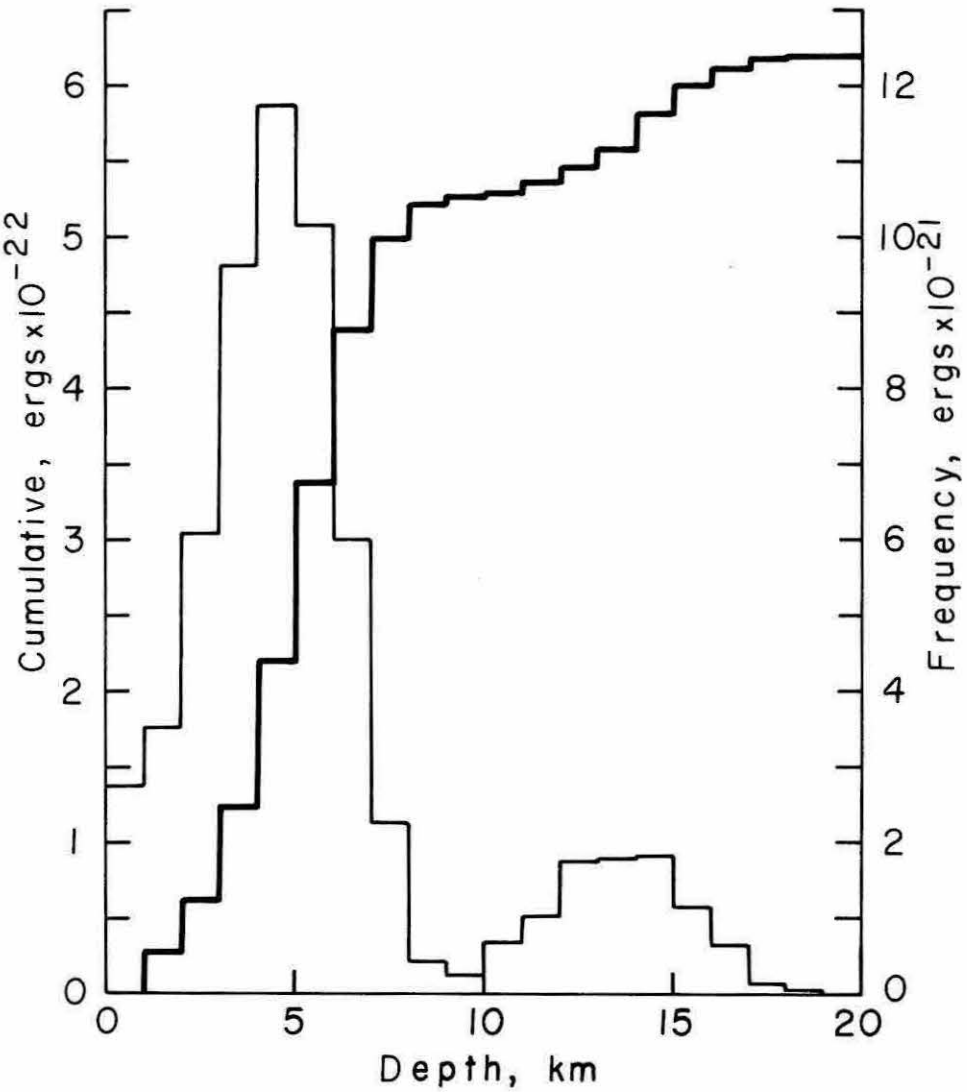
Cumulative, ergs x10^-22
Frequency, ergs x10^-21
Depth, km
0
1
2
3
4
5
6
0
2
4
6
8
10
12
0
5
10
15
20

Figure 11-12

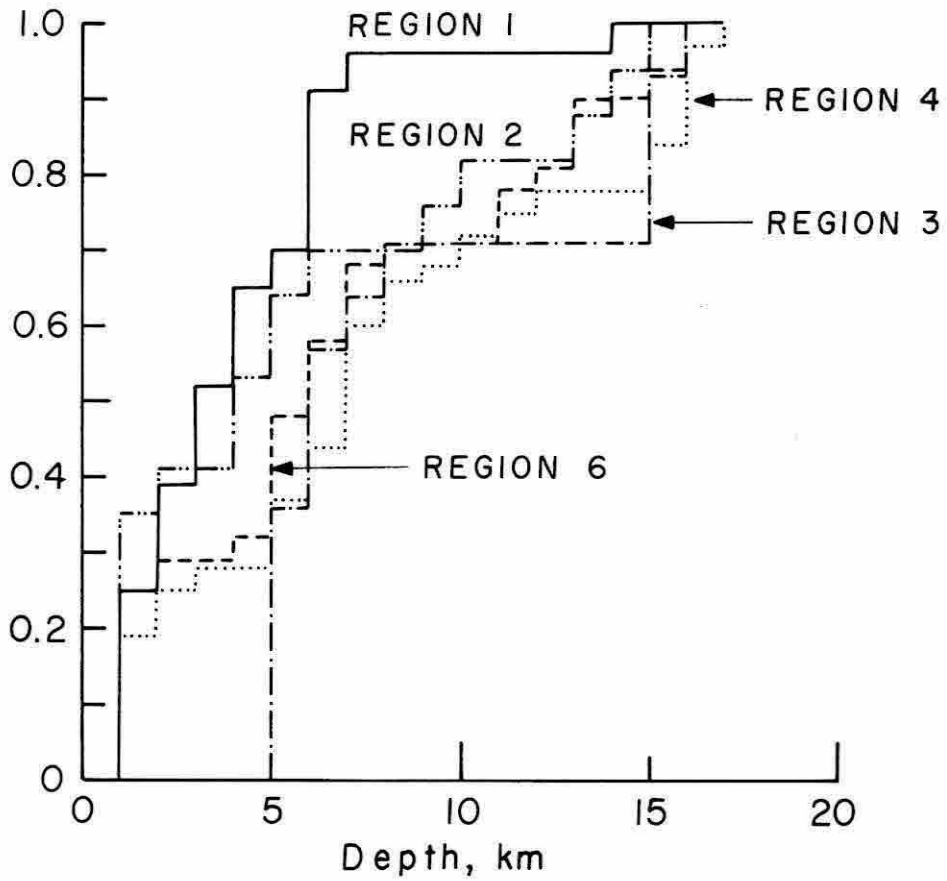
1.0
0.8
0.6
0.4
0.2
0
0
5
10
15
20
Depth, km
REGION 1
REGION 2
REGION 3
REGION 4
REGION 6

Figure 11-13